Università degli Studi di Genova
Dipartimento di Informatica, Bioingegneria,
Robotica ed Ingegneria dei Sistemi

Systems engineering approaches to safety in transport systems

by

Enrico Zero

Theses Series **DIBRIS-TH-2021-XXXIV**

DIBRIS, Università di Genova
Via Opera Pia, 13 16145 Genova, Italy http://www.dibris.unige.it/

Università degli Studi di Genova

Dipartimento di Informatica, Bioingegneria,

Robotica ed Ingegneria dei Sistemi

Ph.D. Thesis in Computer Science and Systems Engineering
Systems Engineering Curriculum

Systems engineering approaches to safety in transport systems

by

Enrico Zero

October, 2021

Dipartimento di Informatica, Bioingegneria, Robotica ed Ingegneria dei Sistemi
Universitá degli Studi di Genova

DIBRIS, Univ. di Genova
Via Opera Pia, 13
I-16145 Genova, Italy
http://www.dibris.unige.it/

Ph.D. Thesis in Computer Science and Systems Engineering
Systems Engineering Curriculum
(S.S.D. ING INF/04)

Submitted by Enrico Zero
Date of submission: October 2021

Title: Systems engineering approaches to safety in transport systems

Advisor: Prof. Roberto Sacile
Dipartimento di Informatica, Bioingegneria, Robotica ed Ingegneria dei Sistemi
Universitá di Genova
Ext. Reviewers:
Prof. Carmelina Ruggiero

Prof. Raul Benitez Iglesias. Polytechnic of Catalunya, Spain

Abstract

During driving, driver behavior monitoring may provide useful information to prevent road traffic accidents caused by driver distraction. It has been shown that 90% of road traffic accidents are due to human error and in 75% of these cases human error is the only cause. Car manufacturers have been interested in driver monitoring research for several years, aiming to enhance the general knowledge of driver behavior and to evaluate the functional state as it may drastically influence driving safety by distraction, fatigue, mental workload and attention. Fatigue and sleepiness at the wheel are well known risk factors for traffic accidents. The Human Factor (HF) plays a fundamental role in modern transport systems. Drivers and transport operators control a vehicle towards its destination in according to their own sense, physical condition, experience and ability, and safety strongly relies on the HF which has to take the right decisions. On the other hand, we are experiencing a gradual shift towards increasingly autonomous vehicles where HF still constitutes an important component, but may in fact become the "weakest link of the chain", requiring strong and effective training feedback.

The studies that investigate the possibility to use biometrical or biophysical signals as data sources to evaluate the interaction between human brain activity and an electronic machine relate to the Human Machine Interface (HMI) framework. The HMI can acquire human signals to analyse the specific embedded structures and recognize the behavior of the subject during his/her interaction with the machine or with virtual interfaces as PCs or other communication systems. Based on my previous experience related to planning and monitoring of hazardous material transport, this work aims to create control models focused on driver behavior and changes of his/her physiological parameters. Three case studies have been considered using the interaction between an EEG system and external device, such as driving simulators or electronical components. A case study relates to the detection of the driver's behavior during a test driver. Another case study relates to the detection of driver's arm movements according to the data from the EEG during a driver test. The third case is the setting up of a Brain Computer Interface (BCI) model able to detect head movements in human participants by EEG signal and to

control an electronic component according to the electrical brain activity due to head turning movements. Some videos showing the experimental results are available at https://www.youtube.com/channel/UCj55jjBwMTptBd2wcQMT2tg.

....alla mia famiglia che in questi anni mi ha sempre supportato ma soprattutto sopportato.....

Acknowledgements

Questi tre anni di dottorato sono stati per me molto intensi e mi hanno portato ad affrontrare insidie nuove come ogni esperienza fa. Volevo ringraziare tutte le persone che nonostante il mio carattere hanno voluto stare al mio fianco in questo mio percorso e mi hanno aiutato ad affrontare e superare le difficoltà.

Il mio primo ringraziamento va al mio tutor Roberto Sacile, tanti sono gli anni in cui ho lavorato per/con te. Beh non finirò mai di ringraziarti per tutto quello che hai fatto per me in questi anni soprattutto verso la fine quando la situazione era delicata ma tu, il mio padre lavorativo, non mi hai lasciato neanche li e mi hai aiutato ad uscirne. Grazie Roberto sei veramente una persona di cuore!

Manu & Simone gli amici di sempre che attraverso una semplice battuta ti rallegrano la giornata. Tanti viaggi abbiamo fatto insieme, tranne Praga, e anche questo ora è arrivato alla fine. In questo lungo viaggio i momenti no sono stati tanti ma voi ci siete sempre stati, nonostante magari io preferissi affrontare le difficoltà da solo sapevo che su di voi potevo sempre contare.

Giuse grazie per le serate di svago a casa tua, dove il tempo passava in allegria dietro sempre ad una battuta od un aneddoto nuovo!

Anita, Massimo, Franky e Mauro il DELAB. Colleghi di molte battaglie, grazie per il sostegno e supporto soprattutto verso la fine, quando il traguardo era vicino.

Chiara grazie per tutti i consigli che mi hai dato in questi anni e per la mano che mi hai dato in tutti i lavori che abbiamo fatto insieme.

Sandro & Laura grazie lo devo dire anche a voi, perché siete sempre disposti ad ascoltare qualche mio ”piccolo” sfogo serale e anche giornaliero. E’ bello avere amici come voi!

Ale grazie per le uscite ”Old + Cinema”, ultimamente causa impegni sono diventate sempre più una chimera, ma sono certo che riusciremo a recuperare.

Alessandro e Simone ultimi compagni di viaggio di questo mio percorso, nella speranza che in futuro si possa continuare a lavorare e divertirsi insieme.

Matteo, non ti ho mai chiesto grandi mani, ma quelle poche volte che l'ho fatto mi hai sempre aiutato. Grazie!

Luca ho perso il conto su quante volte ci siamo scontrati, abbiamo litigato, non ci siamo parlati ma poi alla fine... Grazie per avermi sempre spronato e rincuorato.

Ed ovviamente un enorme grazie va a voi: Mamma e Papà!

Table of Contents

Chapter 1

Introduction

The provision of a safe and a comfortable driving experience is a major concern of motor vehicle manufacturers. As the motor vehicle industry develops, an increasing number of entertainment and information systems is integrated into new vehicles. These systems aim to make the driving experience as enjoyable and as safe as possible.
Human behavior is a major risk factor in goods and people transportation. Car manufacturers have been interested in ”driver monitoring” research for several years, aiming in the first place to enhance the general knowledge of driver behavior and, secondly, to evaluate the functional state, which may drastically influence driving safety by distraction, fatigue, mental workload and attention. Fatigue and sleepiness at the wheel are well known risk factors for traffic accidents. A great number of factors condition driving state, such as: environment (traffic, weather, kind of street), truck maintenance, and driver conditions (e.g. physiological status like fatigue, drowsiness or arouse state). In the automotive context, research and innovation have recently focused on the realization of self-driving vehicles. Autonomous Vehicles (AV) are cars which can detect the environment by devices and sensors installed on board and which can be driven with limited or absent human intervention. According to the SAE International Standard [1], AVs are classified into six levels of automation, from level 0 where the driver is the only decision maker to level 5 where the vehicle is completely managed by the automated driving systems (ADS). Specifically, at level 0 the driver performs all dynamic driving tasks (DDTs), which consist of the tactical and operational functions required for the vehicle motion. Level 1 is applied when the ADS performs the DDTs related to either longitudinal or lateral vehicle motion control. At level 2 the ADS simultaneously performs both longitudinal and lateral vehicle control. At level 3, the ADS also performs the Object and Event Detection and Response (OEDR) to identify and to avoid events or obstacles on the route. At level 4 the ADS also completes DDT fallback [2]. This function consists of a higher automation equipment which may intervene when the ADS fails in case of risk conditions. At low levels of automation (Level 0 to Level 2), the driver is regarded as present and essential to carry out part of the main DDTs. In level 3 the driver may

assist the ADS when a failure occurs during a trip, while at level 4 the ADS performs the overall function included in the DDT fallback. Level 5 is reached when the vehicle is fully autonomous without human user's intervention. To detect and to identify the external environment the ADS must recognize road shape, road signs and different objects on the road in real time [3]. For this reason, the AV must be equipped with specific sensors such as camera, Radar or Light Detection and Ranging (LiDAR) [4]. Recent advances in image treatment provide object-detection models based on multiclass problems where the different elements which can appear on the road may be recognized. A 2D object detection model for vehicles, pedestrian and cyclist identification has been proposed [5]. Both one and two stages deep learning techniques are compared with process images with different resolution in order to identify the method which generates the best trade-off between speed and accuracy of the detection system. A radar-based deep neural network (DNN) has been proposed to recognize road segmentations when different objects such as road-users, obstacles, and other obstructions are present in the street [6]. The use of radar and camera fusion algorithms provides better performances with respect to one sensor applications above all in severe environmental conditions [7]. The LiDAR represents the most expensive solution among detection systems, and because of its high resolution is also the most adequate for SAE level 4 and 5. The 3D LiDAR provides images and measurements not affected by sunlight and tests several classifiers for real time obstacle detection. Among others, support vector machine (SVM) has been used to recognize in real time vehicles on an urban context [8], and a convolutional neural network has been adopted to classify vehicle lane change through LiDAR-based environment analysis [9].

Recent advances in cognitive engineering have taken place as relates to the design, the analysis and the development of complex human-machine-environment systems [10]. Recent research advances have taken place in the identification of cognitive human reaction according to a specific environment perception or to an adaptive human computer interaction (HCI) [11]. HMI relates to systems which allow humans to interact with machines or devices during an assigned task according to different interfaces. Human-as-a-Sensor (HaaS) is a paradigm which considers the human as the main subject which may detect complex hazard events or potential accidents better than automatic sensor systems [12]. Recently this paradigm has been mostly used in the social sensing framework, due to the diffusion of online social networks. By the massive spread of information and communication technology (ICT) devices people can collect large amounts of data and information from the environment and share them by communication systems [13]. The aim of HaaS is to improve and integrate technical systems for safety and security without replacing them. The possibility to complement current ICT with user driver detection systems improves the quality. A cyber-trustworthiness aspect has been introduced in Haas by proposing a mechanism to assign a score for individual reports based on the features of the mobile device that are monitored in real-time[14]. The Haas concept to detect semantic engineering attacks has been described [15] and Haas has been used to improve emergency situation alertness in crisis management. Haas has also been applied for real time detection of earthquake damages [16].
Intelligent automation may also involve HaaS, specifically by putting the human in the loop,

allowing him/her to add information, for example to enhance system's performance, to adjust unforeseen errors adding missing data or supporting the decision making process.

The Electroencephalogram (EEG) provides electrical brain activities by monitoring voltage variations through electrodes allocated on the scalp. EEG analysis started with medical or clinical purposes, but recently its use has also been devoted to the extraction of information about the monitored person while performing some specific task, in order to evaluate how his/her brain reacts in different test cases [17]. The studies that investigate the possibility to use biometrical or biophysical signals as a data source to evaluate the interaction between human brain activity and an electronic machine fall in the HMI framework. HMI acquires human signals to analyse the specific embedded structures, to recognize the behavior of the subject during his/her interaction with the machine or with virtual interfaces as PCs or with other communication systems [18]. Among the paradigms used to implement BCI, EEG analysis represents one of the most frequently adopted [19].
EEG analysis plays an important role in a variety of applications, above all to interpret human emotional states and to produce a feedback to identify the behaviors related to the emotions [20]. A large part of the related scientific work is still dedicated to select the optimal channels or features in the EEG trace, which may markedly improve correlations with emotion recognition [21]. However, most work shows results on different kinds of human sensations recognised by EEG spectral changes. The main basic emotions are anger, disgust, fear, happiness, sadness, and surprise described in a 2-dimensional space with dimensions, valence and arousal [22]. Thanks to the brain's capability to feel sophisticated emotions and to provide complex dynamic information that is reproduced by the cerebral cortex, different methods for the automatic detection of emotions through EEGs have been studied and applied.
A survey on the EEG usability and practicality in this context can be found in [23]. The EEG is one of the most promising tools to monitor brain cognitive functionality, due to the higher temporal precision with respect to other instruments, such as Functional Magnetic Resonance Imaging (FMRI) which presents, higher spatial resolution [24]. EEG-based biometric recognition systems have been used in a wide range of clinical and research applications - among others: interpreting human emotional states [25] [26], monitoring participants' alertness or mental fatigue [27], checking memory workload [28], finding brain area of damage in case of injury or disease [29] or, in general, diagnosing brain disorders [30] [31].
EEG monitoring, processing and analysis are useful techniques to identify intentional cognitive activities from the brain electrical signals. Some work has investigated the event-related potential when the decisions of the monitored subjects are affected by external stimuli during workload sessions. The workload performances depend not only on the operator, but also on the surrounding environment and on their interactions. A cognitive stimulus represents an event that involves the subject while performing different planned tasks during EEG data collection. Recent examples relate to the evaluation of driver's behavior [32] [33] or drowsiness [34] by analyzing the EEGs. In order to prevent road accidents, the driver's fear detected by EEGs has been evaluated when he/she is subjected to unpredictable acoustic or visual external stimuli [35]. Emergency

breaking, a rapid change of lane, or avoiding an obstacle on the route can also be detected by the driver's brain in advance with respect to the vehicle dynamics, and this contribution may improve the quality of the driver's intent prediction [36] and the overall system safety.
Cognitive activities related to motor movements have been observed in the EEG both for actually executed and for imagined actions [37][38]. Actual or imaginary movements examining neural signals, have been compared, concluding that brain activities are similar in the two cases [39]. The classification accuracy to predict the actions of standing and sitting by motor imagery (MI) and motor execution (ME) has been evaluated, and the classification of MI has provided the highest mean accuracy at 82.73±2.54% in the stand-to-sit transition [40]. Another study showed that Artificial Neural Networks (ANNs) perform better than Support Vector Machine (SVM) in the motor imagery classification [41]. Several classification algorithms including Linear Discriminant Analysis (LDA), Quadratic Discriminant Analysis (QDA), k-nearest neighbor (KNN) algorithm, linear SVM, radial basis function (RBF) SVM, and naive Bayesian have been compared to classify left/right hand movement, reaching an accuracy of about 82% by the RBF SVM [42]. A 2D study about the movements of the dominant hand when a participant had to track a moving cursor on a screen by an imaginary mouse on the table has been carried out and the prediction accuracy of horizontal movement intention has been found to be higher than the vertical one[43].
Until 2006, almost 25% of classification algorithms for neural cortical recording were based on Neural Networks (NN) [44]. More recently, NNs have been intensively applied to EEG classification [45]. Neural networks have been adopted for motor imagery classification of hand [46] or foot movements [47], or eye blinking detection [48].
Head movements classification is more complex because, with respect to other monitored actions, EEGs are affected by 'artefacts' to a greater extent [49]. EEGs may also include non-cerebral activities coming from elements such as eye activity, or muscle movements [50]. Many techniques are available to analyze such artefacts [51]. EEG artefacts have been identified using the signal from a gyroscope located on the EEG device [52], and a SVM based automatic detection system where the artefacts were considered as a distinct class has been developed [49]. Artefacts have also been classified according to autoregressive [53] or hidden Markov models [54]. An automatic technique to remove artefacts in head movements has been proposed where the signals from an accelerometer located on the participant's head have been acquired together with the EEGs. Then, EEG components correlated with the accelerometer signals according to a specific threshold have been removed, in order to obtain an EEG free from artefacts[54].
A significant relationship between head movements and the emotions generated by visual stimuli has been found [55][56]. EEG spectral analysis in visual motor tasks has been carried out, in the contex of visual motor tasks. A positive correlation has been found between the task of drawing an image boundary on a screen by hand movement and the brain activities coming from a single frontal electrode in the upper alpha band[57]. A similar experiment, which involved the fingers of one hand, has shown that alpha band variations are correlated to the visual motor performances, while the coherence in alpha and beta oscillations implies an integration among visual motor brain areas[58].

BCI involves a collaboration between the brain and a device which commands the signal from the brain to control some external tool, such as cursor or switch on/off lamps. It can be divided into three steps: brain signal recording, signal analysis and, as a last point, outputting commands to a connected machine according to the brain signal.
BCI technologies for brain activities monitoring may be classified as invasive, semi-invasive or non-invasive. Invasive BCI technologies generally consist of implanting electrodes in the human cortex. Semi-Invasive BCI technologies are based on placing electrodes in the dura mater or in the arachnoid mater in the human scalp, in order to record the electrocorticography (ECoG). ECoG uses the electrodes located on the exposed surface of the brain, to measure the electrical activity from the cerebral cortex. It requires a craniotomy, so it is used only when surgery is necessary. Non-invasive BCI technologies usually relate to positioning the electrodes on the scalp, acquiring the EEG or a magnetoencephalography (MEG). EEG and MEG can respectively monitor the electrical and magnetic fields generated by neuronal activities.
In the specific context of BCI, Haas may be taken into account as a specific human-in-loop feedback control which aims at investigating how human and machine collaborate in an integrated and intelligent way [59]. Several studies consider models which represent the human choice in a complex system as a mixed assembly line in a manufacturing system, considering the techniques based on a human-in- loop approach [60]. In the last few years a challenging trend of the HaaS research deals with the integration of human sensing data coming from the EEG, regarding it as an integral component of the overall automated system and of specific decision making tasks. One of the main hard tasks in a BCI application is the implementation of pattern recognition systems to identify the classes of data coming from the brain activities. Pattern recognition depends on classification algorithms. It has been shown that nonlinear classifiers, such as ANN and SVM, produce slightly better classification results with respect to linear techniques (such as linear discriminant analysis) in the context of mental tasks[61].
Neural activities have been classified when cognitive stimuli are related to olfactory [62] or visual [63] perception. Correlation between the complexity of visual stimuli and the EEG alpha power variations in the parieto-occipital, the right parieto-temporal and central-frontal regions has been found [64]. This is in agreement with findings on linear correlation among EEG data[35]. Software techniques have been used to reduce noise and interferences in the EEGs from the human brain, to classify them, and to process the main information to improve efficiency in the human-device interaction [65]. A steady state visual evoked potential (SSVEP)- BCI systems based on a convolutional neural networks (CNNs) has been developed to classify brain activities coming from a wireless EEG in order to realize a real-time control loop for a mobile robot. The classifier processed the EGG signals of the participants subjected to visual stimuli and generated the commands for the robot as a brain-actuated vehicle in human-in-loop configuration [66]. A SVM classifier has been implemented to manipulate human EEG data in such a way that human intentions can be recognized and motion commands can then be transmitted to a teleoperated robot [67].
In HCI research the use of BCI systems represents one of the most challenging research activities. BCI technologies aim at converting mental activities of the human participant into electrical

brain signals, producing a control command feedback to external devices such as robot systems [68]. In addition, BCIs may also include paradigms that can identify patterns of brain activity for a reliable interpretation of the observed signals [69]. Reviews about BCI and HMI can be found in [70] and [71].
In the BCI context, it is interesting to introduce the concept that the user, who interacts with computer or machine, represents a source of data that can be used to identify critical situations and predict events in different application contexts such as cyber security, transportation, energy or social issues [72]. Traditional approaches which manage system automation often fail in the representation of the relationship among the performances of persons and their human machine co-working environment. A great amount of work concerning EEG analysis versus visual-motor tasks is available. Perspectives are particularly relevant in rehabilitation engineering. A relevant recent example of EEG analysis application in robotics and rehabilitation engineering is provided where an exoskeleton coupled with a BCI elicits EEG brain patterns typical of natural hand motions [73]. Eye or hand movements have also been considered. Some work has been carried out relating to correlation of EEGs in visual-motor tasks associated to the head movement.

This work focuses on driver behavior and changes of his/her physiological parameters.
Specifically the arousal state of the driver, that is the physiological state of being awake, has been considered. It involves the reticular activating system in the brainstem, the autonomic nervous system and the endocrine system, leading to increased heart rate and blood pressure and to a condition of sensory alertness, mobility and readiness to respond. Arousal is important in regulating consciousness, attention and information processing.
It is intended to setup control models able to govern external components using the EEG. Three case studies have been considered.
One relates to the detection of the driver's behavior during a driver test. In this case study an EEG-based Driver Control System (EEG-DCS) is set up to monitor the psychophysical driver state evaluating driver's ability to respond to unexpected or emergent events during a drive session.
Another case study relates to the detection of the driver's arm movement according to the data coming from the EEG during a driver test. The experiment involves 3 measurement sessions for each participant in different days. Three analyses have been carried out on the EEGs.
The third case study is the setting up of a BCI model able to detect head movements in human participants by EEG and to control an electronic component according to the electrical brain activity due to head turning movements. The experiment has been divided into two parts. The first one relates to the acquisition and storing of the EEG of each participant, the second one is the application of a BCI method in a real context. The main goal of this last experiment is to show that it is possible to identify a non-linear input output function to compute the position of the human head (according to three states: left, forward, and right) from its brain electrical activity, which has been acquired by three electrodes.
The first two case studies of the work relate to the evaluation of data deriving from the EEG and to data detection from the brain. Subsequently, in the third case study a new BCI model has

been set up using the findings from the previous experiments to control the switch on/off of the electronic component.

Chapter 2

Methods and tools

2.1 Monitoring dangerous goods transport

In dangerous good transport, many variables must be considered to prevent accidents. The relevant macro areas are the environment, the driver behavior and the truck. The first one can be evaluated using a camera to control the traffic and weather conditions. As relates to the second one, the physiological signal can be monitored acquiring data from EEG, EMG or heart rate to measure variations of the driver's behavior. The third one relates to the automotive damage, and it is possible to monitor automotive data by the CAN bus of trucks or using some external electronic components. The data collected by these three systems are subsequently compared with the target to evaluate if there are anomalies. Fig. 2.1 shows the monitoring system.

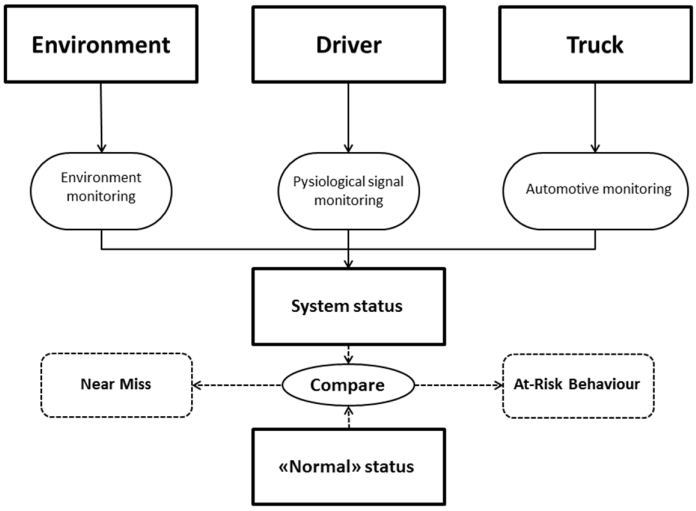

Figure 2.1: A scheme of the monitoring system

This thesis is focused on two macro areas: driver behavior and truck monitoring. The EEG is used to evaluate the driver behavior during driving simulations. A driving position has been built to evaluate and simulate the truck performance during driving simulations.
An integrated approach has been carried out, in order to improve safety in the transport of dangerous goods, mainly by road, focusing on various aspects (risk assessment, real-time monitoring, driver training, traceability systems such as vehicle maintenance means, transport optimization). As part of this research an original hardware prototype has been designed for monitoring the transport of dangerous goods (Fig. 2.2). This prototype consists of an On-Board-Unit and various sensors linked to the physical characteristics of the transported goods (e.g. quantity, temperature), as well as various hardware and software interfaces with other systems such as CAN bus, and electronic head. The system installed on each vehicle sends information ”at frequency” (every 3 minutes) or ”by event” (whenever a particular event occurs such as the opening of the tailgate as detected by appropriate RFID) to a server via TCP / IP on a physical GPRS channel. This prototype, defined in its entirety, both hardware and software, including the syntax present in the transmission protocol was designed and released at the behest of Eni, which subsequently released to MIT (Ministry of Infrastructures and Transport) in order to favor its diffusion, in such a way that the system could be produced by different companies as well as adopted on the territory as a reference model. Currently the system is developed by six companies throughout the country and is adopted in some regions and used in the national logistics platform UIRNET.

Figure 2.2: Truck Monitoring system

Fig. 2.3 shows the TIP – Transport Integrated Platform- a project developed in more than ten years by Delab laboratory and now a basic tool in Eni R&M for monitoring the trucks and to prevent near miss and incident during dangerous goods transport. Since transport services are almost completely outsourced, it's necessary to develop instruments for continuous monitoring of processes and performance, and to ensure an adequate level of control of this important aspect of the supply chain. TIP is a web portal divided into sections, with secure and selective access, accessible via Internet by both internal users (Eni) and by external parties (e.g. transportation suppliers). The main modules of this system relate to remote monitoring, trip planning and technical management.

The **remote monitoring** module is equipped with real-time monitoring of transport through the representation of data in tabular form and on geo-referenced maps and interactive maps. This allows the users to constantly monitor the operations and to extract and export data about the position of the trucks and the quality and quantity of the loaded and unloaded products.

The **trip planning** section is used to provide real time comparison between the planned service and the implemented service. It's possible to compare programmed trips with the data coming from the remote monitoring system which is installed on board.

The **technical management** section manages all technical controls which are constantly updated during each inspection. In addition to the controls, all the expiring dates (audits, insurance, fire extinguishers, certificates, etc...) are available. In this section the technical data of rail tank wagons are also available.

The system is able to collect and control the daily data by the On-Board-Unit of 800 vehicles. This system monitors and controls the trucks in real time. Its goal is to detect anomalies from the data and send alarms in case of dangerous situations, such as: fast speed and sudden stop.

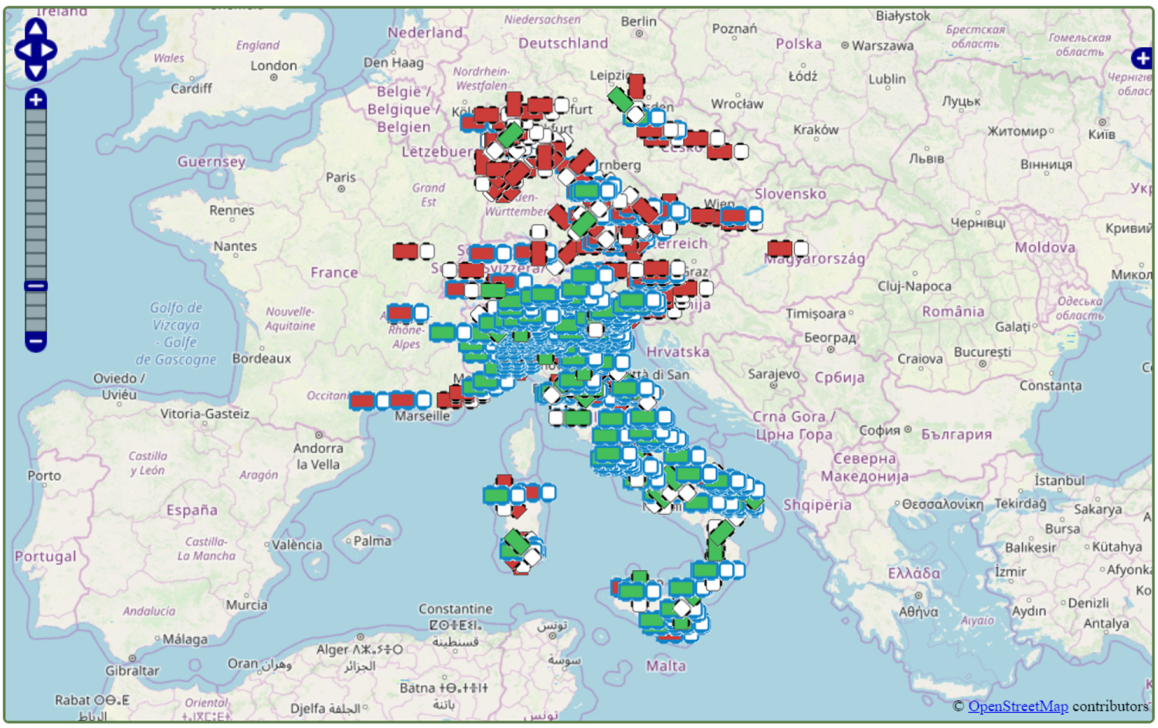

Figure 2.3: Transport Integrated Platform - TIP

In the last three years, a new optimization algorithm has been developed. The algorithm creates an optimization in the daily journeys for the transport of goods starting from a store to many centers arranged around predetermined kilometers. The task of this algorithm is to create the trips taking into account the requests of the individual collection points, reducing the transport costs. In fact, the algorithm takes into account all requests putting together the collection points that are as homogeneous as possible, in such a way as to avoid exceeding the maximum quantities allowed by law for transportation of goods. The optimization model that has been created also takes into account limitations and constraints of the collection points, such as timetables, types of vehicles that can serve them, driving hours - which also include loading and unloading times of the goods for the organization of daily deliveries. The daily deliveries are about 2 thousand, organized on about 800 trips. Fig. 2.4 reports a screen of the web application performed for data processing and analysis.

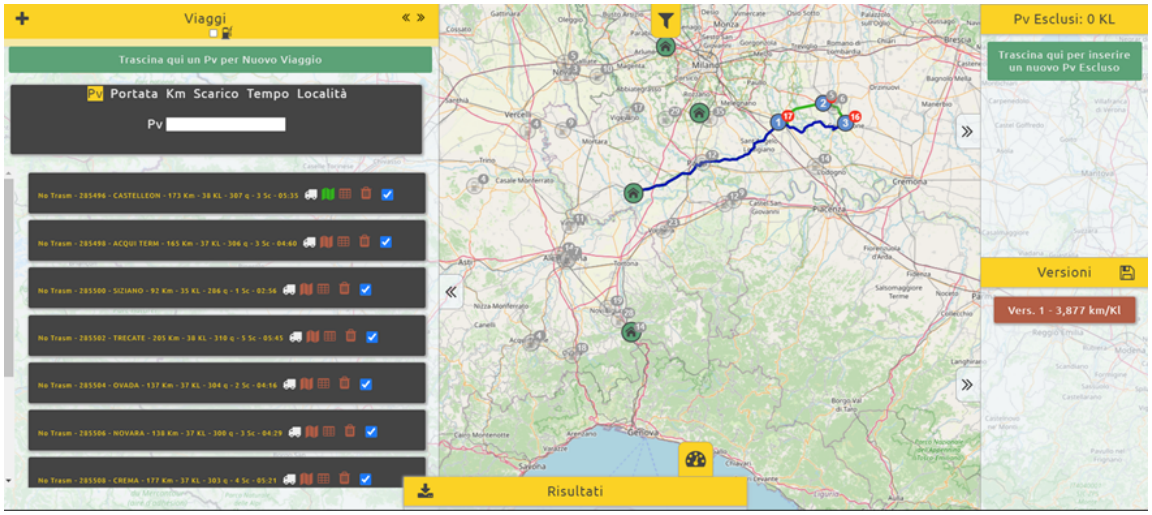

Figure 2.4: Smart Planning Environment for Eni Delivers - SPEED

2.2 Hardware device

2.2.1 EEG

The EEG is a record of the oscillations of electrical potential generated by brain sources and recorded from electrodes on the human scalp. They are highly random in nature and may contain useful information about the brain state. However, it is very difficult to get useful information from these signals directly in the time domain just by observing them. They are basically non-linear and nonstationary in nature [74]. There are two types of EEG recording: monopolar and bipolar. The first one picks up the voltage difference between an active electrode on the scalp and a reference electrode on the ear lobe. The second one records the voltage difference between two scalp electrodes. In all case studies a bipolar recording has been used. The EEG is characterized by four principal rhythms: alpha, delta, theta and beta waves.

- **Alpha** waves are the baseline frequency detected in humans with close eyes and can be identified by the occipital and parietal electrodes. They are classified as: slow (8-9 Hz), mid-term (9-11.5 Hz) and fast (11.5-13 Hz), with an average amplitude of 30 microvolts.
- **Beta** waves are detected in humans with open eyes and they work in low voltage, but they are faster than alpha waves. They can be categorized in: slow (13.5-18 Hz) and fast (18.5-30 Hz), with an average amplitude of 19 microvolts.
- **Theta** waves are detected in half-asleep and they indicate the human attention. They can be slow (4-6 Hz) or fast (6-7.5 Hz), with an average amplitude of 75 microvolts.

- **Delta** waves are usually associated with the non rapid eye movements (R.E.M.) They are detected in the 20 minutes from the beginning of the rest. They have a frequency of oscillation between 0.5 e 4 Hz, with an average amplitude of 150 microvolts.

Brain signals are highly complex and random in nature. Their specifics strongly depend on the individual, age and mental state. The occurrence of symptoms is also random in time scale. Understanding the behavior and dynamics of thousands of interlinked neurons requires diverse linear and nonlinear signal processing techniques and its correlation to the physiological events [74]. An example of EEG is shown in Fig.2.5:

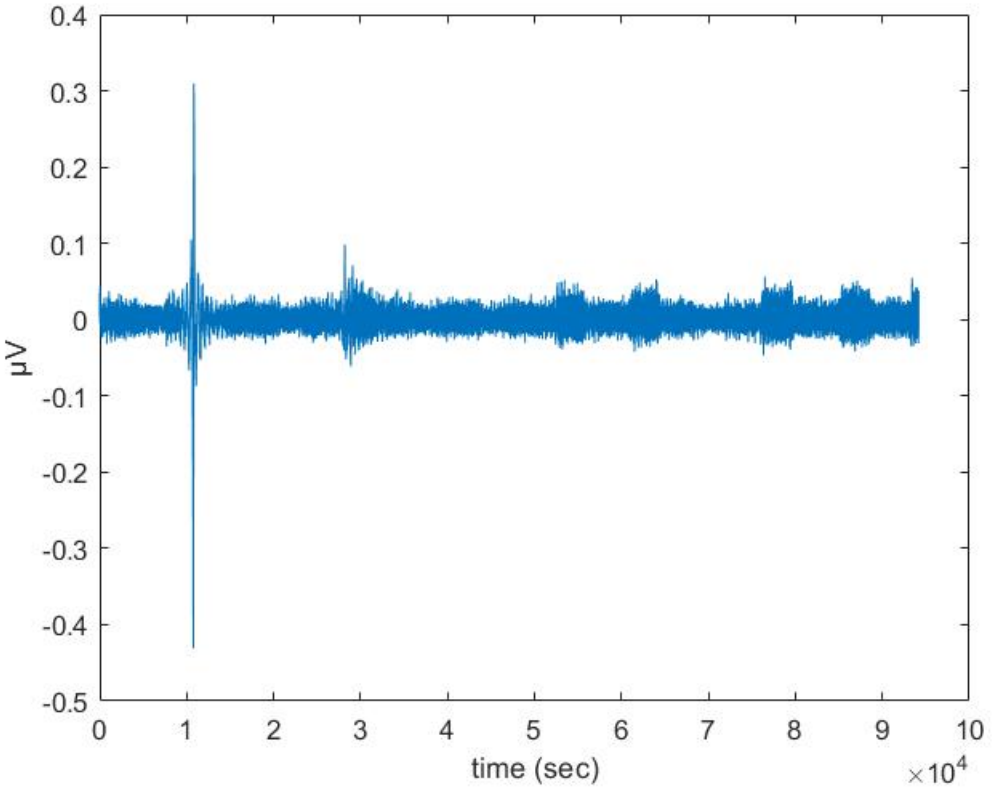

Figure 2.5: EEG

2.2.1.1 Emotion detection by EEG

EEG analysis can refer to the human-in-the-loop control, which combines the human operator's cognitive reaction with the surrounding physical and mechanical environment. This concept may be relevant in the BCI driving system, as relates to estimating driver intentions in simulating

braking [75] ,traffic lights recognition [76], or identification of turning direction [77] during a driving session. Recent studies investigated the EEG in the driving assistant systems in order to identify error-related brain activities [78]. Usually human errors affect the correct use of the interacting machine and the analysis of the brain functions may be used to regulate target directed behavior.

In stressful conditions, when an unexpected event happens, the subject has to react quickly to avoid threatening scenarios. In this context, the real-time detection of users' fear/stress may be crucial for improving safety in different operative work sessions, driving vehicles or aviation. Biometric data such as Heart Rate (HR) or Breathing Rate (BR) are often used to identify the level of stress in driving situations [79]. In general, a person which is subject to external stimuli reflects the emotions in variations of his/her brain waves called evoked potentials (VEP) [80]. More recently, special attention has been given to the prediction of driver's emotional states during driving performances by EEG brain signal recognition [81]. A workload detector has been defined which aimed at quantifying the mental stress for drivers operating under real traffic conditions and, according to it, at regulating the interaction with the car's system [82].

A driver's test has been proposed to identify EEG potentials prediction in emergency braking during simulated driving. A significant event-related association has been observed among EEGs and the critical traffic situation [83].
The relationship between the EEG spectrum and driver's alertness has been estimated in a virtual-reality-based driving simulator [84]. EEG data have been analised to identify an indicator for driver fatigue and the minimum number of electrodes to be used for the analysis [85]. To detect fatigue in drivers the EEG has been used to analyse alpha, beta, delta and theta activities during a monotonous driving session, and the results demonstrated stable delta and theta activities over time, a minor reduction of alpha activity and a significant decrease of beta activity [86]. The driver vigilance performance has been evaluated as effect of the vision of a monotonous road. This study demonstrated that the invariability of the environment in terms of characteristics of the travelled road is a factor that may decrease the drivers alertness [87]. It has been found that the alpha wave fluctuations may reflect the intensification of mental effort to maintain vigilance while the beta wave is associated to high alertness and arousal [88]. Fatigue in human drivers in real and simulated scenarios has been analysed evaluating the entropy values in the wavelet domain. The parameters varied in the same manner in respect to simulated or actual driving conditions [89].

Several studies have been focused on the EEG responses due to acoustical and visual external stimulations on the cortical EEG. Eye blinks and brain activity from EEGs have been used to detect stress in car driving simulations filtering the frequencies between 2 Hz and 40 Hz. The tests have been conducted by introducing stressful emotions to the participants, through straight and curvy roads and with and without billboards during the driving sessions. A strong correlation has been noticed between the EEGs and the visual stimuli during the tests [90]. The stereo-electroencephalography (SEEG) of the drivers was monitored to explore the reactions of the

temporal pole of the brain. It has been found that the stimuli generated by pictures, music and movies affected the theta-alpha frequency range [91]. The correlation between drivers' brain activities and alpha waves has been confirmed under two different situations: during the subject's exposition to unexpected acoustic alarm and during visual external events in driving sessions [35]. The effect of acoustic and visual stimuli on braking response in car drivers with different ages has been tested [92]. The participants had to react to the brake lights in the preceding car, while, contemporary, different secondary stimuli generated by two loudspeakers or by sign on the screen were applied. It was found that stimuli during a workload task affect the braking performances of the drivers and that visual external events had a greater distraction effect than acoustic stimuli. Considering the importance of emotions in human-machine interaction and, in particular, in manual or automated driving, this study aims at showing how stress affects the performance of drivers and examines the effects of emotions on their EEGs, in simple simulation scenarios, relating to driver's behavior [93] .

2.2.1.2 EEG Cap

The EEG is acquired using a wearable cap which could have different numbers of channels located in the human scalp. The number of channels normally used in the acquisition can be: 8, 16 and 32. The signal is recorded by dry or gel electrodes. The gel electrodes are made of silver or nickel, the dry electrodes are made using stainless steel as a conductor to transmit the microvolt signals from the human scalp to the EEG amplifier. The gel electrodes require the use of a gel between the brain surface and the electrode to increase the signal impedance and improve the accuracy of the signal. The EEGs recorded with a wet electrodes have less noise than the EEG recorded with the dry electrodes[94]. However, the use of dry electrodes has been preferred in this work because it is simpler and quicker. In Fig. 2.6 the two types of electrodes previously explained are shown:

Figure 2.6: The dry (left) and gel (right) electrode

The EEG cap that has been used is the Enobio Cap by Neuroelectrics Barcelona SL with 8 electrodes positioned according to the International Standard System 10/20. Two additional reference electrodes are located in a hairless zone behind the ears. The International Standard System 10/20 is an internationally recognized method for EEG recording. The Bandwidth lies between 0 to 125 Hz, the sampling rate is 500 SPS and the resolution is 4 bits – 0,05 microvolts.

In every EEG system an amplifier is necessary, due to this amplification circuit most of signal noises are eliminated and the Signal to Noise Ratio (SNR) is raised. A good EEG amplifier amplifies the EEG and attenuates other undesired noises. The signal from the electrodes has three main signal components coming from electrodes : biological signals,electrode offset signals, and main noise signals.

The dc offset is influenced by electrode's type and material, it's an inherent fluctuating signal, to avoid or to minimize this signal high-quality Ag/AgCl electrodes are highly recommended. The main source of noise relates to the sinusoidal artifacts at 50hz frequency , depending on the presence of electrical devices or motors as pumps and razors.

In the system that has been set up the amplifier is the NECBOX - a bluetooth device connected to a server PC for online recording analysis. In Fig.2.7 the NECBOX device is shown.

Figure 2.7: NecBox device

It is also possible to use the software supplied by Neuroelectrics, the NIC, studying the real time EEG in time domain and frequency domain , as shown in the Fig.2.8. The data can also be saved for offline analysis.

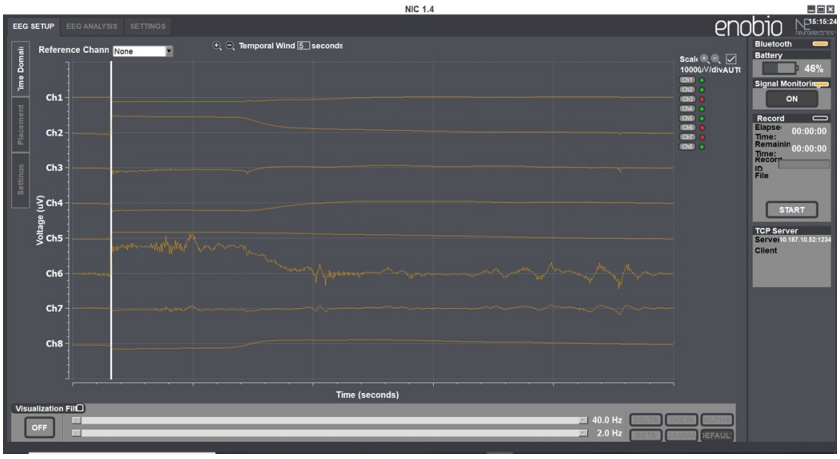

Figure 2.8: NIC software

The software performs the principal band pass filters regarding the: alpha, beta, gamma and theta wave. These waves can be used to extract different information from the data. The position of the electrodes in the different brain areas depends on the aim of the analysis. A possible location of the electrodes is shown in Fig.2.9.

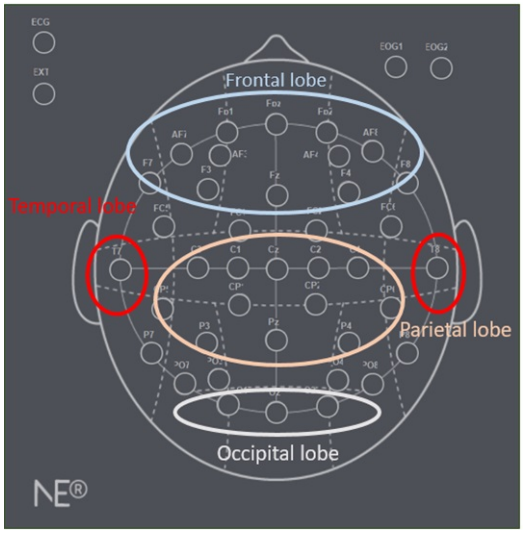

Figure 2.9: Electrode Position

The brain lobes are:

- **Occipital** The occipital lobe is located at the back of the brain and is associated with visual processing, such as visual recognition, visual attention, spatial analysis (moving in a 3-D world) and visual perception of body language - such as postures, expressions and gestures.
- **Frontal** The frontal lobe lies just beneath the forehead and is associated with our brain's ability to reason, organize, plan, speak, move, make facial expressions, serial tasks, problem solve, control inhibition, initiate and self-regulate behaviors, pay attention, remember and control emotions.
- **Parietal** The parietal lobe is located at the upper rear of our brain, and controls our complex behaviors, including senses such as vision, touch, body awareness and spatial orientation. It plays important roles in integrating sensory information from various parts of our body, knowledge of numbers and their relations, and in the manipulation of objects. Portions are involved with our visual spatial processing, language comprehension, the ability to construct, body positioning and movement, neglect/inattention, left-right differentiation and self-awareness/insight.
- **Temporal** The temporal lobe is located near ears, and is associated with processing our perception and recognition of auditory stimuli (including our ability to focus on one sound among many, like listening to one voice among many at a party), comprehending spoken language, verbal memory, visual memory and language production (including fluency and word-finding), general knowledge and autobiographical memories.

2.2.2 EMG

The EMG is used for evaluating and recording the electrical activity by skeletal muscles during their contraction, and it is one of the most important physiological signals that are widely used in clinical and bio engineering applications [95]. The EMG is controlled by the nervous system and is dependent on the anatomical and physiological properties of muscles. It acquires noise while traveling through different tissues. Moreover, the EMG detector, particularly if it is at the surface of the skin, collects signals from different motor units at a time, which may generate interaction of different signals. It is accepted that the amplitude of the EMG is within a range from μV to low mV. The energetic distribution of the EMG is within the 0 to 500 Hz range in frequency domain, with the dominant components in the 50-150 Hz range.
The electric potentials generated by muscle cells are detectd by the electromyograph - the instrument used to record the EMG. The signals can be analyzed to detect abnormalities and activation level to analyze the biomechanics of human movement. In Computer Science the EMG is used as data source able to command external electronic devices. There are still limitations in the detection and characterization of existing nonlinearities in the surface electromyography signal. Various mathematical techniques like wavelet transform, time-frequency approaches and ANNs are used to develop advanced EMG detection and analysis techniques. The Genetic Algorithm has also been applied in evolvable hardware chip for the mapping of EMG inputs [96]. Fig. 2.10 shows the instrument used to record the electrical activity of muscle contraction.

Figure 2.10: EMG device to connect sensor to a PC

The box is connected by wireless with 8 sensors which send the information by USB to the PC. The sensors are located in the interested skin area by gel electrodes. Fig. 2.11 shows one of the

8 sensors that have been used:

Figure 2.11: EMG Sensor

2.2.3 Driver simulator

The simulator has been used to test drive scenarios. The SCANeR Studio software, included in the OKTAL platform, provides the users with tools and models that are able to recreate realistic virtual scenarios addressing automotive and transport simulation. The users can define the features related to road environment and infrastructures, vehicle type to be driven, traffic dynamics, car and pedestrian behavior and weather conditions. Fig. 2.12 shows in the left picture a view of the scenario editor of the OKTAL simulator able to create and modify the scenario of the simulation the driver simulator, the right picture shows a driving interface by a video screen, a seat, a steering wheel and the pedals.

The video screen shows the driver the outside view of the vehicle. The system is able to detect also the pedal pressure applied by the driver's foot and the angle of the steering wheel. At the end of the test drive, the simulator system provides a text file where all information about the driving session is recorded.

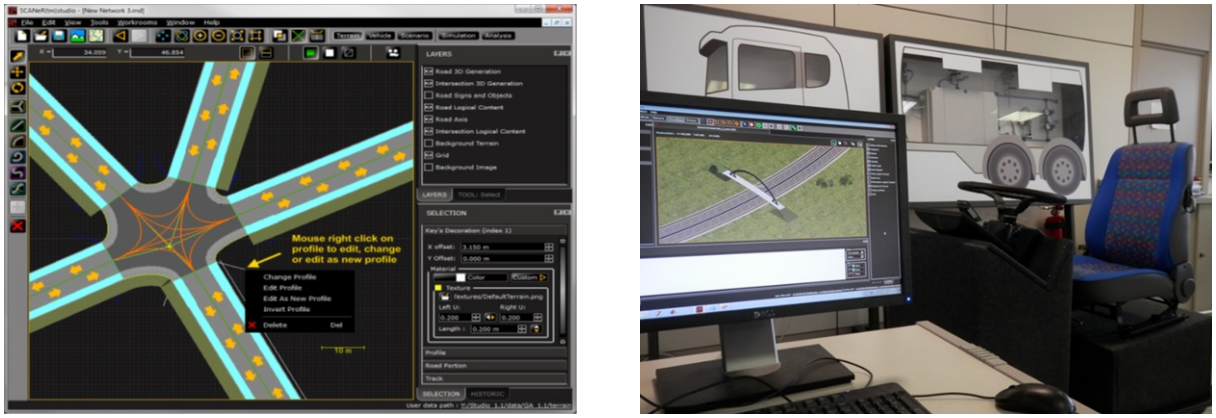

Figure 2.12: Oktal Simulator

2.2.4 Hardware for input/output syncronization

The lamp-system which has been adopted is a homemade device able to control the switch on/off of two LED lamps. The hardware components of the device are:

- AptoFun 2 channels 5V Relay-Interface-Board;
- Raspberry pi 3 - control unit
- USB - TTL converter
- 2 LED lamps
- Server PC

A representation of the subsystem is shown in Fig.2.13:

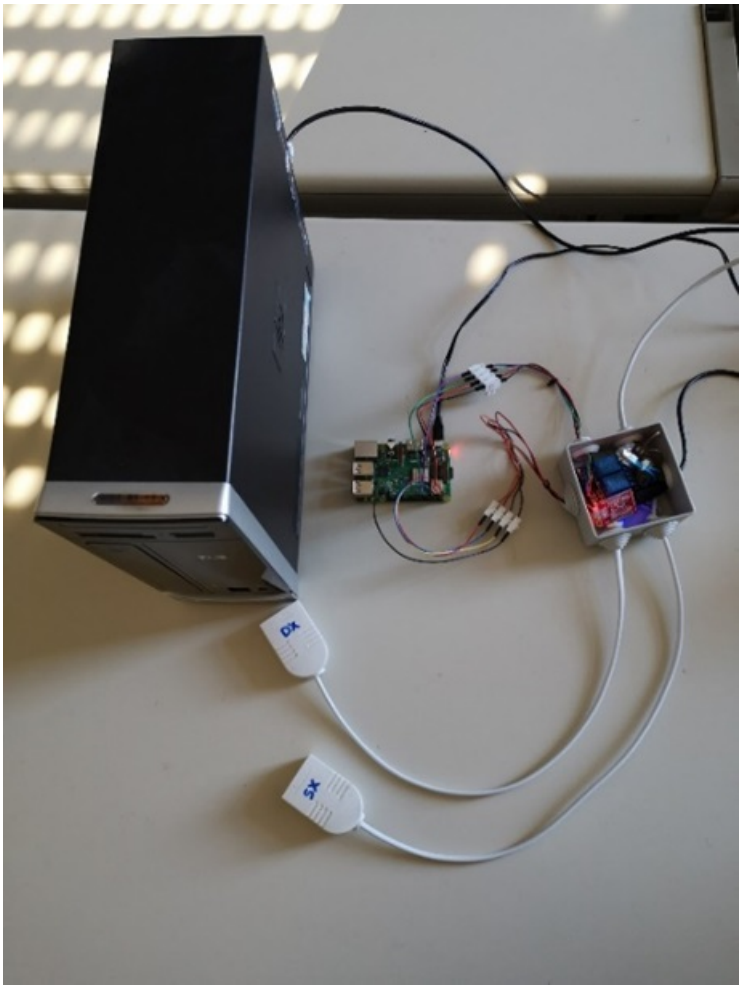

Figure 2.13: Lamp-System

A PC server hosts a python application, which randomly sends an input to the Raspberry unit by a serial cable. The Raspberry unit hosts another python application which receives commands to switch on/off the lamps. The switch on/off of the two lamps is coded with 3 different statuses: 1 switch on the right lamp, -1 switch the left lamp, 0 switch off. It is not possible to have two consecutive switch on codes. The proposed lamp-system is used in two different kinds of trials. In the first part of the experiment, the subject has to follow the visual stimulus and to look toward the switched lamp, while in the second part the participant controls the lighting system.

During the experiments the two lamps are located at the extreme sides of a table 1.3x0.6 meters long, and the participant may rotate the head in the range between -45° and 45°.

2.3 Signal analysis

The EEG as specified in the previous section and in [97] is a multi-frequency non-stationary brain signal. Feature extraction is a very important aspect of the analysis. Linear and non linear methods for data analysis can be used. Linear methods can be applied to non linear signals with the stationarity assumption, but this can cause loss of information. Non linear methods are best suited for non stationary and non linear signals.

2.3.1 Frequency domain analysis

A frequency-domain graph shows how much of the signal lies within each given frequency band over a range of frequencies. Several methods for frequency domain analysis can be used. In this section the Fourier transform and the Wavelet transform are reported. Spectral analysis based on Fourier transform regards the signal as stationary and ignores any time varying spectral content of the signal. Continuous wavelet is a powerful tool for non-stationary signal analysis. This method guarantees better performances in a time–frequency analysis with respect to the more traditional short time Fourier transform (STFT), especially the analysed signals has features whose frequency grows rapidly, as shown in [98], where an example of the two methods is given.

The Fourier transform is a mathematical transform which decomposes a time signal into a magnitude and phase component of its frequency components. The Fourier transform is considered to be the best transformation between time and frequency domains because of its time-shift invariance. The Fourier transformation can be used to display the features of the signal, but can also be used to simplify calculations in order to facilitate problem solving, especially in signal processing. The Fourier transform is shown below:

$$y_{k+1} = \sum_{j=0}^{n-1} \omega^{jk} x_{j+1} \tag{2.1}$$

Where $\omega = e^{-2\pi/n}$ is one of n roots of unity. The Fourier transform of signal is shown in Fig. 2.14a.

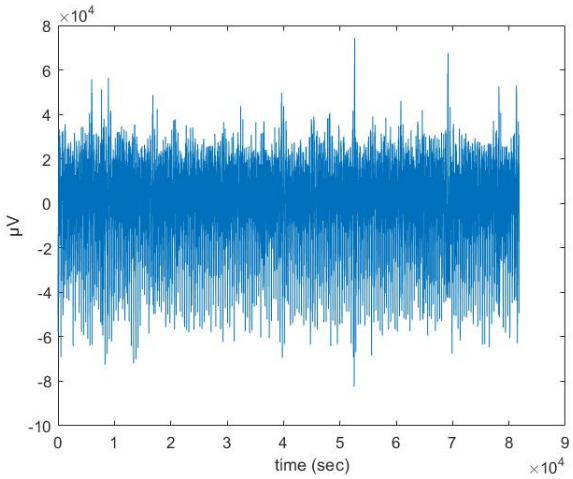

(a) EEG

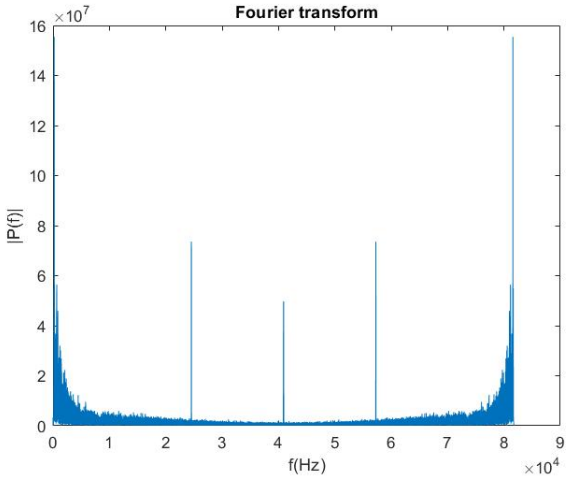

(b) Fourier Transform for a EEG

The wavelet transform transforms a time domain signal into a frequency domain signal. It is used when signal features vary over different scales, such as frequencies varying over time. This method guarantees better performances in a time–frequency analysis with respect to short time Fourier transform, especially for signals whose frequency grows rapidly [99]. The method is based on the concept of mother wavelet, defined as:

$$\psi_{j,k} = 2^{\frac{j}{2}}\psi(2^i t - k) \tag{2.2}$$

Where **k** is the time shift, **j** is the subset of scales of the mother wavelet $\psi(t)$. For **j** and **k** the transformation can be performed as the inner product between the wavelet function and the time-domain signal [100]:

$$W_\psi =< f, \psi_{j,k} > \tag{2.3}$$

The wavelet transformation can be applied the discrete data. The Discrete Wavelet Transform (DWT), derives from the continuous wavelet and can be applied when the input signal and the decomposition can be expressed as in following formula:

$$X_{a,L}[n] = \sum_{k=1}^{N} X_{a-1,L}[2n-k]g[k] \tag{2.4}$$

$$X_{a,H}[n] = \sum_{k=1}^{N} X_{a-1,L}[2n-k]h[k] \tag{2.5}$$

Where $g[k]$ and $h[k]$ are respectively a low pass filter and a high pass filter to capture the low and high frequency components. In Fig.2.15b a representation of wavelet transform of a channel of the EEG in the alpha frequency is shown. The wavelet transform has been used in the first case study to evaluate the variation of driver behavior when an expected event has been happened.

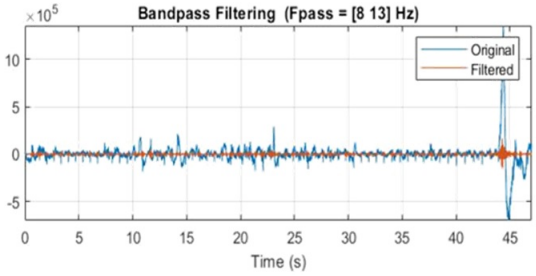

(a) EEG

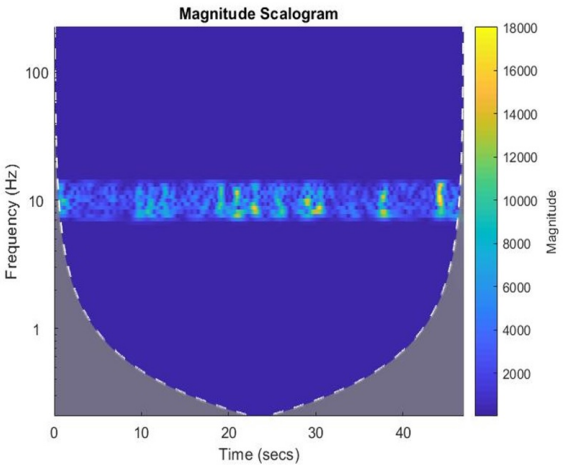

(b) Wavelet Transform

2.3.2 Time domain analysis

Time domain analysis is the study of a signal or time series with respect to time. In case of continuous time the function's value is known for all real numbers, or various separate instants in the case of discrete time. Signals exhibit some periodicity, so that they may be modelled by a sinusoidal signal or a sum of sinusoids with possibly time-varying nature. For this reason it is important during signal processing to be careful to some critical issues. First of all, the EEG must be filtered to focus on only some frequency only, depending on the problem. The possible filters are: low-pass, high-pass and band-pass filter. An adaptive notch filter is used to prevent the main two problem relating to time domain analysis that are noise reduction and signal decomposition [101].
Time domain signal coding techniques and ANNs have been used for discriminating between the sounds of different animal species within a group [102]. The BCI model that has been set up performs a time domain analysis and ANNs for the second and third case study. The artificial neural networks are used to perform a system that coding techniques.
Fig. 2.16 shows one channel of an original EEG and the same signal filtered with a band-pass filter.

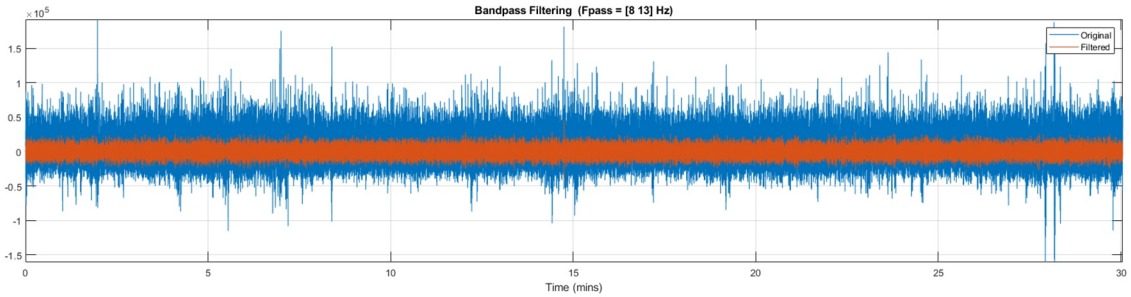

Figure 2.16: EEG for time domain analysis

2.4 Artefacts

In an EEG recording artefacts are any components which are not generated by the brain. In order to reduce artefacts in EEG recordings for clinical purposes acousticallly and electrically shielded cabins are used. Moreover, all interconnected devices use the same mains phase and ground and mains noise filters are used.
There are two different types of artefacts: the exogenous and the endogenous [103].

Exogenous artefacts are mains noise, spurious electrical noise caused by external phenomena like: transmission-line, phone, electrode and physical movements. Each signal generated by the artefacts previously listed has different electrical characteristics able to classify and remove it from the EEG. For the exogenous artefacts of this type typically no action is requested beyond the exclusion of the respective data. However, some artefacts have signal properties which allow the correction by time-domain or spatial filtering. In some case the use of a notch filter is a good solution. A useful and typical method to remove the exogenous artefacts with a spatial filtering is the Independent Components Analysis (ICA). It decomposes the artefacts present in EEG typically into one or two components to be removed from the signal.

Endogenous artefacts relate to the subject's body, such as: eye movements, breath, heart rate, muscle movements and sweat components in the scalp. The heart rate is visible when the electrode is in a blood vessel, and its can influence the EEG-fMRI recording [104]. The acid components of sweat can generate a reaction in contact with the electrode metals producing a battery potential visible in the EEG like slow oscillation: from 0.1 to 0.5 Hz. Breath can cause slow variations in scalp impedance resulting in equally slow shifts. Eye movements have peak values in the order of several hundred microvolts and can be detected by their unique topographies. They can be removed with a regression-based or with a ICA method. Endogenous artefacts relating to muscle movements can affect the EEG at higher frequencies. A low pass filter can be used to remove these artefacts, but sometimes the EEG and muscle activity acting on the same frequency make it difficult to eliminate them. Fig.2.17 gives an example of how artefacts can bias the pure

EEG:

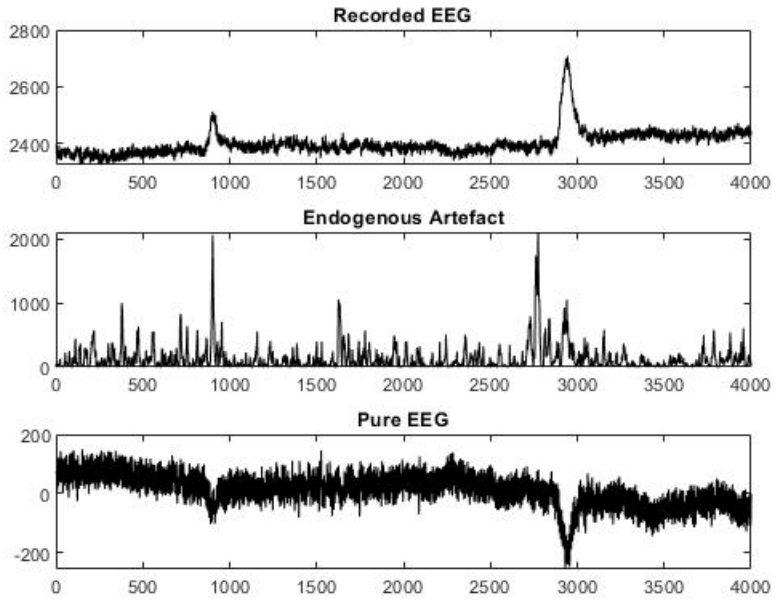

Figure 2.17: Endogenous artefact present in EEG

2.4.1 Artefact Removal Techniques

A range of techniques can be used to remove artefacts in EEGs when they cannot be removed algorithmically [103]:

- **Simple amplitude threshold**: in this case a cut-off value is defined and the positive and negative amplitude above or below this value are removed because they are identified as artifacts.
- **Min-max thresholds**: this technique is similar to the first one, but relates to the amplitude criterion, because in this case it sets a maximally allowed amplitude difference within a specific time length.
- **Gradient criterion**: this method sets a limit based on voltage changes from data point to data point relative to intersample time.
- **Low activity**:this criterion defines a limit of minimally allowed difference between the highest and lowest values in a specific time period.

- **Spectral distribution**: These methods define artefact time periods based on their spectral composition.
- **Standard deviation**: based on the dynamics of artifacts, as expressed by a moving standard deviation index.

2.4.1.1 Blind Source Separation

Blind Source Separation (BSS) includes various unsupervised learning algorithms without prior information and extra reference channels. The focus of this method consists of recovering original sources by sensor observation only.

$$X = AS + N \tag{2.6}$$

where **X** is the matrix of the mixed signal and the rows are the sensor signal, **A** is the unknown nonsingular mixing matrix, **G** is the matrix of independent sources and N is an additive noise matrix. The goal of this method is to find a linear transformation of the sensor signal which makes the outputs to be independent, Let Y the estimation of the sources:

$$Y = BX = BAS + BS \tag{2.7}$$

It is assumed that the number of the sensors is equal to the number of the sources, by definition $A \in \mathbb{R}^{QxQ}$ so the ideal separation $B = A^{-1}$. As previously highlighted the goal of BSS is to define a matrix B which gives a matrix BA diagonal and scaled. Consequently, the estimated source Y can be permuted and normalized because the original sources cannot be permutated and scaled.
This method was developed for an EEG preprocessing technique for the improvement of detection of Alzheimer's disease (AD). The proposed technique [105] is based on filtering of EEG data using BSS and projection of components useful to detect the first stages of the AD. BSS is used not only to separate the artefacts from EEG, but it can be used for all types of signal. The strong point of BSS is a well-known separation method able to extract the desired signal without knowing any information on the source signal[106].

2.4.1.2 Regression method

The statistical regression method can be used to remove artefacts such as eye blink, and horizontal and vertical eye movements. Two regression-based ocular correction algorithm have been proposed [107], [108]. In both algorithms the focus is to find the clink affected data in the electrooculogram (EOG) channel. The correction of the EEG based on the regression weights may however remove important information of the EEG activity along with the true eye movement-borne artefact. For this reason the use of the Independent Components Analysis (ICA) instead of a regression-based approach is suggested [103].

2.4.1.3 Independent Components Analysis

ICA is a statistical method which like Principal Component analysis (PCA), is able to detect the hidden factors which twist a signal or measurement [109]. The hidden factors are supposed to be statistically independent from each other and non – Gaussian. A statistical latent variable model is adopted which consists of *n* linear mixtures $x_1, x_2, ..., x_n$ of n independent components:

$$x_j = c_{j1}s_1 + c - j2s_2 + ... + c_{jn}s_n \quad \forall j \tag{2.8}$$

In this model is assumed that the linear mixtures and the independent components are both random variables, instead of time signals. The current model has been assumed to be zero-mean, if this it's not true the observed variable x_j can be zero centered subtracting the sample mean. Using the vector notation, it is possible to re-write the previous equation as follow:

$$x = Cs \tag{2.9}$$

where C is the matrix with elements c_{ij}, and the random vector **s** contains the elements $s_1, s_2, ..s_n$. The independent components are latent variables, which means that they cannot be observed. The only observed variable is **x**, the other components must be estimated. It is assumed that the components contained in s are statistically independent and that their distribution is unknown. Statistical independence means the joint probability density function of the output factorizes as follows:

$$p(u) = \prod_{i=1}^{N} p_i(u_i) \tag{2.10}$$

Assuming that C is square and it is possible to compute its inverse W as:

$$s = Wx \tag{2.11}$$

The focus of ICA is to separate the signal containing information from the noise signal embedded in the signal. **W** can be estimated by several algorithms, based on a cost function and running an optimization process. Algorithms for the solution of the separation blind source problem are based on: information maximization, maximum likelihood, FastICA and JADE. This work implements ICA for EEG data:

- The sum of different source signals at the sensor is linear
- The propagation delay in the mixing medium can be neglected
- The data sources are statistically independent

2.4.1.4 Wavelet transform for artifact removal

The Wavelet transform previously described is also used to remove artefacts. Limit value is chosen and the remaining details are readded to recompose the clean signal. Despite the DWT is a valid method, it is not able to recognize artefacts when they overlap with the spectral properties, therefore it has recently been used in combination with different methods like ICA. A new method for removing artifacts in EEG records during Galvanic Vestibular Stimulation (GVS) has been proposed, which removes the GVS artifacts from the EEGs using simulated data [110].

2.4.1.5 Principal Components Analysis

PCA is a statistical algorithm used for dimensionally reduction in many applications. PCA is a linear projection which transforms the original data set into a new data set in which the variables are linearly independent and are ordered according to the variance, that is by the mutual information of each component in the new data set. The dual of the problem shows PCA as the linear projection which minimizes the error.
PCA has been used to reduce the artifacts from transcranical magnetic stimulation-EEG data evaluated in a larger number of healthy subjects [111]. Another application of PCA is physiological noise components removal without any physiological monitoring during the scan in FMRI [112].

2.4.1.6 EEG artefact removal by ICA

As described in the previous sections the ICA method is often used for artefact removal in EEGs. In these cases the rows of matrix x in (2.9) are each recording electrode and the columns are the EEG values during recording. The focus of ICA is to find an ”unmixing” matrix W which decomposes the channels of the registration into a sum of temporally independent and spatially fixed components (2.11). The rows of matrix s are the time courses of the independent components of the input data. Each independent component of the EEG consists of activation of the ICA components and of their map. The component map shows the physiological origin of the components. Fig.2.18 shows an ICA decomposition example for an EEG.

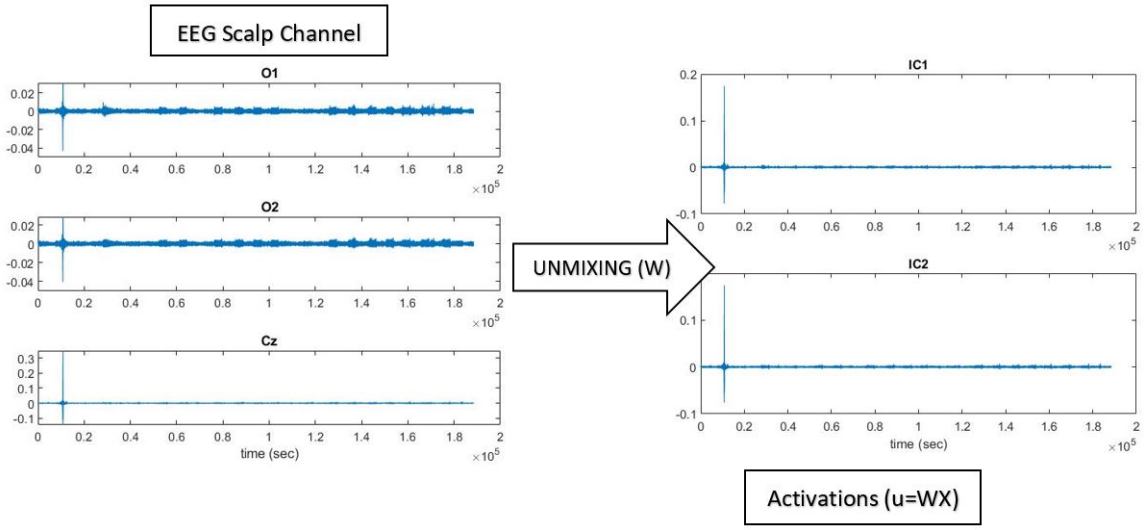

Figure 2.18: ICA decomposition

As shown in the figure, the EEG scalp channel is the original signal recorded during the experiment. Each channel is referred to the original right -mastoid signal, in the right side the activation components calculated with ICA methods are shown. Figure 2.18 shows the interpretation of the formulas in the previous section. The signal obtained by projecting the sum of selected non-artifactual ICA components replaces the original signal after artefact removal.

2.5 Performance Indexes

2.5.1 Mutual Information

Mutual information is an Information Theory metric, which quantifies the dependence between two random variables taking into account the linear and non linear information obtained about one variable observing the other one. It is often used as nonlinear counterpart of the correlation index [113]. When applied to two EEGs, MI gives a measure of the dynamical coupling between them. In comparison with other connectivity measures, mutual information is a measure of statistical dependence between signals that does not make assumptions on the nature of the system generating the signals and gives stable estimates with reasonably long data sets. MI is not limited to real values and determines whether the marginal distribution of the two variables is wider than the joint distribution of the pair.

Considering two random variables $X = x_i$ and $Y = y_i$ with probability distribution respectively $P_X(x_i)$ and $P_Y(y_i)$ and joint probability $P_X(x_i, y_i)$, the MI quantifies the reduction in uncertainty

of X by measurements made on Y and is given as:

$$MI(X,Y) = H(X) - H(X|Y) = H(X) + H(Y) - H(X,Y) \tag{2.12}$$

Where $H(X)$ is the information from measures X, and the uncertainty in X given by y_i is $H(X|Y = y_i)$. Both are defined as:

$$H(X) = -\sum_{x_i} P_X(x_i) log P_X(x_i) \tag{2.13}$$

$$H(X|Y) = \sum_{y_i} P_Y(y_i) H(X|Y = y_i) = -\sum_{x_i,y_i} P_{XY}(x_i, y_i) \log \frac{P_{XY}(x_i, y_i)}{P_Y(y_i)} = H(X,Y) - H(Y) \tag{2.14}$$

2.5.2 Correlation coefficient

The correlation index or dependence quantifies the direction and strength of the linear association between two variables. The goal of the correlation is to indicate whether there is a predictive relationship that can be exploited. Two random variables are dependent if they are not probabilistically independent. The correlation is the measure of the extent to which two or more variables are related to one another. The most commonly used index of the linear relationship between the variables is the Pearson correlation coefficient. If the relationship is not linear the Spearman's rank correlation is the best correlation index, because it is more sensitive to nonlinear relationship and it is more robust than the Pearson coefficient.

2.5.2.1 Pearson correlation coefficient

The Pearson correlation index is defined as:

$$r(y,x) = \frac{cov(y,x)}{\sigma_y \sigma_x} \tag{2.15}$$

where the $cov(y,x)$ is the covariance and σ_y and σ_x are the standard deviations.

Its value is limited to the range -1 and +1 and it only reflects the linear correlation between the variables, without considering other types of correlation. Its value can be classified as: strong correlation if $0.5 < r(y,\bar{y}) \leq 1$, moderate correlation if $0.3 < r(y,\bar{y}) \leq 0.5$ and weak correlation if $r(y,\bar{y}) \leq 0.3$[114].

2.5.2.2 Spearman's rank correlation coefficient

The Spearman's rank correlation coefficient is a non-parametric measure of the rank correlation between two variables. It measures the statistical dependence between the rankings of two variables, and estimates the correlation using a monotonic function. The difference between Pearson and Spearman coefficient is that the first one measures the linear relationship between two variables only, whereas the second one assesses whether the relationship is linear or not. This coefficient has a range between -1 and +1, and the observations of the two variables have similar ranks. When the two variables have a dissimilar rank its value tends to 0. The Spearman's rank correlation index is defined as:

$$\rho_s = r(rg_y, rg_{\bar{y}}) = \frac{cov(rg_y, rg_{\bar{y}})}{\sigma_{rg_y}\sigma_{rg_{\bar{y}}}} \tag{2.16}$$

where $r(rg_y, rg_{\bar{y}})$ is the Pearson correlation indexes calculated using the rank variables, $cov(rg_y, rg_{\bar{y}})$ is the covariance of the rank variables and σ_{rg_y} and $\sigma_{rg_{\bar{y}}}$ are respectively the standard deviation of the two rank variables.

2.5.3 Entropy of a signal

The Entropy of a random discrete variable **H** - called Shannon Entropy - is the average of the information time values of the variable in time. It was introduced in 1948 by Claudie Shannon. The entropy **H** of an information source is given by:

$$H = -\sum_i p_i \log_2(p_i) \tag{2.17}$$

where p_i is the probability of the probability of the event i [115] [116].

2.5.4 Cross Entropy loss function

The Cross Entropy loss function or log function represents the performance of a C - class classification model whose output is the probability to optimize the model during training. Modern neural architectures for classification tasks are trained using the cross-entropy loss, which is widely believed to be empirically superior to the square loss [117]. The cross-entropy loss increases as the predicted probability diverges from the actual label. The objective is often the minimization of the loss function. The lower the loss, the better the model. During model training, the model weights are iteratively adjusted accordingly, aiming to minimize the Cross-Entropy loss. The log loss function penalizes the cases in which the predicted value is near to 1 and the predicted probability decreases, as shown in Fig. 2.19:

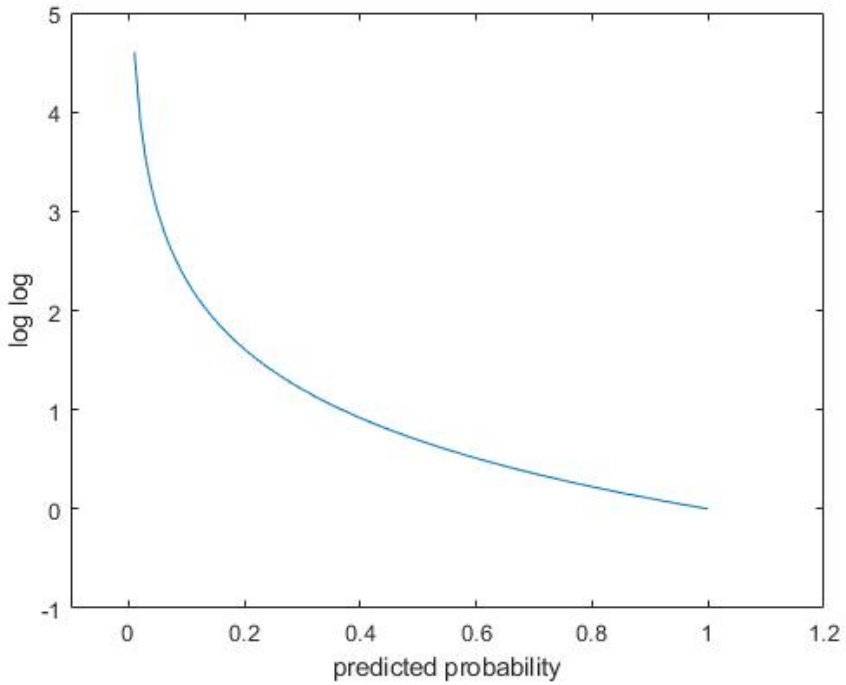

Figure 2.19: Log loss when the true label is 1

The formula of the entropy loss function H is reported below:

$$H = -\sum_{c=1}^{C} y_{o,c} log(p_{o,c}) \tag{2.18}$$

Where C is the number of classes, y is the binary indicator if the class label c is a the correct classification of observation o and p is the predicted probability of observation o being of class c

2.5.5 Mean Square Error

The Mean Square Error (MSE) of a predictor is the average of the errors between the estimated values and the observed values. It is defined in $[0, +\inf)$, and when its value is near 0 it relates to a good model fitting [118]. The MSE of a prediction is given by:

$$MSE = \sum_{t=1}^{n} \frac{(y(t) - \tilde{y}(t))^2}{n} \tag{2.19}$$

Where $y(t)$ and $\tilde{y}(t)$ are respectively the observed value and the predicted value at time instant t.

The MSE is the second moment of the error, and it is composed by the variance and the bias of an estimator $\hat{\theta}$ for a parameter θ. The Bias of an estimator is the difference between the parameter and its mean. In case of unbiased estimator, it is the variance of the estimator:

$$MSE(\hat{\theta}) = \sigma_{\hat{\theta}}^2 + Bias(\hat{\theta}, \theta)^2 \tag{2.20}$$

It can be used as performance index, in fact two or more statistical models may be compared using their MSE as measure of how well they explain a given set of observations[119].

2.5.6 Learning methods

Machine Learning methods may be categorized as supervised, unsupervised and reinforced learning.

In Supervised learning a teacher indicates whether a system is performing correctly, or validates the acceptability of a system's responses, or indicate the amount of error in system performance. A learning task aims to produce the desired output for each input. Labeled data sets are used to train algorithms to help outcome prediction or data classification. The training set is a portion of the original dataset, and the division of the dataset in training and testing is an important operation. In the major application the percentage of the division is 70% for the training and the remain 30% for the test.

In Unsupervised learning the output is trained to respond to clusters of pattern within the input. The system is supposed to discover statistically salient features of the input population. Unlike in supervised learning, there is no a priori set of categories into which the patterns are to be classified but rather the system must develop its own representation of the input stimuli.

Reinforced learning is an intermediate form between the previous two methods, in this case the learning machine does some action on the environment and gets a feedback response from the environment.

2.6 Black box model identification

A black box model describes the relationship between the inputs and the outputs without any knowledge about its internal processes. The main black box model identification methods which are used in BCI are described below.

2.6.1 Linear Discriminant Analysis

LDA is a data classification technique which easily handles the case where the within-class frequencies are unequal and their performances have been examined or randomly generated. The focus of LDA techniques is to project the original dataset into a lower dimensional space. Three steps are necessary: calculation of between - class variance, calculation of within - class variance and construction of the lower dimensional space which maximizes the ratio of between-class variance to within-class variance in a data set, thereby guaranteeing maximal separability [120].

2.6.1.1 Calculating Class Variance

The between-class variance of the *i*-th class S_{B_i} represents the distance between the mean of the *i*-th class indicated by μ_i and the general mean μ.

In the dataset $X = \{x_1, x_2, .., x_N\}$ x_i represent the *i*-th class and *N* is the total number of samples and $x_i \in \mathbb{R}^M$ where *M* is the number of features. The dataset *X* can be partionaed in *K* classes. Before calculating the between - class variance S_B, it is necessary calculate the separation distance between classes:

$$(m_i - m)^2 = (W^T \mu_i - W^T \mu)^2 = W^T (\mu_i - \mu)(\mu_i - \mu)^T W \tag{2.21}$$

Where m_i is the projection of the means of the *i*-th class, m is the projection of the total means, W is the transformation matrix explained in the following section and $(\mu_i - \mu)(\mu_i - \mu)^T$ represent the separation distance between the class mean and the total mean. The mean of the *i*-th class μ_i is :

$$\mu_j = \frac{1}{n_j} \sum_{x_i \in \omega_i} x_i \tag{2.22}$$

and the total mean of all the classes μ is:

$$\mu = \frac{1}{N} \sum_{i=1}^{N} x_i = \sum_{i=1}^{K} \frac{n_i}{N} \mu_i \tag{2.23}$$

Eq. 2.21 can be re-written as:

$$(m_i - m)^2 = W^T S_{B_i} W \tag{2.24}$$

The within-class variance of the *i*-th class S_{W_i} is the difference between the mean and the samples of the class. The focus of the LDA is to minimize the difference between the projected mean m_i

and the projected samples of each class $W^T x_i$.:

$$\begin{aligned}\sum_{x_i \in \omega_j, j=1,...,K} (W^T x_i - m_j)^2 &= \sum_{x_i \in \omega_j, j=1,...,K} (W^T x_{ij} - W^T \mu_j)^2 \\ &= \sum_{x_i \in \omega_j, j=1,...,K} W^T (x_{ij} - \mu_j)(x_{ij} - \mu_j)^T W \\ &= \sum_{x_i \in \omega_j, j=1,...,K} W^T S_{W_j} W \\ &= \sum_{x_i \in \omega_j, j=1,...,K} W^T c_j^T * c_j W\end{aligned} \tag{2.25}$$

where $x_{i,j}$ is the *i*-th sample in the *j*-th class and c_j is the centering data of the class *j*-th class:

$$c_j = \omega_j - \mu_j = \{x_i\}_{i=1}^{n_j} - \mu_j \tag{2.26}$$

2.6.1.2 Constructing the Lower Dimensional Space

The last step of the LDA techniques relates to the calculation of the lower dimensional space. The Fisher's criterion [121] is used to calculate the transformation matrix W :

$$\arg\max_W \frac{W^T S_B W}{W^T S_W W} \tag{2.27}$$

$$S_W W = \lambda S_B W \tag{2.28}$$

Where λ is the eigenvalues of the transformation Matrix W. The solution of this problem can be obtained calculating the eigenvalues $\lambda = \{\lambda_1, \lambda_2, .., \lambda_M\}$ and eigenvectors $V = \{v_1, v_2, ..., v_M\}$ of $W = S_W^{-1} S_B$ if S_W is non-singular. Each eigenvector represent one axis of the LDA space, and the eigenvalue represents the robustness of this eigenvector. The robustness of the eigenvector reflects its ability to discriminate between different classes. The eigenvectors with the k highest eigenvalues are used to construct a lower dimensional space V_k, while the eigenvectors $\{v_{k+1}, v_{k+2}, ..., v_M\}$ are ignored. The new projection of the dataset X in the new dimensional space is:

$$Y = XV_k \tag{2.29}$$

The computational complexity of LDA methods is $O(NM^2)$ if $N > M$, otherwise $O(M^3)$

2.6.2 Support Vector Machine

SVM is a supervisioned learning models with associated learning algorithms which analyze data for classification. SVM is based on a structural risk minimization principle rooted in the statistical learning theory [122]. SVM method is able to manage very large features spaces, because

training is realized in such a way that the size of the classified vectors doesn't affect the performance of the method. The SVM-based classifier has good generalization properties compared to conventional classifiers, because during the training the misclassification error is minimized.

Let the data input $X = \{x_i\} \forall i = 1, 2, ..., M$ where M is the number of samples. The samples have two classes: positive and negative. If the class is positive then the label $y_i = 1$, when it is negative its label is $y_i = -1$. For linearity data it is possible to determine the hyperplane $f(x) = 0$ which separates the data

$$f(x) = w^T x + b = \sum_{j=1}^{M} w_j x_j + b = 0 \tag{2.30}$$

where w is a M-dimensional vector and $b \in \mathbb{R}$. These two parameters are used to define the positions of separating hyperplane. The decision function is made using sign $f(x)$ to create separating hyperplane that classify input data. The separating hyperplane must satisfy the following constraints:

$$y_i f(x_i) = y_i(w^T x_i + b) \geqslant 1 \quad \forall i = 1, 2, .., M \tag{2.31}$$

The optimal separating hyperplane is the hyperplane which maximize the distance between the plane and the nearest data. An optimal hyperplane of two data sets is shown in Fig. 2.20

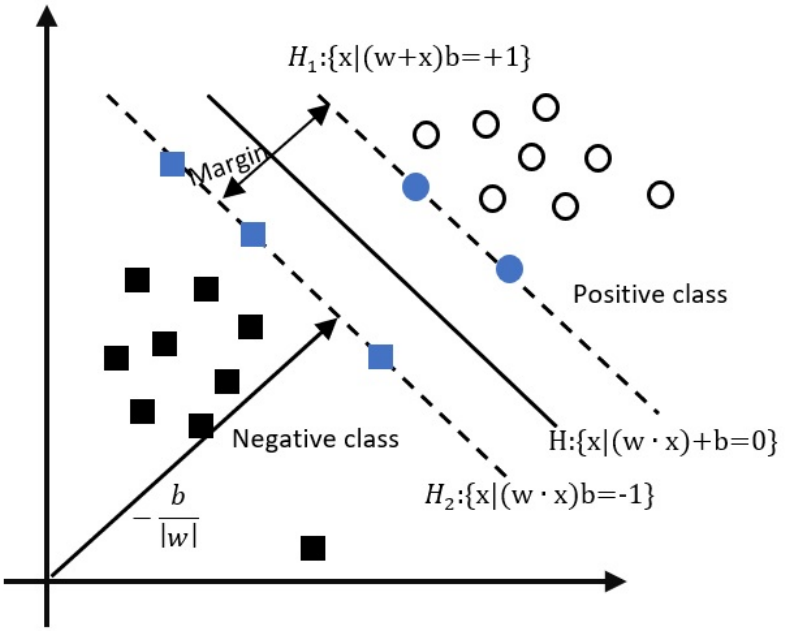

Figure 2.20: Classification of two classes using SVM

Taking into account the noise with the latent variable ϵ_i and the error penalty C, the optimal

hyperplane separating the data as solution of the following problem is:

$$\min \frac{1}{2}||w||^2 + C \sum_{i=1}^{M} \epsilon_i \tag{2.32}$$

where the constraints of the formula above are:

$$\begin{cases} y_i(w^T x_i + b) \geqslant 1 - \epsilon_i \quad \forall i = 1, 2, .., M \\ \epsilon_i \geqslant 0 \quad \forall i = 1, 2, .., M \end{cases} \tag{2.33}$$

It is possible to simplify the calculation of the optimization problem converting the problem with Kuhn-Tucker condition into the equivalent Lagrangian dual problem:

$$\min L(w, b, \alpha) = \frac{1}{2}||w||^2 + C \sum_{i=1}^{M} \alpha_i y_i (w x_i + b) + \sum_{i=1}^{M} \alpha_i \tag{2.34}$$

Minimizing the above formula with respect to w and b the saddle-point equations are:

$$\frac{\partial L}{\partial w} = 0 \quad , \quad \frac{\partial L}{\partial b} = 0 \tag{2.35}$$

which replace into form

$$w = \sum_{i=1}^{M} \alpha_i y_i x_i \quad , \quad \sum_{i=1}^{M} \alpha_i y_i = 0 \tag{2.36}$$

Eq.2.36 demonstrates which w is contained in the subspace of x_i, the dual quadratic optimization problem formulation of Eq.2.34 is:

$$\max L(\alpha) = \sum_{i=1}^{M} \alpha_i - \frac{1}{2} \sum_{i,j=0}^{M} \alpha_i \alpha_j y_i y_j x_i x_j \tag{2.37}$$

subject to the following constraint:

$$\alpha_i \geqslant 0 \quad \forall i = 1, 2, .., M, \quad \sum_{i=1}^{M} \alpha_i y_i = 0 \tag{2.38}$$

The solution of the dual optimization problem α_i allows to solve the original optimization problem. The non-linear decision function obtained is:

$$f(x) = sign(\sum_{i,j=1}^{M} \alpha_i y_i (x_i x_j) + b) \tag{2.39}$$

The use of Kernel functions allows to use the SVM method as non -linear classification. This application is possible when the data are mapped into a high-dimensional feature space, where the linear classification is possible. Using the non-linear vector function $\Phi = \{\phi_1(x), \phi_2(x), .., \phi_l(x)\}$ to map the *n*-dimensional input vector x onto l dimensional feature space, the dual problem is:

$$f(x) = sign(\sum_{i,j=1}^{M} \alpha_i y_i (\Phi^T(x_i) \cdot \Phi(x_j)) + b) \tag{2.40}$$

The high-dimensionality can cause computational problems and overfitting . The latter problem can be solved using the kernel function, which returns a dot product of the feature space mappings of the original data points, $K(x_i, x_j) = (\Phi^T(x_i) \cdot \Phi^T(x_j))$. Using the kernel function Eq.2.40 can be re-written as:

$$f(x) = sign(\sum_{i,j=1}^{M} \alpha_i y_i K(x_i, x_j) + b) \tag{2.41}$$

There are different kernel functions used in SVM: linear, Gaussian and polynomial. The choice of the Kernel function is a very important step because it defines the features space in which the training set examples will be classified[122].

2.6.3 Artificial Neural Network

ANN refers to computing systems whose central theme is borrowed from the analogy of biological neural networks [123]. ANNs are modeled closely following the brain, therefore a great deal of terminology is the same which is used in neuroscience. ANNs are basically massive parallel computational models which imitate the human brain function.

An ANN conists of a large number of simple processors linked by weighted connections which can acquire knowledge from the environment through a learning process and store the knowledge in its connections. The processing nodes are called **neurons**, the output of each node depends only on the information available by the close nodes. Each node receives the input from more nodes and transmits the relative output to another node. A single processing element generates a scalar output with a single numerical value, which is a simple non-linear function of its inputs. In Tab.2.1 the comparison between the biology and ANN terminology:

Table 2.1: Terminology of Neuron

Biological Terminology	**ANN Terminology**
Neuron	Node
Synapse	Connection
Synaptic Efficiency	Connection Weight
Firing Frequency	Node Output

The use of the ANNs is not recommended when the data are noisy, but it is recommended when there is a great amount of data and the problem is poorly understood to derive an approximate model. The ANN does not solve the problem in a strictly mathematical sense, but it demonstrates information processing features that give an approximate solution to a given problem. ANNs have typically been used in complex non linear function mapping, image processing, pattern recognition and classification problems. In this work the Feed-forward approach has been adopted - a common type of neural networks with supervised learning. The learning of ANNs relates to the method of modifying the weights of the connections among the nodes of a specified network. Learning is the process by which the random-values parameters of a neural network are adapted through a continuous process of simulation by the environment in which network is embedded. This type of ANN comprises: input layers where the inputs of the problem are received, hidden layers where the relationships between inputs and outputs are represented and determined by the synaptic weights and output layers where the outputs of the problem are defined[123].

2.6.3.1 Mathematical formulation

A functional model of neurons must take into account three basic components. The synapses of the neuron are modeled as weights whose values represent the strength of the connection. Positive weight values mean excitatory connections, negative values reflect connections. The next two components model the actual activity within the neuron cell. A summing function sums all the inputs modified by their weights. An activation function controls the amplitude of the output of the neuron. A suitable output range is a binary value $(-1, 1)$ or $(0, 1)$. The mathematical model of the ANN is shown in Fig.2.21:

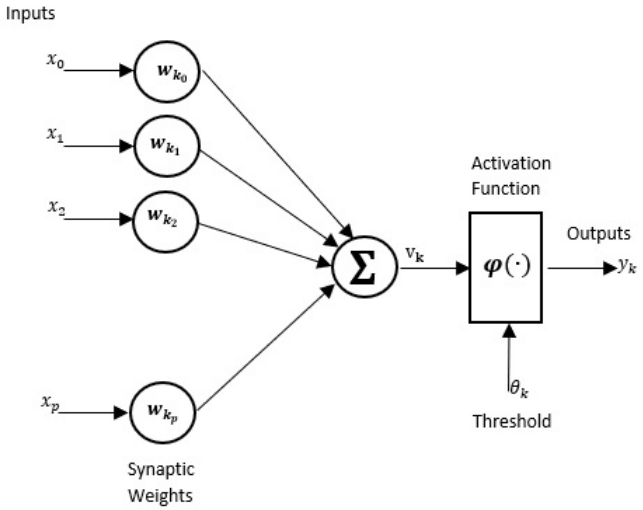

Figure 2.21: Mathematial Model of an ANN

Following the model of the Fig.2.21, the mathematical formulation is:

$$y_k = \varphi(v_k) = \sum_{j=1}^{p} w_{kj} x_j \tag{2.42}$$

where y_k is the output, w_{kj} is the weight between the neuron k of the previous layer and neuron j of the current layer and φ is the activation function a non-linear and differentiable function. Commonly the activation function is the logistic function [123]:

$$\varphi(z) = \frac{1}{1 + e^{-z}} \tag{2.43}$$

2.6.3.2 Back Propagation Network

Feed-forward ANNs use the back propagation algorithm. The neurons are organized in layers and send their information forward, whereas its errors are propagated backwards. The input and the output are located respectively in the input and output layers, between this two layers could be one or more hidden layers are present.

Back propagation algorithms use supervised learning - a learning method where the predicted model is trained with input and output which the network computes, and then the error is calculated. The algorithm is based on the Gradient Descent (GD) method which requires that, at any time, the performance of the dynamical system be assessable through a certain error function E

which measures the discrepancy between the trajectories of the dynamical system and the desired behavior. The methods consists of iteratively adjusting the dynamical parameters in the direction opposite to the gradient of E. Neurons in one layer are connected to all neurons in the next layer. No other connections exist in neural networks of this type. At the initial step the neuron weights are chosen randomly, and they are adjusted step by step until the error is minimal. The parameters regarding the number of the hidden layers and the number of neurons inside the layers must be fixed a priori and they depend on the application problem. The index performance for this algorithms is:

$$V = \frac{1}{2}\sum_{q=1}^{Q}(\underline{t}_q - \underline{a}_q^M)^T(\underline{t}_q - \underline{a}_q^M) = \frac{1}{2}\sum_{q=1}^{Q}\underline{e}_q^T\underline{e}_q \tag{2.44}$$

where $\underline{a}_q^M$ is the output of the network when the q-th input, $\underline{p}_q$ is presented, the $\underline{t}_q$ instead is the corresponding target value [124].

2.6.3.3 Levenberg-Marquardt Method

The Levenberg-Maquardt (LM) algorithm is a back propagation algorithm which is primarily used to solve least-squares curve fitting problems. The LM is an approximation to Newton's method [125].

If $V(\underline{x})$ is the function which to be minimized with respect to the parameter $\underline{x}$ according to the Newton's method [126]:

$$\Delta\underline{x} = -[\nabla^2 V(\underline{x})]^{-1}\nabla V(\underline{x}) \tag{2.45}$$

where $\nabla^2 V(\underline{x})$ is the Hessian matrix and $\Delta V(\underline{x})$ is the gradient. If $V(\underline{x})$ is assumed:

$$V(\underline{x}) = \sum_{i=1}^{N} e_i^2(\underline{x}) \tag{2.46}$$

then

$$\nabla V(\underline{x}) = J^T(\underline{x})\underline{e}(\underline{x}) \tag{2.47}$$

$$\nabla^2 V(\underline{x}) = J^T(\underline{x})J(\underline{x}) + S(\underline{x}) \tag{2.48}$$

where $J(\underline{x})$ is the Jacobian matrix

$$J(\underline{x}) = \begin{bmatrix} \frac{\partial e_1(\underline{x})}{\partial x_1} & \frac{\partial e_1(\underline{x})}{\partial x_2} & \cdots & \frac{\partial e_1(\underline{x})}{\partial x_n} \\ \frac{\partial e_2(\underline{x})}{\partial x_1} & \frac{\partial e_2(\underline{x})}{\partial x_2} & \cdots & \frac{\partial e_2(\underline{x})}{\partial x_n} \\ \vdots & \vdots & \ddots & \vdots \\ \frac{\partial e_N(\underline{x})}{\partial x_1} & \frac{\partial e_N(\underline{x})}{\partial x_2} & \cdots & \frac{\partial e_N(\underline{x})}{\partial x_n} \end{bmatrix} \tag{2.49}$$

and

$$S(\underline{x}) = \sum_{i=1}^{N} e_i(\underline{x}) \nabla^2 e_i(\underline{x}) \tag{2.50}$$

For Gaussian-Newton method it is assumed that $S(\underline{x}) \approx 0$, using this assumption the 2.45 is

$$\Delta \underline{x} = [J^T(\underline{x}) J(\underline{x})]^{-1} J^T(\underline{x}) \underline{e}(\underline{x}) \tag{2.51}$$

The Marquardt-Levenberg modification to the Gauss-Newton method is:

$$\Delta \underline{x} = [J^T(\underline{x}) J(\underline{x}) + \mu I]^{-1} J^T(\underline{x}) \underline{e}(\underline{x}) \tag{2.52}$$

The parameter μ is respectively multiplied or divided by a parameter β depending on whether the function $V(\underline{x})$ increases or decreases. If μ is large the algorithm is steppest descendent, whereas when it is small the algorithm becomes Gauss-Netwon. The Marquardt-Levenberg algorithm can be regarded as a trust region modification to Gauss-Newton [127].

In the LM algorithm the fundamental step relates to the computation of the Jacobian matrix. In ANN mapping problems the components of the Jacobian matrix can be calculated as simple variations of the back-propagation algorithm. Standard back-propagation calculates terms like

$$\frac{\partial \hat{V}}{\partial \omega^k(i,j)} = \frac{\partial \sum_{m=1}^{SM} e_q^2(m)}{\partial \omega^k(i,j)} \tag{2.53}$$

For the elements of the Jacobian matrix necessary for the LM it is necessary to calculate the components:

$$\frac{\partial e_q(m)}{\partial \omega^k(i,j)} \tag{2.54}$$

Using the back-propagation algorithm with a modification on the final layer, it is possible to calculate the term in Eq.2.54 as

$$\Delta^M = \dot{F}^M(\underline{n}^M) \tag{2.55}$$

Chapter 3

Fear detection in driving sessions

During driving, driver behavior monitoring may provide useful information to prevent road traffic accidents caused by driver distraction. It has been shown that 90% of road traffic accidents are due to human error and in 75% of these cases, the human error is the only cause. The main causes are driver distraction and drowsiness.

The HF plays a fundamental role in modern transport systems. Drivers and transport operators control a vehicle towards its destination based on their own sense, physical condition, experience and ability, and the safety of such systems strongly relies on the HF that has to take the right decisions. On the other hand, we are experiencing a gradual shift towards increasingly autonomous vehicles where the HF still constitutes an important component, but may in fact become the "weakest link of the chain", requiring strong and effective training feedback.

In recent years we have experienced how safety management in advanced technological vehicles (planes, ships, trains, road vehicles) may fail due to an at-risk human behavior (HB). Even worse, the consequences in these cases are quite often considerable (cf. cruise ship Costa Concordia disaster; Santiago de Compostela derailment). Conversely, the HF may also be the "strongest link of the chain". An experienced, trained operator with outstanding behavioral and emotional characteristics to manage properly a dangerous event may resolve problems which have not be foreseen in system design.

Recent research advances in technology for safe transport have mostly focused on passive safety technology (PST) and active safety technology (AST). In automotive systems, PST relates to components of the vehicle (primarily airbags, seat belts and the physical structure of the vehicle) that protect occupants during a crash. AST mainly refers to technology assisting in the prevention of a crash (e.g. Antilock Braking System - ABS). Some more recent technology, falling in the broader classification of Advanced Driver Assistance Systems (ADAS), are now shifting their attention towards physiological alterations (e.g. breath alcohol ignition interlock device, lane departure warning system). Related concepts are present in other transport modes. In par-

allel to these technological solutions, professional drivers and transport operators are subject to specific and continuous training and associated verification of requirements and skills, such as the ADR license for the Dangerous Goods Transport (DGT) by road. In this respect, HB observation during a transport process is another important component closely related to safety. A relatively new and successful approach in the field of industrial safety is the application of behavioral science to safety, as in Behavior -Based Safety (BBS), which is the "application of science of behavior change to real world problems" (Cambridge Center for Behavior Studies, http://www.behavior.org/). The results presented here are a part of a more general work devoted to the foundation of a System Behavior Based Safety Technology (SBBST). The SBBST represents a step forward in AST, PST and ADAS. BBS "focuses on what people do, analyses why they do it, and then applies a research-supported intervention strategy to improve what people do" [128] .To be successful, the BBS program used must be based on scientific knowledge. While BBS is still a viable strategy for occupational training, some weak points are emerging. The need to stop reacting to injuries and start predicting them using the available technology has been assessed [128]. In this respect, in BBS it is common to have a huge amount of data generally collected by human data observers, and most of these observations are deemed as safe.

Some work is related to systems for real-time detection of fear by using the ratio of the slow to fast wave powers of the EEG while the user was watching scary images [129] [130] [131] During a transport process where the driver is alone, or interacting with few people, technology must take the place of human observers, and cyber-physical systems may help in this task. HB can be described according to a knowledge base, so that it is possible to activate a proper reaction to the HB, in the form of on-line feedback or as a proactive intervention, such as "behavior al and defensive driving" and general safety management [132].

Two main recent approaches are dedicated to detect driver's conditions. The first one focuses on physical movements of the driver's body as the inclination of the driver's head [133] or eye states identification [134]. The latter approach is related to measuring biometrical and psychophysical parameters of the driver such as for example monitoring heart beat rate [135] or EEG activities [136]. A wearable biometric t-shirt used to collect data about heart rate variability (HRV) of the driver during some test drives has been described, demonstrating the correlation between HRV data with the related georeferenced information about critical points on the road network during driving routes[137]. A systems based on EEG has been realized to classify drivers' behavior as response to pictures related to road accident or hazard events [138]. An ANN has been used to categorize the alert and drowsy states in a driver using EEGs [139].

3.1 System design

An EEG-based Driver Control System (EEG-DCS) has been designed to monitor the psychophysical driver state evaluating driver's ability to respond to unexpected or emergent events during

driving. The proposed EEG-DCS aims at detecting health warning signs to identify driver's near miss accidents to situations at risk of accident and his/her reaction to an unexpected acoustic or visual event. The system is based on the interaction and cooperation of two main subsystems. The first system consists of an electrode cap system (EEG cap) for EEG acquisition in order to monitor drivers' cognitive states and emotional processes. The second one is the OKTAL simulator - which provides the users with virtual driving environment and realistic traffic situations.

More specifically, the electrical activity of the driver's brain has been evaluated using the electrophysiological monitoring method. An EEG cap by Enobio with eight electrodes has been used to acquire and collect data about driver's brain activities. The EEG is a non-invasive exam useful to understand and monitor driver performances in real time during the driving sessions. The EEG cap embeds 8 electrodes which are in contact with the driver scalp to acquire biometrical data in real time with milliseconds precision.

The main aspect relates to the use of the EEG Enobio cap to identify driver's response and behavior when he/she is exposed to an unexpected high acoustical signal and to an unexpected visual disturbance during a test drive session.

Fig.3.1 shows the system configuration which consists of a Wearable System with sensors for measuring EEG and heart rate, and of a device for data pre-processing and transmission by Bluetooth, a smartphone, and a server PC. The output from the wearable system is transmitted via Bluetooth to a smartphone that extracts the results of a real time signal analysis and the position (by a GPS). Thereafter, the smartphone transmits the signals to a PC for processing. The overall on-board model is composed of several devices that are embedded in the on board components: wearable sensors system; sensors and CAN bus; central on board unit and additional information from other sources such as road plans, traffic, weather and cartography.

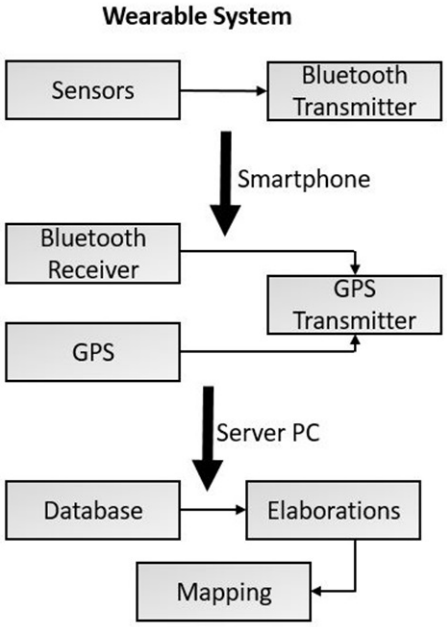

Figure 3.1: Schematic diagram of the proposed detection system

Fig.3.2 shows the proposed logical architecture. At the initial stage the work has focused on wearable sensors, in relation to driver monitoring and CAN bus, for vehicle monitoring.

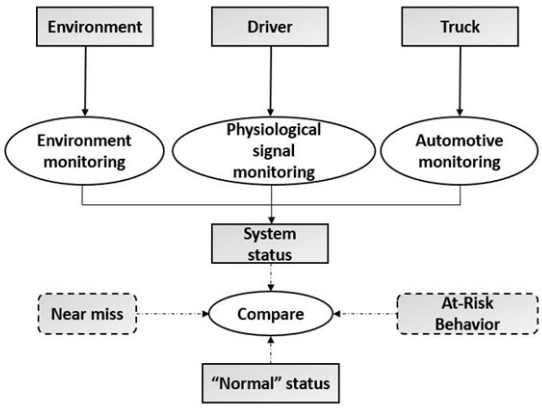

Figure 3.2: The architecture proposed to identify At-risk Behavior

These systems collect crucial parameters about the wellness and the behavior of the driver. The main onboard unit detects abnormal value trends in these parameters and sends GPRS messages to the central system, for storage in a database. All systems are composed by one or more monitoring units. Information may come from the environment, from physiological signals, and

from automotive data defining the status of the system in every time instant in which the system develops. The aim is to identify a "normal status" of the system and then compare this status with the status at every instant.

3.2 Data processing

The NIC software, produced by Enobio for EEG registration, allows visualizing the data by the EEG cap both in time and in frequency for a preliminary analysis. The embedded signal-processing module allows exporting the EEG in the .edf format data, which is an easy and simple format for exchange and storage of multichannel biological and physical signals. A correlation analysis among data coming from the 8 channel of the EEG cap has been carried out. In this preliminary phase the study mainly focuses on the analysis of the values related to the alpha brain activity for each channel. Alpha waves are detected in EEG during a normal wakeful state where the subject is quietly resting [140] and they are mostly associated with mind/body coordination, quietness and attentiveness. The concept that alpha waves play an active role to identify anomalous driver behavior in difficult drive condition is consolidated [141] [142] [143]. An EEG power spectrum analysis in the alpha frequency band has been performed on the data acquired in six drive tests.

3.2.1 Virtual test drive simulations

The virtual test drive simulations consist of two driving sessions, each of which has three drive tests. Each drive test, 30 minutes long, is performed by a twenty-eight years old man with driving license. The driver conducted a car in a simulated highway route at a speed of 80 km/h in the slowest lane while, in the adjacent lanes, other vehicles generated and managed automatically from the simulator are circulating. Simulations have been performed during daylight hours and with stable weather condition. Fig. 3.3 shows the simulation environments in which the subject, who is wearing the EEG cap, drives while sitting in a comfortable chair. In the three tests of the first drive session, between 10 and 15 minutes from the beginning of the test a high intensity sound has been randomly produced for some seconds behind the driver's head, meanwhile the driver was driving. In the three tests of the second driving session, between 10 and 20 minutes from the beginning of the test, the outside driving conditions on the screen of the OKTAL simulator have suddenly got worse for 20 seconds. Specifically, the weather conditions have been modified introducing rapid darkness and strong rain falling. The main purpose has been to identify the brain areas affected by the unpredicted sonic or visual stimuli and the related consequent variation in the EEG. After the external event, the driver is monitored for 10 minutes to detect his/her behavior and the possible changes in his/her EEG. The EEGs, obtained before the external event, have been used as the reference to define driver's standard conditions. The EEGs from

the latter period have been used to test the detection of driver's behavior variations.

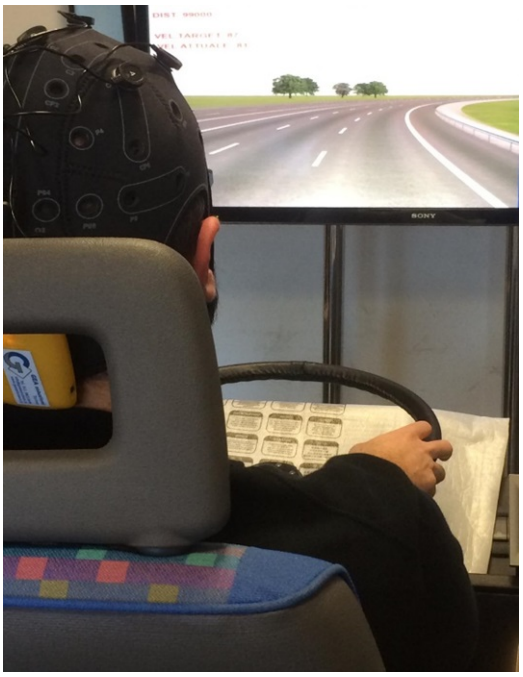

Figure 3.3: Driver's test simulation environment.

3.3 Results

The main objective of the tests that have been carried out consists of evaluating driver's reactions when an unexpected external event perturbs a driving session performed in neutral condition. In this section the results relating the two experiments that have been carried out are shown.

3.3.1 Acoustic external unexpected event

The data coming from the three tests of the first drive session show that the EEG alpha activity reflects, in similar way, the effects related to the acoustic external unexpected event. The data obtained in the tests have given very similar results. The correlation coefficients among the alpha waves in the EEGs coming from the eight different channels for the second drive test are shown in Tab 3.1.

Table 3.1: Correlation coefficients among the 8 EEG channels in acoustic test

	C1	C2	C3	C4	C5	C6	C7	C8
C1	1.00	0.63	0.77	0.85	0.87	0.28	0.27	0.28
C2	0.63	1.00	0.87	0.81	0.61	0.75	0.75	0.77
C3	0.77	0.87	1.00	0.93	0.83	0.74	0.70	0.76
C4	0.85	0.81	0.93	1.00	0.86	0.58	0.60	0.62
C5	0.87	0.61	0.83	0.86	1.00	0.42	0.42	0.44
C6	0.28	0.75	0.74	0.58	0.42	1.00	0.95	0.98
C7	0.27	0.75	0.70	0.60	0.42	0.95	1.00	0.97
C8	0.28	0.77	0.76	0.62	0.44	0.98	0.97	1.00

The alpha waves data have been filtered by a band pass filter, with frequency range 8-13 Hz. The original and filtered signal related to alpha waves for the second test drive after about 15 minutes from the beginning of the drive test, when an external acoustic event has been produced, are shown in Fig.3.4. It is possible to observe that a spike is detected in correspondence with the application of the unexpected stimulus. The spike is highlighted in a black rectangle.

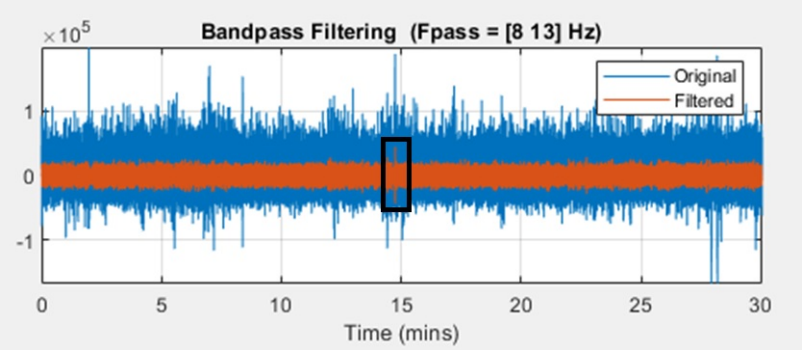

Figure 3.4: Original and filtered signal related to alpha waves acquired during an acoustic event.

The same alpha wave signals plotted in a shorter time window and the related spectrogram in frequency domain are shown in Fig.3.5. The variation in the spectrum of the EEG and the alpha peak frequency demonstrates that the driver behavior is event-related, specially in fear trials.

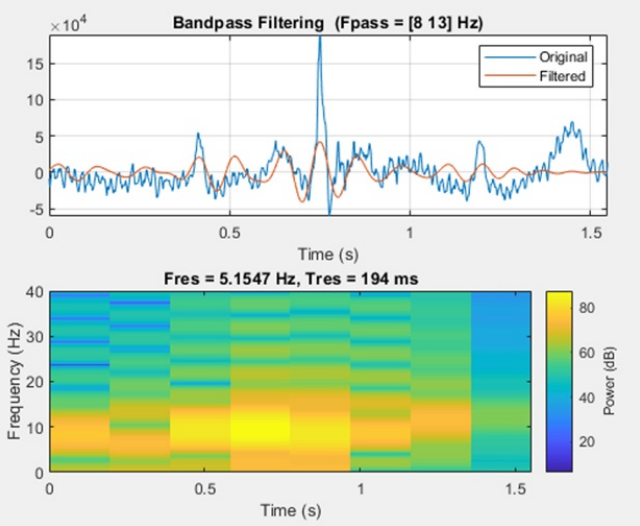

Figure 3.5: Spectrogram of alpha band in EEG for the acoustic event.

The same results are shown in Fig. 3.6, where the EEG recording of the third test drive is shown. The power of the signal increases in the same instants in which the driver is subjected to the external unexpected sound (a whistle).

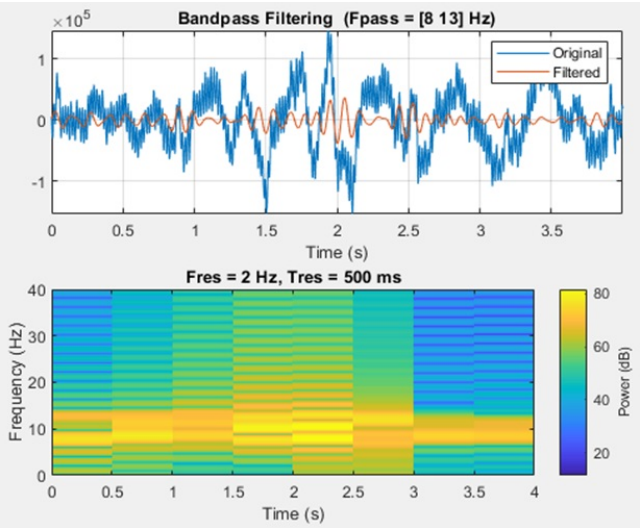

Figure 3.6: Spectrogram of the third test drive

3.3.2 Visual external unexpected event

The second session of the driving test concerns the application of a visual disturbance to the driver, who is subjected to an unpredictable critical external driving condition. As in the previous case for the oscillatory analysis, EEG data have been band-pass filtered into the EEG bands for alpha waves. The band-pass filter for the alpha wave signal of the 8th channel is shown with related spectrogram in Fig.3.7. It shows that frequency and time features are complementary.

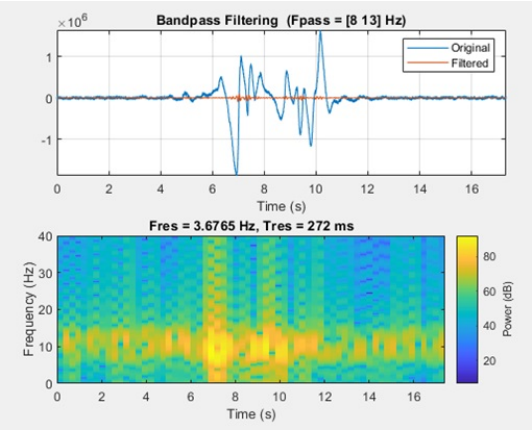

Figure 3.7: Spectrogram of the test drive with visual external event

The maximum spectral power in this time interval is 97155.58 microvolts, while the average power spectral is 3.24 microvolts. The maximum value is calculated when the visual external unexpected event happens. This deviation from the mean value shows the driver's stimulus response. The correlation between the signals coming from 8 channels of the EEG cap detected in a time interval of 20 seconds during the external event application is shown in Tab. 3.2, which demonstrates the positive linear correlation among the data.

Table 3.2: Correlation coefficients among the 8 EEG channels in visual test

	C1	C2	C3	C4	C5	C6	C7	C8
C1	1.00	0.98	1.00	1.00	0.79	1.00	1.00	1.00
C2	0.98	1.00	0.98	0.98	0.89	0.97	0.97	0.97
C3	1.00	0.98	1.00	1.00	0.81	1.00	1.00	1.00
C4	1.00	0.98	1.00	1.00	0.79	1.00	1.00	1.00
C5	0.79	0.89	0.81	0.79	1.00	0.77	0.77	0.78
C6	1.00	0.97	1.00	1.00	0.77	1.00	1.00	1.00
C7	1.00	0.97	1.00	1.00	0.77	1.00	1.00	1.00
C8	1.00	0.97	1.00	1.00	0.78	1.00	1.00	1.00

The analysis of a driver's behavior when he/she is subjected to different types of unexpected stimuli has been carried out using EEGs. Data collection has been performed in a simulator based environment. A significant correlation has been found in time and frequency domain among data related to brain activities associated to alpha waves in both experimental test sessions.
Further developments of this work will focus on defining how brain areas are involved in test drive evaluating driver performance on curved roadways using a driving simulator. Besides, new developments will be focused on setting up an ANN based on EEG data analysis to predict driver's behavior and to prevent possible accidents.

Chapter 4

EEG real time analysis for driver's arm movements identification

In AVs at level 5 the driver is completely absent in the decision framework. To reach this condition, the vehicle must drive in an autonomous way. A propaedeutic analysis of the driver behaviour must be carried out to define the traditional driving style and to identify the relationship between the automated and non-automated driving system, in order to implement the control commands at the operational level. It has been demonstrated that the physical and neurological driver's state affects driving performances [144]. The physiological state of the driver may be detected by different modalities based on the electrooculogram (EOG), on the functional magnetic resonance imaging (fMRI), on the high-frequency electrocardiogram (ECG) or the EEG. Driver's fatigue and distraction represent the major causes of accidents and crashes. The EOG, which detects the electrical signal generated by eye movements, has been acquired and processed to identify driver's drowsiness. The EOG has been found to be a promising drowsiness detector, with detection higher than 80% [145]. FMRI identifies changes in cerebral oxygenation during cognitive tasks and is used to demonstrate the correlation between brain activation and simulated driving actions [146]. In a similar way, functional near infrared spectroscopy (fNIRS) has been applied to quantify cortical activity variations related to changes in workload during driver tasks. The Oxyhaemoglobin significantly increased in the left and right lateral aspects of the prefrontal cortex during both high and low cognitive workload scenarios. Cerebral blood volume significantly increased in the prefrontal cortex in both scenarios, but to a slightly greater degree in the right hemisphere [147]. Heart rate variability has been monitored to extract significant features related to driver drowsiness where the overall accuracy for two-classes such as: normal–drowsy, normal–visual inattention, normal–fatigue and normal–cognitive inattention is 100%, 93.1%, 96.6% and 96.6% respectively[148]. Several methods have been adopted to detect low to moderate and low to high arousal fluctuations in driver workload. Detecting changes from moderate to high arousal may be their major drawback[149] . The possibility of continuously monitoring

the driver's status by the detection of the activation/deactivation states of the autonomic nervous system based on HRV has been confirmed. The proposed method can help prevent accidents caused by sleepiness while driving [150]. EEG monitoring relates to the acquisition of brain signals from different lobes of the brain in order to identify cerebral wave variations when the subjects perform cognitive task. The EEG represents one of the most promising and reliable physiological indicators to describe human state [151]. EEG recording is often used to evaluate driver attention [152], fatigue [85], mental state [153] or, in general, cognitive response in driving environments [154]. EEG acquisition has recently been used to identify human intention for movements. The main objective of this research field, in the context of AV, is to extract the main features from the EEGs while the driver performs a specific movement and to classify brain activities as belonging to the subject's intention to move the related part of his/her body. EEG devices and classification algorithms are the hart of BCI systems. BCI makes it possible for the user to command an external device through brain electrical signals according to his/her intention. Specifically, the EEG acquires the cerebral signals, the classifier interprets human movement intentions by brain activities and finally the BCI translates them into a command for devices. BCI may represent a novel sensor and transducer tool to identify the main parameters of human movements, such as speed, direction and force [155]. Special attention has been given to the classification of hands [156], fingers [157], and eye movements [158]. The detection of movement intention using EEGs has also been considered [159]. Although the BCI may be a significant improvement in the realisation of tools which assist the driver to prevent accidents, limited literature is available in the context of arm movements identification. A classifier based on the SVM to classify three classes of driver movements, left, right and brake has been developed [160]. By the proposed approach the driver's actions have been predicted 500ms ahead with 94,6% accuracy. SVM and CNN have been applied to EEGs acquired during a breaking action to detect pedal pushing and to discriminate between driver's intent to brake in emergency condition and in normal driving state. In these experiments, the average accuracy has reached about 71% [161]. EEGs and waveband specular meteor radar (SMR) have been used to monitor drivers' physiological state and eye-movement electrical waves to identify the relationship between driver fatigue states and driver's grip force on the steering wheel while driving [162]. Recently BCIs have been used in closed loop, to establish a communication with external devices and send them command inputs. Moreover, imagined movement decoding methods have been successfully used to classify horizontal and vertical movements of the right arm using EEGs [163][164]. QDA has been implemented to set up a classifier which has been used to regulate the motion of brushless DC motors for neuro-aid systems. Two classes have been identified from EEG features to move the motor in clockwise and anticlockwise directions[165]. Similar applications based on EEGs for motor imagery classification have been carried out as relates to hand prostheses [166], wheelchair [167] or quadcopter [168]. A wide review on robot controller by motor imagery BCI has been carried out [169].

4.1 Materials and Methods

This work aims at identifying and classifying driver's arm movements according to data from the EEG. Non-invasive EEGs has been used.

4.2 EEG Cap

Experiments have been carried out using the Enobio Cap 8 Features. The Signals have been recorded at 500Hz from six different channels, namely F7, FZ, F8, C4, C3, CZ, in accordance with the 10-20 system which is normally used. The selected channels are shown in Fig. 4.1. The electrodes are located on the medial premotor area and on primary motor cortex.

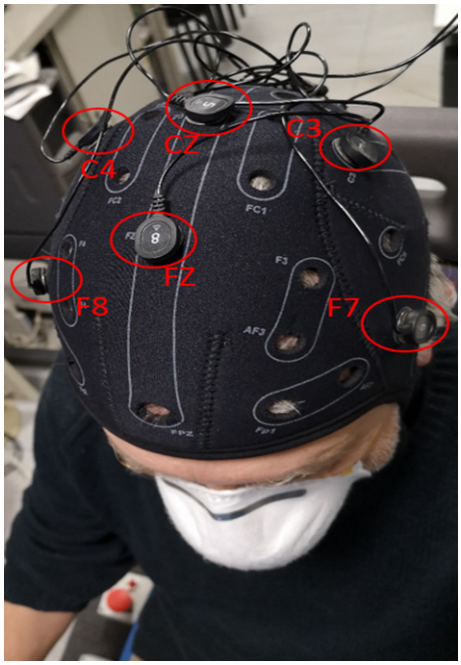

Figure 4.1: Electrodes placement in the ENOBIO cap. (Red circles show the electrodes monitored during the experiments).

4.3 Driving simulation

The driving simulator consists of two components. First a common chair is positioned in front of an LCD screen which projects the driving simulated environment. Second, the user is provided

with a steering wheel connected to the pedal system to perform movements for turning and breaking.

The set of subjects includes 3 participants (P1, P2, P3) with driving license who are, respectively, 25, 26 and 30 years old. Each participant performed three times a test. The driver could rotate the steering wheel, accelerate or brake as if he/she were driving a real car. Each simulation lasts 15 minutes, and the user has to drive along a tour shown in Fig. 4.2. Each driver runs almost eight times on such route. OKTAL Scaner Studio has been used to generate the simulation environment. The correlation between the arm movements of the driver while performing the right/left curves on the road and the related recorded EEGs has been analysed.

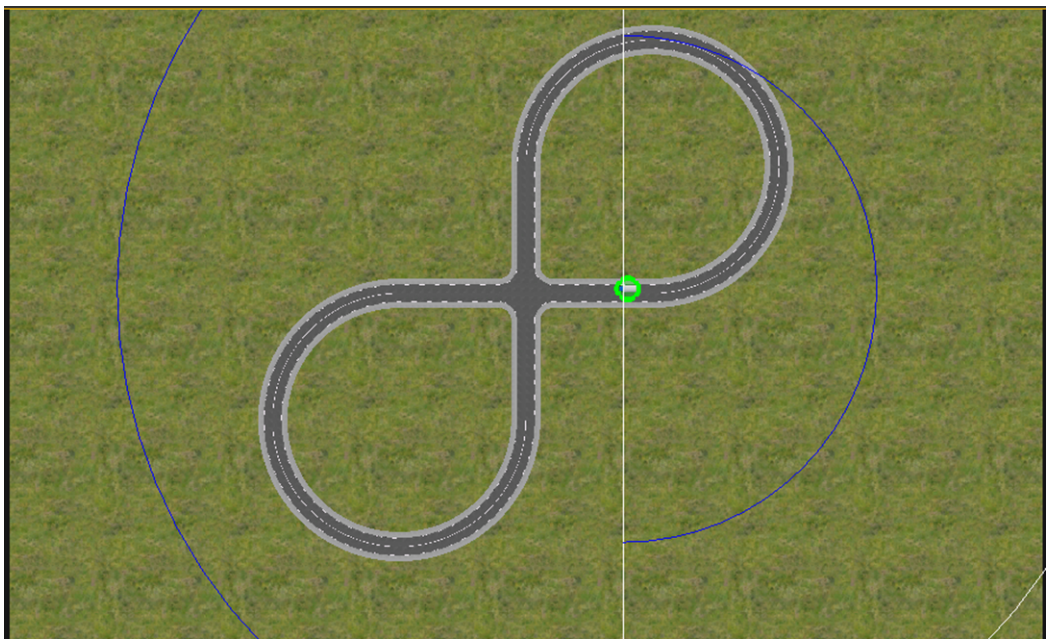

Figure 4.2: Test drive circuit in OKTAL Simulator environment.

4.4 Data Preprocessing

The data has been preprocessed by Matlab R2020b. A high pass filter to 0.167 Hz has been applied to the EEGs to remove the direct current shift. Three analyses have been carried out by a time delay neural network (TDNN) which has been used because of its capability to generate a finite dynamic response to time series input data. TDNN has often been successfully used in complex input-output identification but its great number of applications in EEG analysis is due to the non – stationary nature of brain activities [170]. TDNN has been applied to the classification

of finger movements with a recognition rate of 93.02% [171]. The TDNN that has been used in this work, whose structure is shown in Fig. 4.3, has 10 time delays and 4 hidden units.

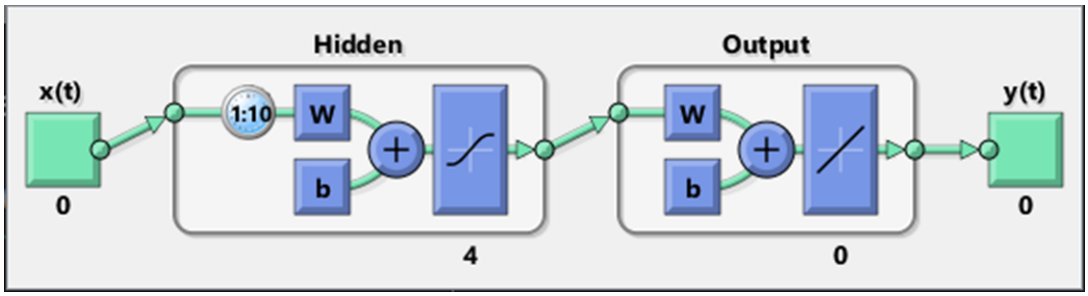

Figure 4.3: TDNN used in this experiment.

4.5 Experiments

Three measurement sessions are foreseen for each participant, in three different days. In the following, the data are identified by the participant ID, P1 or P2 or P3, and by the training sessions chronologically numbered as 1, 2 or 3. Three analyses have been carried out on the monitored EEGs.

4.5.1 First analysis: classifier generation

The first test relates to the classifier generation by the Levenberg-Marquardt algorithm based TDNN. The data acquired in each session for each participant has been divided in two in order to have an equal number of samples, labeled as 1A, 1B, 2A, 2B, 3A, 3B. The different sets of data have been used to train and test six TDNNs in order to identify the best classifier as relates to correlation. The different training and test datasets used in the applications are shown in Table 4.1.

Table 4.1: Dataset used to train and test the TDNNs in the first analysis

TDNN	Training set	Test set
NN1	1A	1B
NN2	2A	2B
NN3	3A	3B
NN4	2A, 2B, 3A	3B
NN5	1A, 1B, 2A	2B
NN6	1A, 1B, 2A, 2B, 3A	3B

The NNs listed in Table 4.1 have been set up for each participant creating 18 TDNNs (6 NNs for each of the three participants). The main objective of this analysis is to assess whether an increased number of input data in the training phase may bring about a better recognition performance.

4.5.2 Second analysis: classifier generation by a weighted cost function

In the second experiment, the TDNNs which have been obtained in the previous test have been modified. Specifically, NN4, NN5 and NN6, for each participant, have been revised modifying the cost function which minimizes the MSE. In this second approach a weight p_i has been introduced, for each sample which belongs to the training set, in the objective function as in 4.1.

$$MSE = \frac{1}{N * S} \sum_{k=1}^{S} \sum_{i=1}^{N} p_i^s (y_i^s - \hat{y}_i^s)^2 \tag{4.1}$$

where

MSE = mean square error;
S = number of dataset s-th used in the training;
N = number of elements in each dataset s-th used in the training set;
p_i^s = weight associated to each data i-th belonging to the s-th dataset;
y_i^s = observed value of the output in the s-th dataset;
$\hat{y}_i^s$ = predicted value for the output in the s-th dataset.

The new TDNNs, namely NN7, NN8 and NN9, have been trained and tested on the same data set which has already been adopted, respectively, in NN4, NN5 and NN6 for each participant. However, the objective functions for the training phase have been modified balancing the different input components, as shown in Table 4.2. The data from the older tests have lower weights with respect to the recent ones. The aim of its analysis is the identification of the set of parameters which, by multiplying the objective components, increase the recognition accuracy.

Table 4.2: TDNNs features

TDNN	Dataset s-th in the objective function	Weights $\mathbf{p}_i^s$	Test set
NN7	2A	0.5	3B
	2B	0.5	
	3A	1	
NN8	1A	0.5	2B
	1B	0.5	
	2A	1	
NN9	1A	0.25	3B
	1B	0.25	
	2A	0.5	
	2B	0.5	
	3A	1	

4.5.3 Third analysis: classifier generation evaluating the model initial weight

The non-linear features of the neural network function may make the results quite different according to the initialization of the weights that are present in its units. This test has been carried out to evaluate TDNN performance variations according to different initializations of the values of the calibrated or randomized weights related to the layers of the neural network.
Specifically, the performances have been evaluated considering the TDNN recognition accuracy taking into account the computational time required by the identification process. When TDNN weights are initialised by values obtained from previous training sessions the required computational time is often lower then the computational time when the TDNN weights are randomly initialised. More specifically, in the former case the values are calibrated according to the values obtained as output of the training phase for the TDNNs shown in Table 4.3, "Initialisation of the weights of TDNN layers" column. The columns "Training set" and "Test set" list, respectively, the datasets used to train and test the related NN in the row. In order to clarify the approach, an example is given. As relates to NN17, a standard TDNN has been created by a specific training on samples 1A, 1B, 2A related to the first and second sessions of experiments for the same participant. Then the generated NN17, where the weights are initialised according to this first training phase, has been trained again on the subset 1A, 1B, 2A, 2B and tested on the 3A subset. NN16 has been trained and tested with the same dataset of NN17 but without specific values of the weight parameters.

Table 4.3: Generation of the weights used in the TDNNs

TDNN	Initialisation of the weights of TDNN layers	Training set	Test set
NN10	weights generated by 1A, 1B, 2A, 2B	3A	3B
NN11	weights generated by 1A,1B	2A	2B
NN12	random weights	1A, 1B	2A
NN13	weights generated by 1A	1A, 1B	2A
NN14	random weights	1A, 1B, 2A	2B
NN15	weights generated by 1A and 1B	1A, 1B, 2A	2B
NN16	random weights	1A, 1B, 2A, 2B	3A
NN17	weights generated by 1A,1B, 2A	1A, 1B, 2A, 2B	3A
NN18	random weights	1A, 1B, 2A, 2B, 3A	3B
NN19	weights generated by 1A,1B, 2A, 2B	1A, 1B, 2A, 2B, 3A	3B

4.6 Evaluation of the results

The results have been evaluated against two main indicators, MSE and R, which is the correlation coefficient of the predicted versus the actual values.
A preliminary analysis of the values for R and the MSE for the TDNNs generated for the three participants is shown in Table 4.4. The results demonstrate that the R value, averaged over the three participants for the overall generated TDNNs, is close to 0.5. Moreover, the MSE values that have been found are much lower than the value which relates to the square of the range between -1 and 1, that is 4 - a value which indicates a poor prediction accuracy.
Table 4.5 shows the R index of each TDNN in the first analysis for the second participant (P2). The results show a significant good correlation between the EEGs and the actual arm movements of the participant. In three cases R is greater than 0.6.
From Table 4.1, it is possible to note that a growing number of datasets has been used to train the NNs, from NN1 to NN6. However, considering the results in Table 4.5, It can be noted that the increasing number of input data for the training phase does not reflect a significant improvement of the performances in terms of R and MSE.

Table 4.4: Mean values of the performance indices computed for each TDNN averaged over the three participants.

TDNN	**R**	**MSE**
NN1	0.6812	0.4310
NN2	0.7001	0.4709
NN3	0.5603	0.5797
NN4	0.5818	0.5077
NN5	0.5348	0.6099
NN6	0.3836	0.6597
NN7	0.5950	0.5102
NN8	0.5774	0.5726
NN9	0.5364	0.5570
NN10	0.5811	0.5529
NN11	0.6316	0.5285
NN12	0.1001	1.0378
NN13	0.3802	0.8660
NN14	0.3917	0.7167
NN15	0.5169	0.6356
NN16	0.2713	0.7666
NN17	0.2132	0.8039
NN18	0.4379	0.6480
NN19	0.4075	0.6453
Mean	**0.48**	**0.64**

Table 4.5: First analysis results for subject P2.

TDNN	**R**	**MSE**
P2_NN1	0.6628	0.3838
P2_NN2	0.6610	0.4506
P2_NN3	0.5492	0.6213
P2_NN4	0.6435	0.4174
P2_NN5	0.2773	0.7922
P2_NN6	0.2907	0.7383

In the second analysis, a higher correlation is found in the P2_NN7. Moreover, the modified objective function produces better values, both for R and MSE, in the P2_NN8 versus the P2_NN5 and in P2_NN9 versus P2_NN6. The couple of NN5 and NN8 and the couple NN6 and NN9 respectively are trained and tested by the same dataset for each participant, but with different

weight p_i^s (see Table 4.1 and Table 4.2).
In the third analysis, reported in Table 4.7 relating to participant P2, the recognition accuracy for TDNNs, initialized randomly or with accurate weight input values, appear very similar. The different approaches that have been followed to initialize the layer parameters are not significant in terms of prediction. However, from a computation viewpoint, the TDNNs with accurate custom initialization appear, in general, less time expensive with respect to the ones with random initialization.

Table 4.6: Second analysis results for P2.

TDNN	**R**	**MSE**
P2_NN7	0.6356	0.4363
P2_NN8	0.4851	0.6200
P2_NN9	0.4197	0.6080

Table 4.7: Second analysis results for P2.

TDNN	**R**	**MSE**	**Time (sec)**
P2_NN10	0.6234	0.5489	47.0743
P2_NN11	0.6234	0.5873	34.6633
P2_NN12	0.2824	0.7039	241.2782
P2_NN13	0.4214	0.6526	205.9559
P2_NN14	0.1913	0.8688	451.9295
P2_NN15	0.3794	0.7182	185.1008
P2_NN16	0.3053	0.6668	418.4075
P2_NN17	0.0687	0.8356	276.9772
P2_NN18	0.3793	0.6414	245.0443
P2_NN19	0.1547	0.7996	583.0464

Table 4.8: First analysis results for P1.

TDNN	**R**	**MSE**
P2_NN1	0.8159	0.3657
P2_NN2	0.8538	0.2828
P2_NN3	0.6079	0.5130
P2_NN4	0.6079	0.4528
P2_NN5	0.8507	0.2920
P2_NN6	0.6588	0.4622

The three analyses have been performed for the other two participants and the results relating to the first analysis in the first participant (P1) are reported in Table 4.8. For the first analysis, a higher correlation is obtained with respect to the results reported for participant P2. In this case, the value R is higher than 0.8 for NN1, NN2, and NN5.

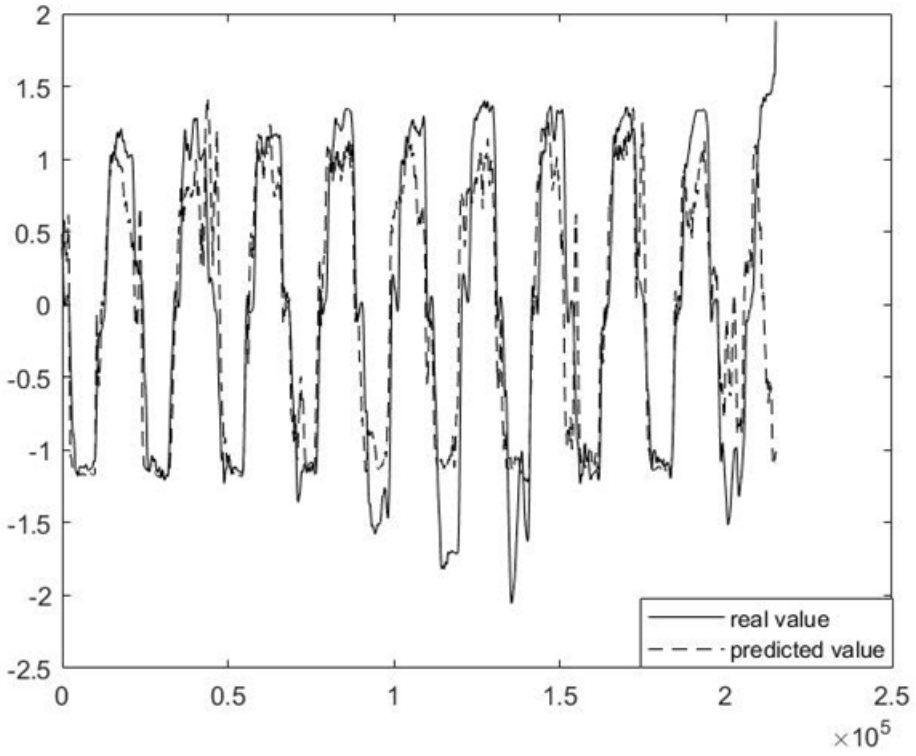

Figure 4.4: Predictive and real value in P1_NN2 .

Specifically, Fig. 4.4 shows the comparison between the values relating to the actual angles associated to the rotation of the steering wheel realized by the participant during the simulation and the predicted values generated by the NN2 relating to the direction of the arm movements. The graph shows a significant overlapping of the peaks (values -1 and 1) associated to the correct prediction of the right and left driver's arms movement. The results relating to the second analysis regarding participant P1 are shown in Table 4.9.

Table 4.9: Second analysis results for P1.

TDNN	R	MSE
P2_NN7	0.6408	0.4633
P2_NN8	0.8502	0.2892
P2_NN9	0.6442	0.4464

In this case also the R value is higher than 0.64, which shows a good correlation among predicted data and actual data. Conversely, the modified objective function does not introduce any significant variation in terms of prediction accuracy. The third analysis for P1 is reported in Table 4.10.

Table 4.10: Second analysis results for P2.

TDNN	R	MSE	Time (sec)
P2_NN10	0.6040	0.4949	100.052
P2_NN11	0.8517	0.2864	24.882
P2_NN12	0.4501	0.8698	114.260
P2_NN13	0.4696	0.7928	54.245
P2_NN14	0.8542	0.2854	196.969
P2_NN15	0.8495	0.2912	567.360
P2_NN16	0.5545	0.6188	442.865
P2_NN17	0.5983	0.5841	127.593
P2_NN18	0.6056	0.5841	209.203
P2_NN19	0.6392	0.4781	644.334

In this analysis, the R value is greater than 0.5 for 80% of tests, while the MSE is lower than 0,5 for the 50%.
In general, anyway, it can be concluded that the initialization of the weights for the neural network layers is not relevant in terms of accuracy of prediction with respect to the NNs which are randomly initialized.

This work aims at implementing a TDNN based classifier of EEGs for driver's arm movement recognition for two main purposes. First, the driver's style recognition is crucial for driving safety in order to prevent accidents and to react to critical situations. Second, the identification of the driver's behavior during specific driving tasks may support the understanding of the relationship between the driver and the automated driving systems (ADS), above all, in AVs at level 3 and 4.
The main aspect of the analysis that has been carried out relates to the development of a classifier for driver's arm movements recognition using EEGs when the user rotates the steering wheel in order to perform a turn in a driving simulated scenario. The EEG data acquired by a non-invasive

EEG cap, whose electrodes are in contact with the scalp, have been processed to classify those movements according to three classes: right or left turns and central position. Moreover, three different methods have been implemented to evaluate possible improvements of the accuracy of the driver's arm movements prediction.
The TDNNs generated for the recognition of movements have been modified by increasing the number of the datasets which have been used to train the NNs. In this second approach the different components of the objective function have been differently weighted in order to minimize the MSE. Finally, the initialization of the weights associated to the layers of the neural network has been considered in order to evaluate possible benefits with respect to the random initialization which is often used.
The results have shown a statistically significant positive correlation of the EEGs with the actual participant's actions to realize a turning in a car, which cover a curvilinear path in a simulated environment. On the contrary, the approaches that have been taken to increase the accuracy of movement's prediction do not seem particularly relevant in the experiments that have been carried out. Due to the complexity of the problem and to the relevance of the first preliminary analyses, further work would be worthwhile increasing the number of participants and evaluating new techniques for the classifier implementation.

Chapter 5

BCI model to detect head movement

In this section a case study is reported regarding the recognition of head movement by EEG. The experiment has been divided in two parts, the first one relating to EEG data storing for of each participant, and the second one relating to the application of BCI methods in a real context.

This work deals with a specific issue that has rarely been addressed. The main objective is the development of a BCI system that can predict the participants' head position. The EEGs have been recorded on 22 healthy participants between 16 and 62 years - 7 female 15 male - 4 of which left handed.

The output data of the experiments have been treated according to the consecutive application of a TDNN and a Neural Network Pattern Recognition (PCNN), in order to classify the left or right head position as responses to external visual stimuli. This has been propaedeutic to realize a closed loop BCI to translate the user's signals into commands to control the switching on/off of the lamps in real time. The main purpose is to find significant correlations between the head position and EEGs, in order to use human signals as inputs to the BCI to manage external devices.

The proposed EEG based BCI consists of two main components (Fig. 5.1). The first component is the lamp system which has a twofold role: it generates the external visual stimuli for the participants used to train and test the ANNs and it evaluates the pattern recognition performances . The EEG Enobio cap is the second subsystem for the EEG acquisition users. The two subsystems send their input to a common PC server by a serial port and a Bluetooth connector.

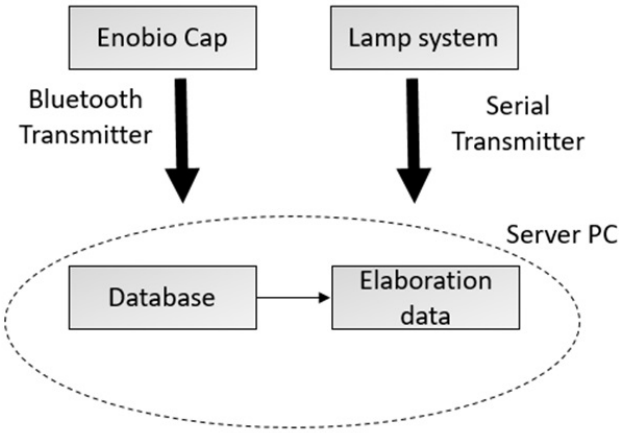

Figure 5.1: System design

5.1 EEG System

For the EEG acquisition an Enobio cap containing 8 electrodes positioned according to the International Standard System 10/20 has been used. Moreover, 2 additional signals from electrodes positioned in the neck have been considered in order to perform a differential filtering and to limit artifacts due to the electrical muscles' activity. In the experiments, three channels labeled O1, O2 in the occipital lobe, and CZ in the parietal lobe have been taken into account (Fig. 5.2). It has been found that the occipital lobe is associated to visual processing, while the parietal one is associated to recognition, perception of stimuli, movement and orientation. In addition, visual motor performance may be detected in the occipital and centroparietal areas [172]. These three electrodes only have been used because they are located in a brain part which is not affected by movements.

Figure 5.2: Electrodes position

5.2 Preliminary identification of Brain Electrical Activity related to head yaw rotation

Automatizing the identification of human brain stimuli during head movements could lead towards a significant step forward for HCI, with important applications for severely impaired people and for robotics. In this preliminary study a neural network-based identification technique is presented to recognize, by EEGs, the participant's head yaw rotations when he/she is subjected to a visual stimulus. The goal is to identify an input-output model between the brain electrical activity and the head movement triggered by switching on/off a light on the participant's left/right hand side. This identification process is based on TDNN with "Levenberg–Marquardt" back-propagation algorithm.
The results obtained on ten participants, spanning more than two hours of experiments, show the ability of the proposed approach to identify the brain electrical stimulus associated with head turning. The analysis has been carried out in order to evaluate the model for each participant.

5.2.1 Data Set

The trials involved 10 participants: one woman (P1) and nine men (P2–P10), aged 25 to 60, with no known history of neurological abnormalities. All participants, except P5, are right-handed. P2 and P4 are hairless. For two participants, namely P1 and P2, 10 different experiments have been recorded. For P10 2 experiments have been recorded while for the others, namely P3–P9, only one experiment has been recorded. All tests lasted 5 min. Table 5.1 shows the main file features.

Table 5.1: The data used to identify the function f

Part. ID	File ID	Duration Time (s)	Start Time	Head Position Occurrence (Left L, Forward F, Right R)
P1	F1	328	0	L 14.2%, F 59.5%, R 26.3%
P1	F2	310	51d	L 28.9%, F 60.7%, R 10.5%
P1	F3	319	51d	L 18.0%, F 59.9%, R 22.1%
P1	F4	336	54d	L 12.0%, F 60.3%, R 27.7%
P1	F5	335	54d	L 11.9%, F 60.3%, R 27.8%
P1	F6	328	54d	L 18.5%, F 60.9%, R 20.6%
P1	F7	306	100d	L 17.9%, F 61.5%, R 20.6%
P1	F8	307	100d	L 20.2%, F 59.6%, R 20.2%
P1	F9	328	100d	L 16.7%, F 59.9%, R 23.4%
P1	F10	305	100d	L 22.8%, F 61.1%, R 16.1%
P2	F1	341	0	L 21.6%, F 60.7%, R 17.7%
P2	F2	341	68d	L 19.1%, F 59.8%, R 21.2%
P2	F3	321	68d	L 12.7%, F 60.3%, R 27.1%
P2	F4	325	68d	L 22.9%, F 61.7%, R 15.4%
P2	F5	354	68d	L 17.5%, F 61.3%, R 21.2%
P2	F6	384	85d	L 11.0%, F 60.4%, R 28.6%
P2	F7	304	85d	L 17.0%, F 59.5%, R 23.5%
P2	F8	314	85d	L 30.5%, F 60.9%, R 8.7%
P2	F9	312	85d	L 23.3%, F 62.0%, R 14.7%
P2	F10	316	85d	L 17.0%, F 60.1%, R 22.9%
P3	F1	314	0	L 19.1%, F 59.6%, R 21.3%
P4	F1	300	0	L 25.9%, F 59.3%, R 14.8%
P5	F1	399	0	L 16.8%, F 60.0%, R 23.2%
P6	F1	308	0	L 11.0%, F 60.7%, R 28.4%
P7	F1	356	0	L 23.0%, F 61.7%, R 15.8%
P8	F1	304	0	L 25.5%, F 61.7%, R 12.8%
P9	F1	366	0	L 19.7%, F 60.4%, R 19.9%
P10	F1	377	0	L 24.8%, F 59.6%, R 15.6%
P10	F2	339	1h	L 22.1%, F 59.9%, R 18.0%

From left to right, the columns show: participant ID; file ID; number of samples in each file; time elapsed from participant's first trial; occurrences percentage related to the three coded head positions (1 R , 0 F, -1 L). For example, Fig. 5.3 shows P4F1 trend in the three EEG channels versus head movement signals.

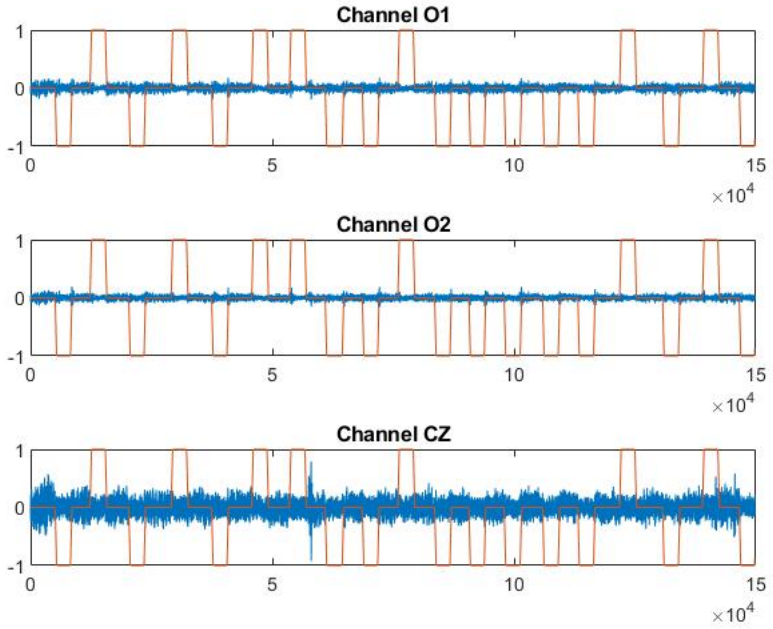

Figure 5.3: EEG of channels O1, O2 and CZ (blue) vs the visual stimulus (orange) y in file P4F1

5.2.2 Identification of the function f on the first half file and verification on the second half

Each file has been divided into two equal parts; the first has been named ”training set,” and the second ”test set.” The training sets always include samples related to the three possible positions (R, F, L). The results on the testing set can be further classified according to r value ranges reported in Table 5.2 [114]:

Table 5.2: Threshold values to evaluate correlation index.

R	Correlation
$0.50 \leq$ r	strong
$0.30 \leq$ r <0.50	moderate
r <0.30	weak

Table 5.3 shows the performance indexes of the testing set. Out of 29 files, only two (P1F8 and P1F10) show a moderate correlation; the others show a strong correlation.

Table 5.3: Prediction performances in the test set

Part. ID	File ID	MSE	r
P1	F1	0.12	0.86
P1	F2	0.20	0.80
P1	F3	0.32	0.78
P1	F4	0.14	0.84
P1	F5	0.26	0.78
P1	F6	0.21	0.71
P1	F7	0.30	0.61
P1	F8	0.37	0.48
P1	F9	0.42	0.79
P1	F10	0.38	0.38
P2	F1	0.31	0.71
P2	F2	0.19	0.86
P2	F3	0.12	0.88
P2	F4	0.16	0.86
P2	F5	0.16	0.82
P2	F6	0.29	0.82
P2	F7	0.30	0.78
P2	F8	0.28	0.57
P2	F9	0.27	0.76
P2	F10	0.35	0.87
P3	F1	0.31	0.82
P4	F1	0.02	0.98
P5	F1	0.13	0.91
P6	F1	0.37	0.59
P7	F1	0.35	0.66
P8	F1	0.33	0.76
P9	F1	0.33	0.78
P10	F1	0.18	0.89
P10	F2	0.32	0.93

Tables 5.4 and 5.5 report r and MSE values produced by extracting the functions from the 10 different tests on P1 (rows) and applying them to each test for the same subject (columns). Tables 5.6 and 5.7 report the same data produced from P2 tests. The colors of the cells are in accordance with the correlation values represented in Table 5.2

Table 5.4: r Values (P1)

r	F1	F2	F3	F4	F5	F6	F7	F8	F9	F10
F1	0.90	-0.18	-0.21	-0.73	-0.39	-0.74	0.40	-0.17	-0.35	-0.15
F2	-0.23	0.78	0.59	-0.79	-0.70	-0.78	-0.32	-0.21	-0.42	-0.47
F3	-0.33	0.52	0.71	-0.8	-0.65	-0.81	-0.19	-0.35	-0.10	-0.14
F4	0.01	-0.59	-0.56	0.84	0.73	0.82	0.04	0.57	0.15	0.19
F5	0.06	-0.53	-0.5	0.84	0.82	0.84	0.49	-0.09	-0.01	0.08
F6	0.17	-0.54	-0.47	0.84	0.76	0.85	0.37	-0.15	0.13	0.13
F7	0.70	-0.14	-0.14	0.70	0.60	0.70	0.67	0.27	-0.07	-0.02
F8	-0.11	-0.48	-0.40	0.80	0.68	0.81	0.35	0.55	0.31	0.08
F9	-0.69	-0.06	0.22	0.41	0.33	0.45	0.39	0.07	0.80	0.68
F10	-0.66	-0.32	0.00	0.78	0.52	0.77	0.20	0.31	0.83	0.79

Table 5.5: MSE Values (P1)

MSE	F1	F2	F3	F4	F5	F6	F7	F8	F9	F10
F1	0.09	0.51	0.41	0.52	0.49	0.47	0.35	0.41	0.40	0.40
F2	0.54	0.17	0.46	0.93	1.23	1.33	0.86	0.78	0.78	0.68
F3	0.48	0.41	0.31	1.10	1.72	1.73	0.50	0.41	0.40	0.38
F4	1.25	2.64	2.18	0.11	0.19	0.13	2.39	2.46	2.26	2.79
F5	0.79	1.88	1.41	0.14	0.13	0.13	1.95	1.84	1.50	1.93
F6	1.05	2.13	1.64	0.12	0.17	0.11	2.25	2.11	1.70	2.16
F7	0.28	0.43	0.40	0.58	0.47	0.45	0.25	0.38	0.40	0.38
F8	0.48	0.47	0.42	1.01	1.08	1.07	0.33	0.30	0.37	0.40
F9	0.85	0.45	0.37	0.34	0.35	0.35	0.34	0.41	0.32	0.35
F10	0.88	0.42	0.43	0.55	0.71	0.51	0.36	0.38	0.35	0.34

Table 5.6: r Values (P2)

r	F1	F2	F3	F4	F5	F6	F7	F8	F9	F10
F1	0.78	0.62	0.77	0.62	0.77	0.41	-0.01	0.01	0.02	0.0
F2	0.09	0.86	0.86	0.86	0.85	0.29	0.51	0.61	0.70	0.52
F3	0.01	0.77	0.87	0.77	0.84	0.21	0.31	0.11	0.26	0.33
F4	0.00	0.78	0.86	0.76	0.86	0.27	0.37	0.38	0.42	0.43
F5	-0.14	0.83	0.86	0.83	0.87	0.30	0.60	0.58	0.72	0.60
F6	0.15	0.42	0.60	0.42	0.83	0.75	0.70	0.69	0.77	0.80
F7	-0.00	-0.12	0.44	-0.12	0.39	0.42	0.80	0.72	0.84	0.86
F8	0.15	-0.22	-0.24	-0.22	-0.11	0.37	0.71	0.72	0.8	0.65
F9	0.16	-0.20	-0.15	-0.20	-0.21	0.53	0.62	0.66	0.81	0.72
F10	-0.11	-0.36	0.05	-0.36	0.04	0.41	0.78	0.71	0.83	0.87

Table 5.7: MSE Values (P2)

MSE	F1	F2	F3	F4	F5	F6	F7	F8	F9	F10
F1	0.29	0.26	0.29	0.43	0.31	0.31	0.63	1.13	0.93	0.68
F2	0.40	0.16	0.15	0.17	0.15	0.51	0.47	0.30	0.36	0.46
F3	0.43	0.20	0.13	0.18	0.16	0.40	0.44	0.34	0.35	0.45
F4	0.44	0.17	0.15	0.15	0.54	0.58	0.33	0.43	0.59	0.21
F5	0.42	0.20	0.15	0.16	0.15	0.48	0.51	0.31	0.40	0.51
F6	0.40	0.34	0.28	0.32	0.29	0.25	0.36	0.52	0.41	0.35
F7	0.38	0.42	0.38	0.33	0.36	0.36	0.29	0.33	0.28	0.31
F8	0.39	0.55	0.57	0.41	0.47	0.47	0.39	0.26	0.30	0.39
F9	0.37	0.55	0.50	0.39	0.44	0.37	0.35	0.27	0.26	0.34
F10	0.39	0.44	0.40	0.36	0.38	0.32	0.30	0.34	0.28	0.30

Out of example, Fig. 5.4 shows the trend of three different prediction cases against the actual head positions. The best case (i.e. on P4F1, r=0.98), the medium case (r=0.82 and MSE=0.31) and the worst one (i.e. on P1F10, r=0.38,) are shown:

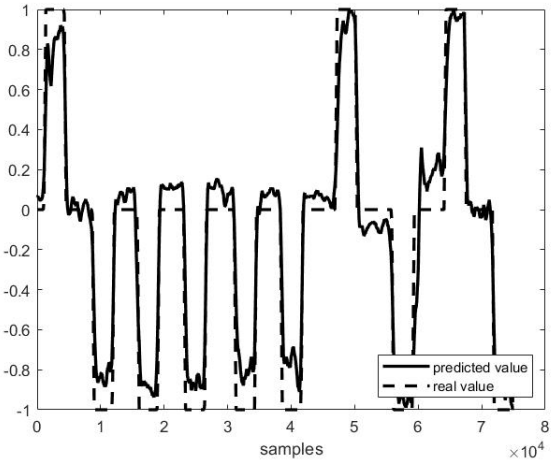

(a) Relates to r=0.98

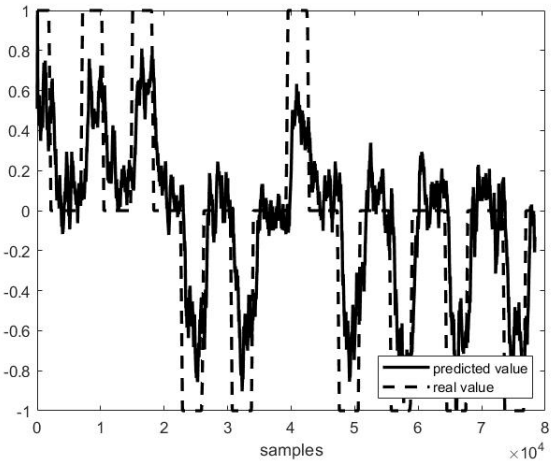

(b) Relates to r=0.82

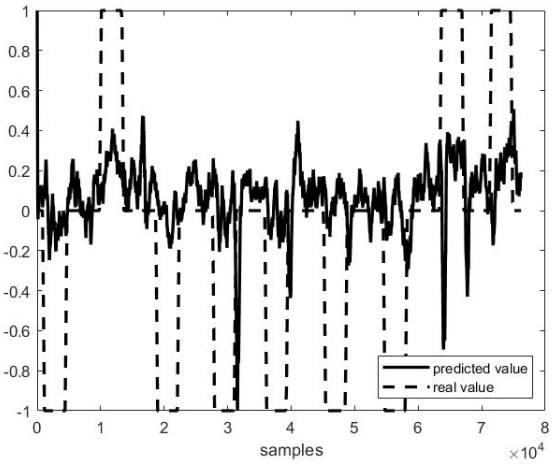

(c) Relates to r=0.38

Figure 5.4: Prediction (solid line) against real values (dotted line).

This preliminary analysis highlights the possibility of identifying human head movements (yaw rotation) by EEG - an issue that so far has received little attention. The trials on ten participants, spanning more than two hours of experiments, show that this goal is achievable considering the results obtained by this experiment, a next step concerning the creation of a new BCI model will be made.

5.3 Experimental setup for the creation of a new BCI model

The lamp-system is used in the two phases of the experiments. Fig 5.5 shows the experimental environment.

Figure 5.5: Experimental environment

In the first phase of the experiment (hereinafter referred to as ”ANN training”), the participant follows the visual stimulus with a yaw rotation, and looks towards the switched-on lamp, while in the second phase (hereinafter referred as ”binary controller”), he/she decides whether to rotate the head or not, and according to a runtime interpretation of the EEG, the lamp switches on/off.

During the ANN training the lamps are switched on randomly, one by one, for a 5 second period. Subsequently, they are both switched off for a period varying between 6 and 9 seconds. As soon as one lamp is switched on, the participant has to turn his/her head towards the light. When the lamp is switched off, the participant cames back in the forward position. Each ANN training experiment lasts 5 minutes and the participants wear the Enobio cap for EEG recording with dry sensors. The EEG is used to identify an input output relation between the EEG (input) and

the state of the lamp system (defined by which lamp is switched on). The identification of this function is described in the next section.

In the second phase of the experiment the participant decides to turn his/her head on the left or right side, controlling the lamp system using his/her EEG and generating the control through the input-output function. This control phase lasts 3 minutes.

5.4 Data acquisition protocol

The transmission protocol regarding the EEG cap to a Server PC is the TCP/IP. The two systems are connected by bluethoot and the raw data streaming is managed by the TCP/IP protocol by EDF+ data format. For the lamp system a protocol in a raw data format has been used. The csv log file from a Python script stores: the time and the corresponding lamp value. No protocol has been used for the artefacts because the neck/head movements are obtained from the EEG. The whole signal is acquired during the experiment, and subsequently artifacts are identified and removed in the data processing phase.

5.5 Data processing and analysis

5.5.1 Pre-processing

The main issue in EEG processing relates to the artefacts and to the exogenous and endogenous noises which affect the acquired data. For example, the electrical fields present in the environment, the movements of the eyes and the muscles activity can contaminate the EEG [51]. Muscle artefacts have been limited introducing the signals coming from the differential electrodes placed in the neck. In addition, a bandstop/notch filter between 49 and 51 Hz has been applied to reduce the noise deriving from the electrical frequency of devices [173]. Further techniques have been applied to limit the artefacts. The resulting time-series data are still contaminated with signal artefacts, like eye blink and movements, that have the potential to considerably distort any further analysis. During data acquisition two electrodes located in the hairless part of the head are used like a dual reference electrode. Reference and ground EEG electrodes are fixed on the mastoids of the user for noise reduction. The EEG Cap is extremely lightweight in order to reduce artifacts deriving from movement. The cap fits perfectly to different head shapes and keeps the device in position to guarantee the solid contact of the electrode to the scalp, which is a key requirement for high-quality EEG recordings. In EEG-Based BCI systems the implementation of simple low-pass, high-pass, or bandpass filters has been successfully used to remove physiological artifacts [174] [175]. ICA can also be applied to remove these artefacts [176]. A

high-pass filter with 1Hz threshold has been used. An ICA has also been tested in this respect, and the results have been similar to the ones obtained by high-pass filtering.

Preliminary tests including correlation analysis and the need to speed up computation as a controller have suggested to limit the available information to the signals coming from the three main electrodes labeled O1, O2 and CZ. Finally, to limit precision errors, the resulting samples have been divided by 10^6, and subsequently limited between -1 and 1. In order to set up a suitable classifier, the signal which identifies the head position has been set to -1 for left, 1 for right and 0 for forward positions. The transition between one position and another (e.g. left to forward) has been linearly smoothed using a moving average computed on a window of 300 samples i.e. for a 0.6 s duration. This is the time needed to reach the final position by the participant. An empirical analysis has been carried out to choose the window size. 0.6 sec is the time average of all head movement measurements that have been collected during the simulations.

5.5.2 Input output function identification

The main objective in this phase is to define the best direct input output function generated according to the relationship among a specific set of EEG samples and the related value of the head position. In this context it has been shown that the variance [24] and the participants' sensibility [10] affect the results of the experiments. Because of the complexity of this task, a two-step approach has been adopted to obtain the classification of left or right head position as responses to visual stimuli. The scheme of the architecture, where two ANN's - a TDNN and a PCNN - have been sequentially applied is shown in Fig.5.6.

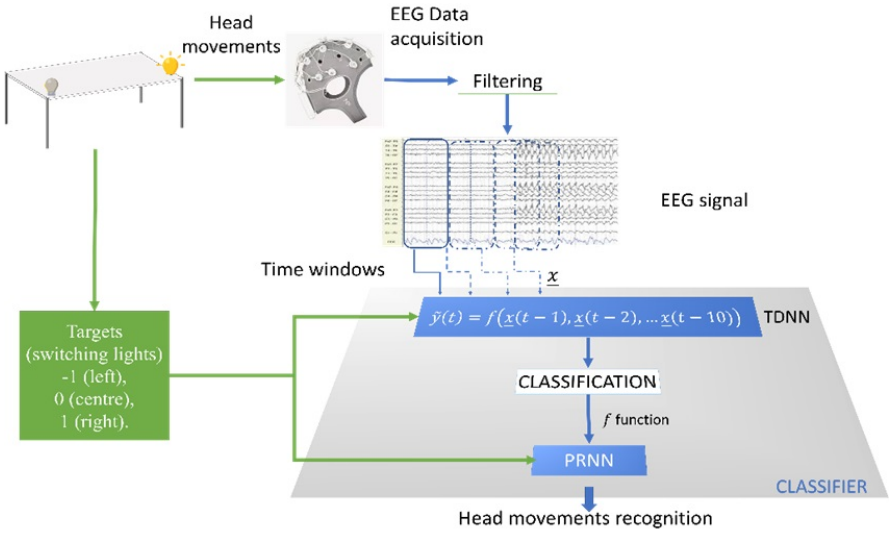

Figure 5.6: Architecture of the proposed system

First, a TDNN is adopted to model the temporal relationships of the input EEGs. Then, the TDNN outputs are used as input to an additional PRNN.

5.5.3 Time Delay Neural Network (TDNN)

The main goal has been to identify a non-linear input output function between 10 consecutive EEG samples (hereinafter defined as $\underline{x}(t)$) taken from O1, O2, and Cz, and the value of the head position in the sample just following the EEG recording (hereinafter defined as $y(t)$). A non-linear function f between input $\underline{x}(t)$ and output $y(t)$ has been identified, so that the values $\tilde{y}(t)$

$$\tilde{y}(t) = f(\underline{x}(t-1), \underline{x}(t-2), ..., \underline{x}(t-10)) \tag{5.1}$$

minimize the MSE between $y(t)$ and $\tilde{y}(t)$. To make predictions less affected by input noise, the predicted values $\tilde{y}(t)$ have then been averaged by a moving mean of 300 preceding samples, that is:

$$\bar{y} = \sum_{\hat{t}=0}^{299} \frac{\tilde{y}(t-\hat{t})^2}{300} \tag{5.2}$$

The TDNN with 10 neurons in the hidden layer identifies the non-linear input-output function. The identification process is based on the Levenberg-Marquardt backpropagation algorithm [177], [178] (Matlab® software version 2020). The training process has taken an average of 87 steps (about 45 s) on a common laptop.

Two key performance indexes have been used to evaluate the reliability of the proposed function f generated by the TDNN: MSE and the Pearson correlation coefficient *r* as defined respectively in (2.15) and (2.19)

5.5.4 The Pattern Recognition Neural Network (PRNN)

The aim of this second computation has been to generate the binary control. The PRNN has been defined with 3 layers. The input layer has been set up with $k = 98$ units, relating to an input pattern, in which the *i*-th pattern p_i has the values resulting from

$$p_i = \bar{y}(t(p_i)) \tag{5.3}$$

$$t(p_i) = (k+2)i + t \quad i = 0, .., N-1 \quad t = 0, .., k-1 \tag{5.4}$$

where N is the number of time intervals with duration $2 * 10^{-1}$ s contained in each resulting $\bar{y}(t)$. A 10 unit hidden layer has been used. A three unit output layer has been chosen to match the output binary target $g_{i,b}$, defined on three bits b=1..3, coded as 100 for left, 010 for right, and 001 for forward positions. For each pattern, the position was the one at the end of each time

interval made. The PRNN has been identified by the scaled conjugate gradient back-propagation algorithm (Matlab® software version 2020).

The results have been evaluated by the cross–entropy loss H [179]: The Cross Entropy loss function applied in this case is shown below:

$$H = -\frac{\sum_{i=0}^{N-1}\sum_{b=1}^{C} g_{i,b}\log(\tilde{g}_{i,b})}{N} \tag{5.5}$$

Where C is the number of pattern class, in this case its value is 3. To evaluate the accuracy of the results obtained in case of unbalanced class the Matthews correlation coefficient has been used. This index is frequently encountered in biomedical applications [180] and is generally applied in machine learning problems to evaluate the quality of binary classifications. Its generalization to a multiclass case is also used:

$$MCC = \frac{\sum_k \sum_l \sum_m C_{kk}C_{lm} - C_{kl}C_{mk}}{\sqrt{\sum_k(\sum_l C_{kl})(\sum_{k'|k'\neq k}\sum_{l'} C_{k'l'})}\sqrt{\sum_k(\sum_l C_{lk})(\sum_{k'|k'\neq k}\sum_{l'} C_{l'k'})}} \tag{5.6}$$

Where C_{kk} is the number of correctly predicted that is in category k. C_{kl} is the number predicted to belong to class k, but belonging to class l where $l \neq k$.

5.5.5 Binary controller testing in real-time

To test the reliability of the binary controller, the same participants have been involved in a second phase of the experiments. In this phase, the participant, wearing the Enobio cap, decided the direction of the head yaw rotations towards one of the two lamps. Consequently, the real-time binary controller, implemented in Matlab® software version 2020, based on the classifier previously identified for each participant (Fig.5.7) if properly working, should have switched on the related lamp. If again properly working, the binary controller could switch off the lamp once the user turned the head in the frontal position. In the testing protocol the participant turned the head on the right or left at his/her preference for about 5 seconds and he/she stayed in the frontal position for about 8 seconds. The switching on/off control test has been performed by the participants both with open and with closed eyes.

In this test, the action resulting from the binary controller has been defined as correct:

- if in the period with the head turned on one side (i.e. left/right) the lamp on the same side (i.e. left/right) switched on with no switches of the other lamp (i.e. right/left);
- if in the period with the head in the forward position the lamp switched off with no other switches.

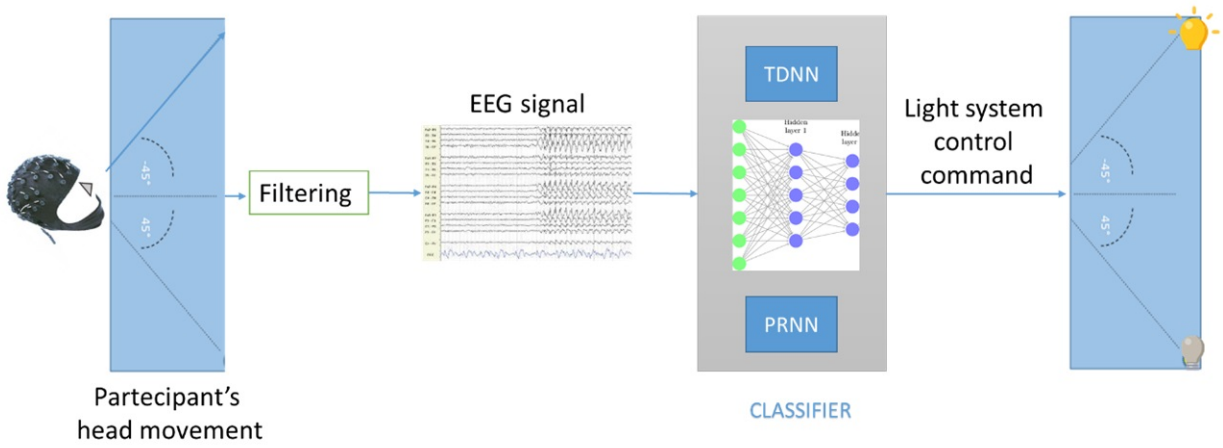

Figure 5.7: Binary controller framework

5.6 Results

5.6.1 Prediction accuracy

The trials involved 22 participants: 5 women and 17 men, aged 18 to 62 years including 4 left-handed. For each participant one ANN training, lasting 5 minutes, has been carried out. Each file has been divided into equal parts, with the training performed on the first half, and the testing performed on the second half. Table 5.8 shows the results related to the MSE and correlation coefficient resulting from the TDNN just for the testing. According to Cohen classification [114], the r values demonstrate a strong correlation, which guarantees that the TDNN classifier is reliable. In all experiments, the r values are greater than 0.5 and, in 15 out of 22 of cases, they overcome the value r =0.75 with a related MSE smaller than 0.55.

The results related to the PRNN performances are shown in Table 5.9. In this model, the 70% of the EEG has been adopted for the training phase, while the remaining 30% has been used for the test. Table 5.9 shows the testing patterns accuracy and the cross-entropy loss H. The PRNN accuracy is greater than 74% in all cases, with a mean value of 88%. The best performance is 96% for P1. The H values in Table 5.9 confirm that a good accuracy of the model relates to lower entropy. In the cases in which the participants obtained an accuracy greater than 90%, the H value is limited to 0.3. However, the average value for H on the overall experiments is 0.67 with the minimum for P10 (accuracy=94,72% and H=0,16) and a maximum for P18 (accuracy = 74.19% and H=0.6751).

Table 5.8: TDNN performance indices

Part ID	r	MSE		Part ID	r	MSE
P1	0.89	0.177		P12	0.91	0.225
P2	0.78	0.335		P13	0.87	0.441
P3	0.76	0.719		P14	0.59	1.047
P4	0.90	0.468		P15	0.91	0.249
P5	0.79	0.522		P16	0.78	0.411
P6	0.85	0.560		P17	0.84	0.514
P7	0.64	0. 575		P18	0.61	0.598
P8	0.65	0.636		P19	0.64	0.530
P9	0.72	0.523		P20	0.90	0.451
P10	0.92	0.224		P21	0.69	0.862
P11	0.91	0.322		P22	0.87	0.316

Table 5.9: Results for the PRNN

Part ID	%correct prediction	H		Part ID	%correct prediction	H
P1	96.85	0.1814		P12	93.04	0.1979
P2	90.55	0.2862		P13	91.67	0.3069
P3	89.75	0.4447		P14	81.82	0.5116
P4	93.08	0.2410		P15	91.92	0.2960
P5	82.93	0.4559		P16	90.55	0.3124
P6	90.21	0.3247		P17	85.48	0.3701
P7	78.85	0.6257		P18	74.19	0.6751
P8	83.64	0.4802		P19	79.21	0.5458
P9	83.64	0.4659		P20	93.36	0.1932
P10	94.72	0.1634		P21	79.83	0.5567
P11	93.88	0.1911		P22	95.82	0.2127

The accuracy results have been evaluated by the Matthews correlation coefficient, which is used for the P22 data. Table 5.10 shows the confusion matrix. The data on the matrix diagonal show the number of times in which the classifier correctly predicts the head position associated to, respectively, label 1 (right movement of the head), label 0 (forward position), label -1 (left movements). The values out of the diagonal represent the failed predictions between output class and related target.

Table 5.10: Confusion Matrix for P22

Actual class /Predicted class	-1	0	1	Total
-1	38	3	0	41
0	3	163	1	167
1	0	4	51	55
Total	41	170	52	263

The MCC (5.6) for data in Table 5.10 is 92.04 %. This value is high and confirms a good prediction, according to the previously calculated H value. The global confusion matrix is shown for the test set of each participant in Table 5.11:

Table 5.11: Confusion Matrix for P22

Actual class /Predicted class	-1	0	1	Total
-1	759	148	1	908
0	272	3200	212	3684
1	0	137	899	1036
Total	1031	3485	1112	5628

The MCC (5.6) for the data shown in Table IV is 74.3%. The Matthews index confirms that good results have been obtained, which are shown in Table II. As relates to comparative performance analysis in term of classifier accuracy, it is important to note that EEG classification for BCI applications in the context of human movements mainly focuses on hands, eyes, arms or movement intention detection. The proposed classifier, and the resulting BCI controller, focuses on head movements and aims to evaluate the possibility to identify the head turning of participants when they are subjected to visual stimuli, to provide a non-invasive interface tool to control external devices.

5.6.2 Binary controller performance

Table 5.12 shows the percentage of correct predictions for BCI used as a binary controller. The tests have been performed both with open and with closed eyes. The percentage of correct predictions is greater than 75% for 20 participants out of 22 with opened eyes and 11 out of 22 for closed eyes. The average difference between the performance between open eyes vs closed eyes is always in favor of open eyes, with an average difference of 9%. Participant P1 controlled the light system without errors during both experiments with 100% success.

Table 5.12: The BCI accuracy

Part ID	%correct with open eyes	%correct with closed eyes		Part ID	%correct with open eyes	%correct with closed eyes
P1	100%	100%		P12	96%	96%
P2	86%	83%		P13	76%	73%
P3	80%	63%		P14	54%	26%
P4	82%	80%		P15	94%	88%
P5	79%	44%		P16	88%	86%
P6	91%	68%		P17	88%	73%
P7	85%	79%		P18	81%	59%
P8	81%	79%		P19	78%	68%
P9	77%	73%		P20	97%	87%
P10	100%	96%		P21	78%	71%
P11	87%	90%		P22	71%	62%

This work relates to the implementation of a BCI system to implement a binary controller, in the case study applied to switch on/off lamp system according to the electrical brain activity due to the head turning movement. As shown by the reported results, it appears to be feasible to identify human left or right head movements by a non-linear input output function recording brain signals from three channels of an EEG cap.

The correlation is quite relevant and, for a set of 22 participants, it is greater than 0.75 in 68% of the experiments. The approach tha has been taken, which consists of applying two consecutive NNs, a TDNN firstly and subsequently a PRNN, gives promising outcomes as relates to the prediction of movements acquired by participants' EEG. The accuracy of the classifier has a mean value of 88%. In addition, the low computational time required by TDNN and PRNN allows for their application in a real time context.

The main result of this work is the reliability of the controller that has been realised. The tests related to the application of the classifier to user movements and consequently to control the light system by monitoring the EEGs demonstrated a relevant capability of the BCI to identify the intention of the subjects to move the head on the right and left sides. On the contrary, a drawback may be recognized in the customisation of the classifier. When the TDNN-PRNN system is identified on one participant it cannot be applied to another participant, since the performance assessment is not reliable.
However, several issues may be raised. The first relates to the presence of artifacts in the EEG, which may affect the overall identification process. In fact, while classic filtering has been adopted, electrical stimuli coming from different sources (such as for example the effect of the lamp light on the participant's eyes) can still be present. However, as relates to the effects of the light on the participant's eyes, it is encouraging to observe that the controller works quite well

with no need of stimulus, since lamps are switched on by the controller. In addition, quite good results are also obtained with closed eyes. Another aspect may be related to the objective of the study.In fact with a simple accelerometer positioned on the head, better results could have surely been obtained. That is why it is important to underline that the goal of this study is understanding the association between the electrical brain activity and a specific action. The further step, which could not be achieved by an accelerometer, is to verify such an association when the actual movement is not performed, while the participant is "just thinking" to make a such movement. Some studies [181] show that this further step is feasible.

Chapter 6

Conclusion and further developments

The main aspect of this work is the linking human behavior and an external device. The results of the three case studies that have been carried out confirm that it is possible to detect, process and analyse the human emotional state. The main achievement relates to the identification of human head movements (yaw rotation) by EEG - BCI issue that has received little attention so far. BCI has recently started to be present in commercial systems at prototypal level, and is increasingly being used in the automotive context, with proprietary systems which are mainly based on ANN applications.

The first case study, focused on the analysis of a driver's behaviour when he/she is subjected to several types of unexpected stimuli by EEG has found a significant correlation in time and frequency among data related to brain activities associated to alpha waves. The results have been used to develop the second case study, which has focused on defining how brain areas are involved in driving, evaluating driver performance on curved roadways by a driving simulator. Both studies introduce an innovative research goal, relating to setting up a predictive model aiming to detect human behavior during driving sessions and to manage the interaction with an external device. The results and acquired knowledge have led to the implementation of a BCI system.

As relates to the head yaw rotation in BCI - which is the third case study - from the trials on several subjects, it seems clear that — under some specific limitations — human head movements can be used for the control of automotive systems. It has been found after identifying a proper function over a short period of time, head positions can be predicted with high accuracy for a quite longer time span. However, the results obtained on different days showed that EEGs on the same subject are time variant. The EEGs recorded in a short time interval can be used to set up a classifier for human head movements following visual stimuli. This correlation is also more likely, susceptible to sensors' positioning. A further result which may represent a drawback, and also an important finding, relates to the fact that the correlation is certainly dependent on the

specific subject, therefore it not possible to make predictions on a subject when the classifier has been trained on another subject. This may be a disadvantage for the implementation of the EEG classifier, because it does not allow to achieve an acceptable generalization level. However, further work could address the identification of a classifier which takes into account groups of subjects. Other important findings relate to EEG acquisition reliability, which is extremely dependent on the adherence of the electrodes to the scalp.
Foreseeable developments could address different aspects of BCI. The EEG has been found to be affected both by electrical and by light stimuli, and further work could focus on the separation of these aspects. Moreover, foreseeable EEG analysis could consider input-output relations for specific frequency bands. BCI systems could be extended including the acquisition of EMGs together with EEGs during simulations, in order to consider the information which is present in each signal. Very preliminary work is being carried out in this respect. Brain imagery in order to set up BCI systems focused on the intention to move the head is also being carried out and is at an initial stage.

This work has been sponsored by Eni S.p.A. with the goal to enhance safety in the trasportation of dangerous goods.

Bibliography

[1] "Sae, taxonomy and definitions for terms related to on-road motor vehicle automated driving systems, j3016, sae international standard (2014). https://www.sae.org/standards/content/j3016_201806/.LastaccessJune2020."

[2] W. Xue, B. Yang, T. Kaizuka, and K. Nakano, "A fallback approach for an automated vehicle encountering sensor failure in monitoring environment," in *2018 IEEE Intelligent Vehicles Symposium (IV)*, pp. 1807–1812, IEEE, 2018.

[3] D. Li and Q. Xu, "An efficient framework for road sign detection and recognition," *Sensors & Transducers*, vol. 165, no. 2, p. 112, 2014.

[4] S. Chavhan, R. A. Kulkarni, and A. R. Zilpe, "Smart sensors for iiot in autonomous vehicles," in *Smart Sensors for Industrial Internet of Things*, pp. 51–61, Springer, 2021.

[5] M. Carranza-García, J. Torres-Mateo, P. Lara-Benítez, and J. García-Gutiérrez, "On the performance of one-stage and two-stage object detectors in autonomous vehicles using camera data," *Remote Sensing*, vol. 13, no. 1, p. 89, 2021.

[6] I. Orr, M. Cohen, and Z. Zalevsky, "High-resolution radar road segmentation using weakly supervised learning," *Nature Machine Intelligence*, vol. 3, no. 3, pp. 239–246, 2021.

[7] Z. Liu, Y. Cai, H. Wang, L. Chen, H. Gao, Y. Jia, and Y. Li, "Robust target recognition and tracking of self-driving cars with radar and camera information fusion under severe weather conditions," *IEEE Transactions on Intelligent Transportation Systems*, 2021.

[8] H. Wang and X. Zhang, "Real-time vehicle detection and tracking using 3d lidar," *Asian Journal of Control*, 2021.

[9] A. Díaz-Álvarez, M. Clavijo, F. Jiménez, and F. Serradilla, "Inferring the driver's lane change intention through lidar-based environment analysis using convolutional neural networks," *Sensors*, vol. 21, no. 2, p. 475, 2021.

[10] J. Sharit, *A Human Factors Engineering Perspective to Aging and Work*, pp. 191–218. Springer, 2020.

[11] J. Zhang, Z. Yin, and R. Wang, "Recognition of mental workload levels under complex human–machine collaboration by using physiological features and adaptive support vector machines," *IEEE Transactions on Human-Machine Systems*, vol. 45, no. 2, pp. 200–214, 2014.

[12] D. Wang, M. T. Amin, S. Li, T. Abdelzaher, L. Kaplan, S. Gu, C. Pan, H. Liu, C. C. Aggarwal, and R. Ganti, "Using humans as sensors: an estimation-theoretic perspective," in *IPSN-14 proceedings of the 13th international symposium on information processing in sensor networks*, pp. 35–46, IEEE.

[13] S. S. Deogade, "A survey of human-sensing methods for detecting presence and identity," 2018.

[14] S. S. Rahman, R. Heartfield, W. Oliff, G. Loukas, and A. Filippoupolitis, "Assessing the cyber-trustworthiness of human-as-a-sensor reports from mobile devices," in *2017 IEEE 15th International Conference on Software Engineering Research, Management and Applications (SERA)*, pp. 387–394, IEEE.

[15] R. Heartfield and G. Loukas, "A taxonomy of attacks and a survey of defence mechanisms for semantic social engineering attacks," *ACM Computing Surveys (CSUR)*, vol. 48, no. 3, pp. 1–39, 2015.

[16] T. Sakaki, M. Okazaki, and Y. Matsuo, "Earthquake shakes twitter users: real-time event detection by social sensors," in *Proceedings of the 19th international conference on World wide web*, pp. 851–860.

[17] S. Paszkiel, *Analysis and Classification of EEG Signals for Brain-Computer Interfaces*. Springer, 2020.

[18] A. Ferreira, W. C. Celeste, F. A. Cheein, T. F. Bastos-Filho, M. Sarcinelli-Filho, and R. Carelli, "Human-machine interfaces based on emg and eeg applied to robotic systems," *Journal of NeuroEngineering and Rehabilitation*, vol. 5, no. 1, pp. 1–15, 2008.

[19] A. Roman-Gonzalez, *Eeg signal processing for bci applications*, pp. 571–591. Springer, 2012.

[20] M. Mohammadpour, S. M. R. Hashemi, and N. Houshmand, "Classification of eeg-based emotion for bci applications," in *2017 Artificial Intelligence and Robotics (IRANOPEN)*, pp. 127–131, IEEE.

[21] G. Chen, X. Zhang, Y. Sun, and J. Zhang, "Emotion feature analysis and recognition based on reconstructed eeg sources," *IEEE Access*, vol. 8, pp. 11907–11916, 2020.

[22] N. K. Al-Qazzaz, M. K. Sabir, S. H. B. M. Ali, S. A. Ahmad, and K. Grammer, "Electroencephalogram profiles for emotion identification over the brain regions using spectral, entropy and temporal biomarkers," *Sensors*, vol. 20, no. 1, p. 59, 2020.

[23] S. Yang and F. Deravi, "On the usability of electroencephalographic signals for biometric recognition: A survey," *IEEE Transactions on Human-Machine Systems*, vol. 47, no. 6, pp. 958–969, 2017.

[24] V. Sakkalis, "Review of advanced techniques for the estimation of brain connectivity measured with eeg/meg," *Computers in biology and medicine*, vol. 41, no. 12, pp. 1110–1117, 2011.

[25] P. Zhong, D. Wang, and C. Miao, "Eeg-based emotion recognition using regularized graph neural networks," *IEEE Transactions on Affective Computing*, 2020.

[26] M. Stikic, R. R. Johnson, V. Tan, and C. Berka, "Eeg-based classification of positive and negative affective states," *Brain-Computer Interfaces*, vol. 1, no. 2, pp. 99–112, 2014.

[27] T. G. Monteiro, C. Skourup, and H. Zhang, "Using eeg for mental fatigue assessment: A comprehensive look into the current state of the art," *IEEE Transactions on Human-Machine Systems*, vol. 49, no. 6, pp. 599–610, 2019.

[28] S. Wang, J. Gwizdka, and W. A. Chaovalitwongse, "Using wireless eeg signals to assess memory workload in the n-back task," *IEEE Transactions on Human-Machine Systems*, vol. 46, no. 3, pp. 424–435, 2015.

[29] H. Yu, L. Zhu, L. Cai, J. Wang, C. Liu, N. Shi, and J. Liu, "Variation of functional brain connectivity in epileptic seizures: an eeg analysis with cross-frequency phase synchronization," *Cognitive neurodynamics*, vol. 14, no. 1, pp. 35–49, 2020.

[30] U. R. Acharya, S. V. Sree, G. Swapna, R. J. Martis, and J. S. Suri, "Automated eeg analysis of epilepsy: a review," *Knowledge-Based Systems*, vol. 45, pp. 147–165, 2013.

[31] S. Borhani, R. Abiri, Y. Jiang, T. Berger, and X. Zhao, "Brain connectivity evaluation during selective attention using eeg-based brain-computer interface," *Brain-Computer Interfaces*, vol. 6, no. 1-2, pp. 25–35, 2019.

[32] E. Gonzalez-Trejo, H. Mögele, N. Pfleger, R. Hannemann, and D. J. Strauss, "Electroencephalographic phase–amplitude coupling in simulated driving with varying modality-specific attentional demand," *IEEE Transactions on Human-Machine Systems*, vol. 49, no. 6, pp. 589–598, 2019.

[33] D. He, B. Donmez, C. C. Liu, and K. N. Plataniotis, "High cognitive load assessment in drivers through wireless electroencephalography and the validation of a modified n-back task," *IEEE Transactions on Human-Machine Systems*, vol. 49, no. 4, pp. 362–371, 2019.

[34] G. Li and W.-Y. Chung, "Combined eeg-gyroscope-tdcs brain machine interface system for early management of driver drowsiness," *IEEE Transactions on Human-Machine Systems*, vol. 48, no. 1, pp. 50–62, 2017.

[35] E. Zero, C. Bersani, L. Zero, and R. Sacile, "Towards real-time monitoring of fear in driving sessions," *IFAC-PapersOnLine*, vol. 52, no. 19, pp. 299–304, 2019.

[36] Y. Xing, C. Lv, and D. Cao, *Advanced Driver Intention Inference: Theory and Design*. Elsevier, 2020.

[37] J. Sleight, P. Pillai, and S. Mohan, "Classification of executed and imagined motor movement eeg signals," *Ann Arbor: University of Michigan*, vol. 110, 2009.

[38] J. J. Liao, J. J. Luo, T. Yang, R. Q. Y. So, and M. C. H. Chua, "Effects of local and global spatial patterns in eeg motor-imagery classification using convolutional neural network," *Brain-Computer Interfaces*, vol. 7, no. 3-4, pp. 47–56, 2020.

[39] A. Athanasiou, E. Chatzitheodorou, K. Kalogianni, C. Lithari, I. Moulos, and P. Bamidis, "Comparing sensorimotor cortex activation during actual and imaginary movement," in *XII Mediterranean Conference on Medical and Biological Engineering and Computing 2010*, pp. 111–114, Springer.

[40] R. Chaisaen, P. Autthasan, N. Mingchinda, P. Leelaarporn, N. Kunaseth, S. Tammajarung, P. Manoonpong, S. C. Mukhopadhyay, and T. Wilaiprasitporn, "Decoding eeg rhythms during action observation, motor imagery, and execution for standing and sitting," *IEEE Sensors Journal*, vol. 20, no. 22, pp. 13776–13786, 2020.

[41] M. L. Al-dabag and N. Ozkurt, "Eeg motor movement classification based on cross-correlation with effective channel," *Signal, Image and Video Processing*, vol. 13, no. 3, pp. 567–573, 2019.

[42] S. Bhattacharyya, A. Khasnobish, A. Konar, D. Tibarewala, and A. K. Nagar, "Performance analysis of left/right hand movement classification from eeg signal by intelligent algorithms," in *2011 IEEE Symposium on Computational Intelligence, Cognitive Algorithms, Mind, and Brain (CCMB)*, pp. 1–8, IEEE.

[43] R. Abiri, S. Borhani, J. Kilmarx, C. Esterwood, Y. Jiang, and X. Zhao, "A usability study of low-cost wireless brain-computer interface for cursor control using online linear model," *IEEE Transactions on Human-Machine Systems*, vol. 50, no. 4, pp. 287–297, 2020.

[44] A. Bashashati, M. Fatourechi, R. K. Ward, and G. E. Birch, "A survey of signal processing algorithms in brain–computer interfaces based on electrical brain signals," *Journal of Neural engineering*, vol. 4, no. 2, p. R32, 2007.

[45] A. Kawala-Sterniuk, N. Browarska, A. Al-Bakri, M. Pelc, J. Zygarlicki, M. Sidikova, R. Martinek, and E. J. Gorzelanczyk, "Summary of over fifty years with brain-computer interfaces—a review," *Brain Sciences*, vol. 11, no. 1, p. 43, 2021.

[46] R. Alazrai, M. Abuhijleh, H. Alwanni, and M. I. Daoud, "A deep learning framework for decoding motor imagery tasks of the same hand using eeg signals," *IEEE Access*, vol. 7, pp. 109612–109627, 2019.

[47] M. Tariq, P. M. Trivailo, and M. Simic, "Mu-beta event-related (de) synchronization and eeg classification of left-right foot dorsiflexion kinaesthetic motor imagery for bci," *Plos one*, vol. 15, no. 3, p. e0230184, 2020.

[48] B. Chambayil, R. Singla, and R. Jha, "Eeg eye blink classification using neural network," in *Proceedings of the world congress on engineering*, vol. 1, pp. 2–5, 2010.

[49] S. O'Regan, S. Faul, and W. Marnane, "Automatic detection of eeg artefacts arising from head movements using eeg and gyroscope signals," *Medical engineering & physics*, vol. 35, no. 7, pp. 867–874, 2013.

[50] N. Uke and D. Kulkarni, "Recent artifacts handling algorithms in electroencephalogram," 2020.

[51] X. Jiang, G.-B. Bian, and Z. Tian, "Removal of artifacts from eeg signals: a review," *Sensors*, vol. 19, no. 5, p. 987, 2019.

[52] S. O'Regan and W. Marnane, "Multimodal detection of head-movement artefacts in eeg," *Journal of Neuroscience Methods*, vol. 218, no. 1, pp. 110–120, 2013.

[53] V. Lawhern, W. D. Hairston, K. McDowell, M. Westerfield, and K. Robbins, "Detection and classification of subject-generated artifacts in eeg signals using autoregressive models," *Journal of neuroscience methods*, vol. 208, no. 2, pp. 181–189, 2012.

[54] N. A. Chadwick, D. A. McMeekin, and T. Tan, "Classifying eye and head movement artifacts in eeg signals," in *5th IEEE International Conference on Digital Ecosystems and Technologies (IEEE DEST 2011)*, pp. 285–291, IEEE.

[55] B. J. Li, J. N. Bailenson, A. Pines, W. J. Greenleaf, and L. M. Williams, "A public database of immersive vr videos with corresponding ratings of arousal, valence, and correlations between head movements and self report measures," *Frontiers in psychology*, vol. 8, p. 2116, 2017.

[56] B. J. Li, J. N. Bailenson, A. Pines, W. J. Greenleaf, and L. M. Williams, "A public database of immersive vr videos with corresponding ratings of arousal, valence, and correlations between head movements and self report measures," *Frontiers in psychology*, vol. 8, p. 2116, 2017.

[57] J. N. Mak, R. H. Chan, and S. W. Wong, "Evaluation of mental workload in visual-motor task: Spectral analysis of single-channel frontal eeg," in *IECON 2013-39th Annual Conference of the IEEE Industrial Electronics Society*, pp. 8426–8430, IEEE.

[58] A. J. Rilk, S. R. Soekadar, P. Sauseng, and C. Plewnia, "Alpha coherence predicts accuracy during a visuomotor tracking task," *Neuropsychologia*, vol. 49, no. 13, pp. 3704–3709, 2011.

[59] E. Zareian, V. Kathpalia, J. Chen, and T. Smith, "A cost effective approach for the practical realisation of a demonstration platform for brain machine interface," 2014.

[60] M. Busogi and N. Kim, "Analytical modeling of human choice complexity in a mixed model assembly line using machine learning-based human in the loop simulation," *IEEE Access*, vol. 5, pp. 10434–10444, 2017.

[61] F. Lotte, M. Congedo, A. Lécuyer, F. Lamarche, and B. Arnaldi, "A review of classification algorithms for eeg-based brain–computer interfaces," *Journal of neural engineering*, vol. 4, no. 2, p. R1, 2007.

[62] A. Saha, A. Konar, A. Chatterjee, A. Ralescu, and A. K. Nagar, "Eeg analysis for olfactory perceptual-ability measurement using a recurrent neural classifier," *IEEE Transactions on Human-Machine Systems*, vol. 44, no. 6, pp. 717–730, 2014.

[63] J. Jiang, A. Fares, and S.-H. Zhong, "A context-supported deep learning framework for multimodal brain imaging classification," *IEEE Transactions on Human-Machine Systems*, vol. 49, no. 6, pp. 611–622, 2019.

[64] V. Müller, W. Lutzenberger, H. Preißl, F. Pulvermüller, and N. Birbaumer, "Complexity of visual stimuli and non-linear eeg dynamics in humans," *Cognitive Brain Research*, vol. 16, no. 1, pp. 104–110, 2003.

[65] L. Angrisani, P. Arpaia, and D. Casinelli, "Instrumentation and measurements for non-invasive eeg-based brain-computer interface," in *2017 IEEE International Workshop on Measurement and Networking (M&N)*, pp. 1–5, IEEE.

[66] M. Attia, I. Hettiarachchi, S. Mohamed, M. Hossny, and S. Nahavandi, "A frequency domain classifier of steady-state visual evoked potentials using deep separable convolutional neural networks," in *2018 IEEE International Conference on Systems, Man, and Cybernetics (SMC)*, pp. 2134–2139, IEEE.

[67] S. Zhao, Z. Li, R. Cui, Y. Kang, F. Sun, and R. Song, "Brain–machine interfacing-based teleoperation of multiple coordinated mobile robots," *IEEE Transactions on Industrial Electronics*, vol. 64, no. 6, pp. 5161–5170, 2016.

[68] A. Nourmohammadi, M. Jafari, and T. O. Zander, "A survey on unmanned aerial vehicle remote control using brain–computer interface," *IEEE Transactions on Human-Machine Systems*, vol. 48, no. 4, pp. 337–348, 2018.

[69] R. Abiri, S. Borhani, E. W. Sellers, Y. Jiang, and X. Zhao, "A comprehensive review of eeg-based brain–computer interface paradigms," *Journal of neural engineering*, vol. 16, no. 1, p. 011001, 2019.

[70] D. Tan and A. Nijholt, *Brain-computer interfaces and human-computer interaction*, pp. 3–19. Springer, 2010.

[71] P. Stegman, C. S. Crawford, M. Andujar, A. Nijholt, and J. E. Gilbert, "Brain–computer interface software: A review and discussion," *IEEE Transactions on Human-Machine Systems*, vol. 50, no. 2, pp. 101–115, 2020.

[72] M. Avvenuti, M. G. Cimino, S. Cresci, A. Marchetti, and M. Tesconi, "A framework for detecting unfolding emergencies using humans as sensors," *SpringerPlus*, vol. 5, no. 1, pp. 1–23, 2016.

[73] L. Randazzo, I. Iturrate, S. Perdikis, and J. d. R. Millán, "mano: A wearable hand exoskeleton for activities of daily living and neurorehabilitation," *IEEE Robotics and Automation Letters*, vol. 3, no. 1, pp. 500–507, 2017.

[74] D. P. Subha, P. K. Joseph, R. Acharya, and C. M. Lim, "Eeg signal analysis: a survey," *Journal of medical systems*, vol. 34, no. 2, pp. 195–212, 2010.

[75] I.-H. Kim, J.-W. Kim, S. Haufe, and S.-W. Lee, "Detection of braking intention in diverse situations during simulated driving based on eeg feature combination," *Journal of neural engineering*, vol. 12, no. 1, p. 016001, 2014.

[76] Z. Khaliliardali, R. Chavarriaga, L. A. Gheorghe, and J. del R Millán, "Action prediction based on anticipatory brain potentials during simulated driving," *Journal of neural engineering*, vol. 12, no. 6, p. 066006, 2015.

[77] H. Zhang, R. Chavarriaga, L. Gheorghe, and J. d. R. Millán, "Inferring driver's turning direction through detection of error related brain activity," in *2013 35th Annual international conference of the IEEE engineering in medicine and biology society (EMBC)*, pp. 2196–2199, IEEE.

[78] H. Zhang, R. Chavarriaga, Z. Khaliliardali, L. Gheorghe, I. Iturrate, and J. d R Millán, "Eeg-based decoding of error-related brain activity in a real-world driving task," *Journal of neural engineering*, vol. 12, no. 6, p. 066028, 2015.

[79] S. De Nadai, M. Benza, M. D'Incà, F. Parodi, and R. Sacile, "A system of systems approach to evaluate at-risk human behaviour in the transport by road," in *2015 IEEE International Symposium on Systems Engineering (ISSE)*, pp. 212–215, IEEE.

[80] A. Hashemi, V. Saba, and S. N. Resalat, "Real time driver's drowsiness detection by processing the eeg signals stimulated with external flickering light," *Basic and clinical neuroscience*, vol. 5, no. 1, p. 22, 2014.

[81] M. Hajinoroozi, Z. Mao, T.-P. Jung, C.-T. Lin, and Y. Huang, "Eeg-based prediction of driver's cognitive performance by deep convolutional neural network," *Signal Processing: Image Communication*, vol. 47, pp. 549–555, 2016.

[82] J. Kohlmorgen, G. Dornhege, M. Braun, B. Blankertz, K.-R. Müller, G. Curio, K. Hagemann, A. Bruns, M. Schrauf, and W. Kincses, "Improving human performance in a real operating environment through real-time mental workload detection," *Toward brain-computer interfacing*, vol. 409422, pp. 409–422, 2007.

[83] S. Haufe, M. S. Treder, M. F. Gugler, M. Sagebaum, G. Curio, and B. Blankertz, "Eeg potentials predict upcoming emergency brakings during simulated driving," *Journal of neural engineering*, vol. 8, no. 5, p. 056001, 2011.

[84] C.-T. Lin, R.-C. Wu, T.-P. Jung, S.-F. Liang, and T.-Y. Huang, "Estimating driving performance based on eeg spectrum analysis," *EURASIP Journal on Advances in Signal Processing*, vol. 2005, no. 19, pp. 1–10, 2005.

[85] W. Li, Q.-c. He, X.-m. Fan, and Z.-m. Fei, "Evaluation of driver fatigue on two channels of eeg data," *Neuroscience letters*, vol. 506, no. 2, pp. 235–239, 2012.

[86] B. T. Jap, S. Lal, P. Fischer, and E. Bekiaris, "Using eeg spectral components to assess algorithms for detecting fatigue," *Expert Systems with Applications*, vol. 36, no. 2, pp. 2352–2359, 2009.

[87] G. S. Larue, A. Rakotonirainy, and A. N. Pettitt, "Driving performance impairments due to hypovigilance on monotonous roads," *Accident Analysis & Prevention*, vol. 43, no. 6, pp. 2037–2046, 2011.

[88] R. P. Balandong, R. F. Ahmad, M. N. M. Saad, and A. S. Malik, "A review on eeg-based automatic sleepiness detection systems for driver," *Ieee Access*, vol. 6, pp. 22908–22919, 2018.

[89] S. Kar, M. Bhagat, and A. Routray, "Eeg signal analysis for the assessment and quantification of driver's fatigue," *Transportation research part F: traffic psychology and behaviour*, vol. 13, no. 5, pp. 297–306, 2010.

[90] M. Haak, S. Bos, S. Panic, and L. Rothkrantz, "Detecting stress using eye blinks and brain activity from eeg signals," *Proceeding of the 1st driver car interaction and interface (DCII 2008)*, pp. 35–60, 2009.

[91] S. Sonkusare, V. T. Nguyen, R. Moran, J. van der Meer, Y. Ren, N. Koussis, S. Dionisio, M. Breakspear, and C. Guo, "Intracranial-eeg evidence for medial temporal pole driving amygdala activity induced by multi-modal emotional stimuli," *Cortex*, vol. 130, pp. 32–48, 2020.

[92] M. Karthaus, E. Wascher, M. Falkenstein, and S. Getzmann, "The ability of young, middle-aged and older drivers to inhibit visual and auditory distraction in a driving simulator task," *Transportation research part F: traffic psychology and behaviour*, vol. 68, pp. 272–284, 2020.

[93] N. Du, F. Zhou, E. M. Pulver, D. M. Tilbury, L. P. Robert, A. K. Pradhan, and X. J. Yang, "Examining the effects of emotional valence and arousal on takeover performance in conditionally automated driving," *Transportation research part C: emerging technologies*, vol. 112, pp. 78–87, 2020.

[94] K. E. Mathewson, T. J. Harrison, and S. A. Kizuk, "High and dry? comparing active dry eeg electrodes to active and passive wet electrodes," *Psychophysiology*, vol. 54, no. 1, pp. 74–82, 2017.

[95] A. Phinyomark, C. Limsakul, and P. Phukpattaranont, "Application of wavelet analysis in emg feature extraction for pattern classification," *Measurement Science Review*, vol. 11, no. 2, p. 45, 2011.

[96] M. B. I. Reaz, M. S. Hussain, and F. Mohd-Yasin, "Techniques of emg signal analysis: detection, processing, classification and applications," *Biological procedures online*, vol. 8, no. 1, pp. 11–35, 2006.

[97] V. K. Harpale and V. K. Bairagi, "Time and frequency domain analysis of eeg signals for seizure detection: A review," in *2016 International Conference on Microelectronics, Computing and Communications (MicroCom)*, pp. 1–6, 2016.

[98] M. Akin, "Comparison of wavelet transform and fft methods in the analysis of eeg signals," *Journal of medical systems*, vol. 26, no. 3, pp. 241–247, 2002.

[99] P. S. Kumar, R. Arumuganathan, K. Sivakumar, and C. Vimal, "Removal of ocular artifacts in the eeg through wavelet transform without using an eog reference channel," *Int. J. Open Problems Compt. Math*, vol. 1, no. 3, pp. 188–200, 2008.

[100] J. Chen, Z. Li, J. Pan, G. Chen, Y. Zi, J. Yuan, B. Chen, and Z. He, "Wavelet transform based on inner product in fault diagnosis of rotating machinery: A review," *Mechanical systems and signal processing*, vol. 70, pp. 1–35, 2016.

[101] M. Mojiri, M. Karimi-Ghartemani, and A. Bakhshai, "Time-domain signal analysis using adaptive notch filter," *IEEE Transactions on Signal Processing*, vol. 55, no. 1, pp. 85–93, 2006.

[102] E. D. Chesmore, "Application of time domain signal coding and artificial neural networks to passive acoustical identification of animals," *Applied Acoustics*, vol. 62, no. 12, pp. 1359–1374, 2001.

[103] S. Tong and N. V. Thakor, *Quantitative EEG analysis methods and clinical applications*. Artech House, 2009.

[104] S. Debener, A. Strobel, B. Sorger, J. Peters, C. Kranczioch, A. K. Engel, and R. Goebel, "Improved quality of auditory event-related potentials recorded simultaneously with 3-t fmri: removal of the ballistocardiogram artefact," *Neuroimage*, vol. 34, no. 2, pp. 587–597, 2007.

[105] A. Cichocki, S. L. Shishkin, T. Musha, Z. Leonowicz, T. Asada, and T. Kurachi, "Eeg filtering based on blind source separation (bss) for early detection of alzheimer's disease," *Clinical Neurophysiology*, vol. 116, no. 3, pp. 729–737, 2005.

[106] D. A. Ramli, Y. H. Shiong, and N. Hassan, "Blind source separation (bss) of mixed maternal and fetal electrocardiogram (ecg) signal: A comparative study," *Procedia Computer Science*, vol. 176, pp. 582–591, 2020.

[107] G. Gratton, M. G. Coles, and E. Donchin, "A new method for off-line removal of ocular artifact," *Electroencephalography and clinical neurophysiology*, vol. 55, no. 4, pp. 468–484, 1983.

[108] H. V. Semlitsch, P. Anderer, P. Schuster, and O. Presslich, "A solution for reliable and valid reduction of ocular artifacts, applied to the p300 erp," *Psychophysiology*, vol. 23, no. 6, pp. 695–703, 1986.

[109] A. Hyvärinen, "Independent component analysis: recent advances," *Philosophical Transactions of the Royal Society A: Mathematical, Physical and Engineering Sciences*, vol. 371, no. 1984, p. 20110534, 2013.

[110] M. Adib and E. Cretu, "Wavelet-based artifact identification and separation technique for eeg signals during galvanic vestibular stimulation," *Computational and mathematical methods in medicine*, vol. 2013, 2013.

[111] E. M. ter Braack, B. de Jonge, and M. J. Van Putten, "Reduction of tms induced artifacts in eeg using principal component analysis," *IEEE transactions on neural systems and rehabilitation engineering*, vol. 21, no. 3, pp. 376–382, 2013.

[112] D. A. Soltysik, D. Thomasson, S. Rajan, and N. Biassou, "Improving the use of principal component analysis to reduce physiological noise and motion artifacts to increase the sensitivity of task-based fmri," *Journal of neuroscience methods*, vol. 241, pp. 18–29, 2015.

[113] M. C. B. Pravitha Ramanand and E. N. Bruce, "Mutual information analysis of eeg signals indicates age-related changes in cortical interdependence during sleep in middle-aged vs. elderly women," *Journal of clinical neurophysiology: official publication of the American Electroencephalographic Society*, vol. 27, no. 4, p. 274, 2010.

[114] L. H. Cohen, *Life events and psychological functioning: Theoretical and methodological issues*, vol. 90. SAGE Publications, Incorporated, 1988.

[115] E. M. Guizzo, *The essential message: Claude Shannon and the making of information theory*. Thesis, 2003.

[116] A. Lesne, "Shannon entropy: a rigorous notion at the crossroads between probability, information theory, dynamical systems and statistical physics," *Mathematical Structures in Computer Science*, vol. 24, no. 3, 2014.

[117] L. Hui and M. Belkin, "Evaluation of neural architectures trained with square loss vs cross-entropy in classification tasks," *arXiv preprint arXiv:2006.07322*, 2020.

[118] H. Parmar and D. Hindoliya, "Artificial neural network based modelling of desiccant wheel," *Energy and Buildings*, vol. 43, no. 12, pp. 3505–3513, 2011.

[119] A. S. Goldberger, "Best linear unbiased prediction in the generalized linear regression model," *Journal of the American Statistical Association*, vol. 57, no. 298, pp. 369–375, 1962.

[120] A. Tharwat, T. Gaber, A. Ibrahim, and A. E. Hassanien, "Linear discriminant analysis: A detailed tutorial," *AI communications*, vol. 30, no. 2, pp. 169–190, 2017.

[121] S. Z. Li and A. Jain, eds., *Fisher Criterion*, pp. 549–549. Boston, MA: Springer US, 2009.

[122] A. Widodo and B.-S. Yang, "Support vector machine in machine condition monitoring and fault diagnosis," *Mechanical systems and signal processing*, vol. 21, no. 6, pp. 2560–2574, 2007.

[123] A. Dongare, R. Kharde, A. D. Kachare, *et al.*, "Introduction to artificial neural network," *International Journal of Engineering and Innovative Technology (IJEIT)*, vol. 2, no. 1, pp. 189–194, 2012.

[124] P. Baldi, "Gradient descent learning algorithm overview: A general dynamical systems perspective," *IEEE Transactions on neural networks*, vol. 6, no. 1, pp. 182–195, 1995.

[125] M. T. Hagan and M. B. Menhaj, "Training feedforward networks with the marquardt algorithm," *IEEE transactions on Neural Networks*, vol. 5, no. 6, pp. 989–993, 1994.

[126] D. T. La Corte, "Newton's method backpropagation for complex-valued holomorphic neural networks: Algebraic and analytic properties," 2014.

[127] R. Battiti, "First-and second-order methods for learning: between steepest descent and newton's method," *Neural computation*, vol. 4, no. 2, pp. 141–166, 1992.

[128] E. S. Geller, "Behavior-based safety: a solution to injury prevention: behavior-based safety "empowers" employees and addresses the dynamics of injury prevention," *Risk & Insurance*, vol. 15, no. 12, p. 01, 2004.

[129] J.-S. Choi, J. W. Bang, H. Heo, and K. R. Park, "Evaluation of fear using nonintrusive measurement of multimodal sensors," *Sensors*, vol. 15, no. 7, pp. 17507–17533, 2015.

[130] S. Cheemalapati, M. Gubanov, M. Del Vale, and A. Pyayt, "A real-time classification algorithm for emotion detection using portable eeg," in *2013 IEEE 14th International Conference on Information Reuse & Integration (IRI)*, pp. 720–723, IEEE.

[131] P. Putman, J. van Peer, I. Maimari, and S. van der Werff, "Eeg theta/beta ratio in relation to fear-modulated response-inhibition, attentional control, and affective traits," *Biological psychology*, vol. 83, no. 2, pp. 73–78, 2010.

[132] B. C. PETTINGER, "Is behavior-based safety dead?,"

[133] B. Öz, T. Özkan, and T. Lajunen, "An investigation of professional drivers: Organizational safety climate, driver behaviours and performance," *Transportation research part F: traffic psychology and behaviour*, vol. 16, pp. 81–91, 2013.

[134] I. Teyeb, O. Jemai, M. Zaied, and C. B. Amar, "A drowsy driver detection system based on a new method of head posture estimation," in *International Conference on Intelligent Data Engineering and Automated Learning*, pp. 362–369, Springer.

[135] T. Hong and H. Qin, "Drivers drowsiness detection in embedded system," in *2007 IEEE International Conference on Vehicular Electronics and Safety*, pp. 1–5, IEEE.

[136] C.-T. Lin, C.-J. Chang, B.-S. Lin, S.-H. Hung, C.-F. Chao, and I.-J. Wang, "A real-time wireless brain–computer interface system for drowsiness detection," *IEEE transactions on biomedical circuits and systems*, vol. 4, no. 4, pp. 214–222, 2010.

[137] S. De Nadai, M. D'Incà, F. Parodi, M. Benza, A. Trotta, E. Zero, L. Zero, and R. Sacile, "Enhancing safety of transport by road by on-line monitoring of driver emotions," in *2016 11th System of Systems Engineering Conference (SoSE)*, pp. 1–4, Ieee.

[138] B. Liang and Y. Lin, "Using physiological and behavioral measurements in a picture-based road hazard perception experiment to classify risky and safe drivers," *Transportation research part F: traffic psychology and behaviour*, vol. 58, pp. 93–105, 2018.

[139] A. Vuckovic, V. Radivojevic, A. C. Chen, and D. Popovic, "Automatic recognition of alertness and drowsiness from eeg by an artificial neural network," *Medical engineering & physics*, vol. 24, no. 5, pp. 349–360, 2002.

[140] P. Sauseng, W. Klimesch, C. Gerloff, and F. C. Hummel, "Spontaneous locally restricted eeg alpha activity determines cortical excitability in the motor cortex," *Neuropsychologia*, vol. 47, no. 1, pp. 284–288, 2009.

[141] M. A. Schier, "Changes in eeg alpha power during simulated driving: a demonstration," *International Journal of Psychophysiology*, vol. 37, no. 2, pp. 155–162, 2000.

[142] G. Borghini, G. Vecchiato, J. Toppi, L. Astolfi, A. Maglione, R. Isabella, C. Caltagirone, W. Kong, D. Wei, and Z. Zhou, "Assessment of mental fatigue during car driving by using high resolution eeg activity and neurophysiologic indices," in *2012 Annual International Conference of the IEEE Engineering in Medicine and Biology Society*, pp. 6442–6445, IEEE.

[143] M. Simon, E. A. Schmidt, W. E. Kincses, M. Fritzsche, A. Bruns, C. Aufmuth, M. Bogdan, W. Rosenstiel, and M. Schrauf, "Eeg alpha spindle measures as indicators of driver fatigue under real traffic conditions," *Clinical Neurophysiology*, vol. 122, no. 6, pp. 1168–1178, 2011.

[144] L. Yan, T. Wen, J. Zhang, L. Chang, Y. Wang, M. Liu, C. Ding, and F. Yan, "An evaluation of executive control function and its relationship with driving performance," *Sensors*, vol. 21, no. 5, p. 1763, 2021.

[145] T. C. Chieh, M. M. Mustafa, A. Hussain, S. F. Hendi, and B. Y. Majlis, "Development of vehicle driver drowsiness detection system using electrooculogram (eog)," in *2005 1st International Conference on Computers, Communications, & Signal Processing with Special Track on Biomedical Engineering*, pp. 165–168, IEEE, 2005.

[146] V. D. Calhoun, "Functional magnetic resonanc e imaging (fmri)," *OXFORD SERIES IN HUMAN-TECHNOLOGY INTERACTION*, p. 51, 2007.

[147] P. M. Bloomfield, H. Green, and N. Gant, "Cerebral haemodynamics during simulated driving: Changes in workload are detectable with functional near infrared spectroscopy," *PLoS one*, vol. 16, no. 3, p. e0248533, 2021.

[148] S. Murugan, J. Selvaraj, and A. Sahayadhas, "Detection and analysis: driver state with electrocardiogram (ecg)," *Physical and engineering sciences in medicine*, vol. 43, no. 2, pp. 525–537, 2020.

[149] J. R. Perello-March, C. G. Burns, R. Woodman, M. T. Elliott, and S. A. Birrell, "Driver state monitoring: Manipulating reliability expectations in simulated automated driving scenarios," *IEEE Transactions on Intelligent Transportation Systems*, 2021.

[150] L. Salvati, M. d'Amore, A. Fiorentino, A. Pellegrino, P. Sena, and F. Villecco, "On-road detection of driver fatigue and drowsiness during medium-distance journeys," *Entropy*, vol. 23, no. 2, p. 135, 2021.

[151] S. K. Lal, A. Craig, P. Boord, L. Kirkup, and H. Nguyen, "Development of an algorithm for an eeg-based driver fatigue countermeasure," *Journal of safety Research*, vol. 34, no. 3, pp. 321–328, 2003.

[152] C.-T. Lin, C.-H. Chuang, C.-S. Huang, S.-F. Tsai, S.-W. Lu, Y.-H. Chen, and L.-W. Ko, "Wireless and wearable eeg system for evaluating driver vigilance," *IEEE Transactions on biomedical circuits and systems*, vol. 8, no. 2, pp. 165–176, 2014.

[153] H. Zeng, C. Yang, G. Dai, F. Qin, J. Zhang, and W. Kong, "Eeg classification of driver mental states by deep learning," *Cognitive neurodynamics*, vol. 12, no. 6, pp. 597–606, 2018.

[154] C.-T. Lin, I.-F. Chung, L.-W. Ko, Y.-C. Chen, S.-F. Liang, and J.-R. Duann, "Eeg-based assessment of driver cognitive responses in a dynamic virtual-reality driving environment," *IEEE Transactions on Biomedical Engineering*, vol. 54, no. 7, pp. 1349–1352, 2007.

[155] N. Robinson, T. W. J. Chester, and K. Smitha, "Use of mobile eeg in decoding hand movement speed and position," *IEEE Transactions on Human-Machine Systems*, vol. 51, no. 2, pp. 120–129, 2021.

[156] N. Robinson, C. Guan, and A. Vinod, "Adaptive estimation of hand movement trajectory in an eeg based brain–computer interface system," *Journal of neural engineering*, vol. 12, no. 6, p. 066019, 2015.

[157] A. Y. Paek, H. Agashe, and J. L. Contreras-Vidal, "Decoding repetitive finger movements with brain activity acquired via non-invasive electroencephalography," *Frontiers in neuroengineering*, vol. 7, p. 3, 2014.

[158] M. Kim, B. H. Kim, and S. Jo, "Quantitative evaluation of a low-cost noninvasive hybrid interface based on eeg and eye movement," *IEEE transactions on neural systems and rehabilitation engineering*, vol. 23, no. 2, pp. 159–168, 2014.

[159] A. Shakeel, M. S. Navid, M. N. Anwar, S. Mazhar, M. Jochumsen, and I. K. Niazi, "A review of techniques for detection of movement intention using movement-related cortical potentials," *Computational and mathematical methods in medicine*, vol. 2015, 2015.

[160] R. A. Gougeh, T. Y. Rezaii, and A. Farzamnia, "An automatic driver assistant based on intention detecting using eeg signal," in *Proceedings of the 11th National Technical Seminar on Unmanned System Technology 2019*, pp. 617–627, Springer, 2021.

[161] L. G. Hernández, O. M. Mozos, J. M. Ferrández, and J. M. Antelis, "Eeg-based detection of braking intention under different car driving conditions," *Frontiers in neuroinformatics*, vol. 12, p. 29, 2018.

[162] R. Li, Y. V. Chen, and L. Zhang, "A method for fatigue detection based on driver's steering wheel grip," *International Journal of Industrial Ergonomics*, vol. 82, p. 103083, 2021.

[163] P. Ofner and G. R. Müller-Putz, "Using a noninvasive decoding method to classify rhythmic movement imaginations of the arm in two planes," *IEEE transactions on biomedical engineering*, vol. 62, no. 3, pp. 972–981, 2014.

[164] J.-H. Kim, F. Bießmann, and S.-W. Lee, "Decoding three-dimensional trajectory of executed and imagined arm movements from electroencephalogram signals," *IEEE Transactions on Neural Systems and Rehabilitation Engineering*, vol. 23, no. 5, pp. 867–876, 2014.

[165] G. S. Gupta, G. B. Dave, P. R. Tripathi, D. K. Mohanta, S. Ghosh, and R. K. Sinha, "Brain computer interface controlled automatic electric drive for neuro-aid system," *Biomedical Signal Processing and Control*, vol. 63, p. 102175, 2021.

[166] M. Owen and C. Au, "The development of a brain controlled interface employing electroencephalography to control a hand prostheses," *International Journal of Biomedical Engineering and Technology*, vol. 35, no. 2, pp. 173–190, 2021.

[167] N. Sulaiman, N. M. M. A. Al-Fakih, M. Rashid, M. S. Jadin, M. Mustafa, and F. Samsuri, "Offline eeg-based dc motor control for wheelchair application," in *Proceedings of the 11th National Technical Seminar on Unmanned System Technology 2019*, pp. 965–980, Springer, 2021.

[168] A. S. Royer, A. J. Doud, M. L. Rose, and B. He, "Eeg control of a virtual helicopter in 3-dimensional space using intelligent control strategies," *IEEE Transactions on neural systems and rehabilitation engineering*, vol. 18, no. 6, pp. 581–589, 2010.

[169] J. Zhang and M. Wang, "A survey on robots controlled by motor imagery brain–computer interfaces," *Cognitive Robotics*, 2021.

[170] R. Rao and R. Derakhshani, "A comparison of eeg preprocessing methods using time delay neural networks," in *Conference Proceedings. 2nd International IEEE EMBS Conference on Neural Engineering, 2005.*, pp. 262–264, IEEE, 2005.

[171] G. Emayavaramban, S. Ramkumar, A. Amudha, and K. S. Kumar, "Classification of hand gestures using ffnn and tdnn networks," *International Journal of Pure And Applied Mathematics*, vol. 118, no. 8, pp. 27–32, 2018.

[172] E. Zero, C. Bersani, and R. Sacile, "Identification of brain electrical activity related to head yaw rotations," *Sensors*, vol. 21, no. 10, p. 3345, 2021.

[173] V. Singh, K. Veer, R. Sharma, and S. Kumar, "Comparative study of fir and iir filters for the removal of 50 hz noise from eeg signal," *International Journal of Biomedical Engineering and Technology*, vol. 22, no. 3, pp. 250–257, 2016.

[174] M. Tariq, P. M. Trivailo, and M. Simic, "Eeg-based bci control schemes for lower-limb assistive-robots," *Frontiers in human neuroscience*, vol. 12, p. 312, 2018.

[175] F. Lotte, M. Congedo, A. Lécuyer, F. Lamarche, and B. Arnaldi, "A review of classification algorithms for eeg-based brain–computer interfaces," *Journal of neural engineering*, vol. 4, no. 2, p. R1, 2007.

[176] S. K. Goh, H. A. Abbass, K. C. Tan, A. Al-Mamun, C. Wang, and C. Guan, "Automatic eeg artifact removal techniques by detecting influential independent components," *IEEE transactions on emerging topics in computational intelligence*, vol. 1, no. 4, pp. 270–279, 2017.

[177] S. Sapna, A. Tamilarasi, and M. P. Kumar, "Backpropagation learning algorithm based on levenberg marquardt algorithm," *Comp Sci Inform Technol (CS and IT)*, vol. 2, pp. 393–398, 2012.

[178] C. Lv, Y. Xing, J. Zhang, X. Na, Y. Li, T. Liu, D. Cao, and F.-Y. Wang, "Levenberg–marquardt backpropagation training of multilayer neural networks for state estimation of a safety-critical cyber-physical system," *IEEE Transactions on Industrial Informatics*, vol. 14, no. 8, pp. 3436–3446, 2017.

[179] Z. Qin, D. Kim, and T. Gedeon, "Rethinking softmax with cross-entropy: Neural network classifier as mutual information estimator," *arXiv preprint arXiv:1911.10688*, 2019.

[180] S. Boughorbel, F. Jarray, and M. El-Anbari, "Optimal classifier for imbalanced data using matthews correlation coefficient metric," *PloS one*, vol. 12, no. 6, p. e0177678, 2017.

[181] S. Bhattacharyya, A. Konar, and D. Tibarewala, "Motor imagery and error related potential induced position control of a robotic arm," *IEEE/CAA Journal of Automatica Sinica*, vol. 4, no. 4, pp. 639–650, 2017.